Geohydrologic Conditions on a Steep Forested Slope: Modeling Transient Piezometric Response to Precipitation

by

Mark Bransom

A THESIS

Submitted to

Oregon State University

In partial fulfillment of
the requirements for the
degree of

Doctor of Philosophy

Completed December 6, 1996

Commencement June 1997

AN ABSTRACT OF THE THESIS OF

Mark Bransom for the degree of Doctor of Philosophy in Civil Engineering presented on December 6, 1996. Title: Geohydrologic Conditions on a Steep Forested Slope: Modeling Transient Piezometric Response to Precipitation

Abstract approved: ______________________________
Marvin R. Pyles

Two hillslope sites in the central Oregon Coast Range were instrumented and monitored for winter precipitation and saturated and unsaturated subsurface conditions. The study sites were near-ridge depressions typically known as headwalls. Based on results of the monitoring, two existing mathematical models were adapted to predict piezometric levels in headwalls during storms. The first is a statistically based model, using an Antecedent Precipitation Index (API) as an independent variable in a regression model. The second is a mass balance model based on the kinematic assumption that the hydraulic gradient is equal to the slope of the impermeable base of the control volume. Several extreme storm events recorded during the monitoring period were used to calibrate the models. Precipitation data from a subsequent extreme event was then used in verification runs of both the API and the kinematic storage models.

Soil from one site was sampled for index properties, strength parameters, and hydraulic properties. The soil is a non-plastic, sand-silt mixture derived from sandstone. A relatively undisturbed sample tested in a consolidated-undrained

triaxial test had a ϕ' value of 32.5° and a c' value of 5.2 kPa. Laboratory testing suggests that the soil is hydraulically similar to other soils in similar geographic and topographic locations. An estimate of the "effective" saturated hydraulic conductivity, considering both macropore and matrix flow, is approximately 10^{-2} cm/s.

In general, the API models for individual storms were capable of reproducing observed piezometric hydrographs. However, the use of API was limited by the high degree of variability in API values and antecedent hydraulic head conditions from storm to storm. A multi-storm API model was developed to overcome these limitations, and produced reasonably good results. The kinematic storage model also performed well for this site, for two of three methods of determining drainable porosity of the soil.

Hillslope discharge measurements made on one occasion suggested that approximately 70% of flow at the outlet was occurring in pores larger than 2.5 centimeters in diameter. Macropore flow would seem to be an important feature of the subsurface flow regime under certain precipitation and antecedent soil moisture conditions.

Acknowledgments

The author wishes to acknowledge the professional guidance and personal friendship of the major professor, Dr. Marvin Pyles; I am richer for both. Thanks are extended to Drs. Jack Istok, John Selker, and Paul Adams for playing a vital role in directing and improving the work. The support of the Forest Engineering Department and the College of Forestry, and all her people, is greatly appreciated.

Simple words of gratitude cannot convey the degree of thanks due my family, but I try nonetheless. Thanks to my wife, Kay, for all her support, and to our daughter, Ciera, for being a light of inspiration. Never stop asking why?.

Doctor of Philosophy thesis of Mark Bransom presented on December 6, 1996

APPROVED:

Major Professor, representing Civil Engineering

Head of Department of Civil, Construction, and Environmental Engineering

Dean of Graduate School

I understand that my thesis will become part of the permanent collection of Oregon State University libraries. My signature below authorizes release of my thesis to any reader upon request.

Mark Bransom, Author

Table of Contents

Page

Table of Contents (continued)

Table of Contents (continued)

Page

Table of Contents (continued)

Table of Contents (continued)

List of Figures

Figure | Page

List of Figures (continued)

List of Figures (continued)

List of Tables

This thesis is dedicated to my parents, Laura and Bruce Bransom, with love, and gratitude for your guidance.

Geohydrologic Conditions on a Steep Forested Slope:
Modeling Transient Piezometric Response to Precipitation

1. INTRODUCTION

Knowledge of subsurface conditions is the principle objective of every geotechnical and geohydrologic investigation. These investigations typically rely on some level of testing and monitoring to obtain information relevant to the objectives. In many geotechnical studies, an examination of landslides or earth-structure failure involves back-analysis of subsurface conditions at the time of failure. More commonly, however, a site is monitored in order to make predictions about its behavior under a different set of site conditions. This scenario is typical where construction of low-volume transportation systems or related timber harvest activities has been proposed for potentially unstable areas.

In the central Oregon coastal mountain range, engineering activities are often conducted on very steep terrain. Design of engineering works on steep natural slopes, or construction of steep embankments, can pose significant technical challenges. Knowledge of groundwater conditions on such sites is critical to any analysis of the stability of that site. The primary focus of this work is steep slopes where the significant management activity is timber harvesting and related activities such as road building.

On natural forested slopes in the Oregon coast range, groundwater flow in response to precipitation and snowmelt is typically shallow and highly transient.

Slope failures are thought to occur primarily as a result of rapid buildup of pore-water pressures in all or some portion of the slope as a result of wet antecedent conditions and the addition of high intensity precipitation. Local failures often propagate significant distances down slope as debris flows.

In order to analyze failure potential for a particular slope, one must know how hydraulic head is distributed throughout the slope, for either a range of storm events, or for a particular design storm. Those with need for a method to predict piezometric levels on steep slopes generally have been forced to chose between complex models with enormous data requirements, and models with assumptions that grossly oversimplify field conditions. Furthermore, acquisition of meaningful information about the soil properties is complicated by the high degree of heterogeneity common to soils on natural slopes where colluvial action is an important geomorphic force. Such sites typically have significant variability in soil properties. Characterization of the variability can require a great deal of testing. For large engineering projects, expensive testing and monitoring of site conditions can be justified, but for most other projects it cannot. Yet engineers, hydrologists, and foresters must move ahead with the best information at hand in order to make predictions about the response of a site to a proposed use, or the ability of a site to withstand a change in conditions.

For classification of slopes based on a failure risk index, a simple physically based model that allows for prediction of subsurface response to precipitation, but does not require detailed site data, would be a valuable tool for land managers and engineers. The purpose of this work was to address this need, and determine whether it is feasible to construct a reliable model requiring a minimum of data inputs. Previous research has recognized that there is a strong correlation between the timing and magnitude of precipitation, antecedent conditions, and the resulting runoff that appears in surface waterways (Fedora 1987, Istok et al. 1986). There had been, however, relatively few attempts to investigate the correlation between antecedent conditions and piezometric levels on steep slopes.

Many landslides in the Oregon coast range are thought to originate in small near-ridge depressions, commonly referred to as headwalls. These sites are typically very steep, show evidence of colluvial activity, and have little or no overstory vegetation (Bransom, 1991). They are often characterized by converging topography, terminating in a constriction sometimes called a critical point. Below this critical point, surface channelization of water is often evident. Headwalls are thought to be a principle source of sediment delivered to small streams. Much work has been done to classify headwall failure risk, and determine ways to recognize those sites that have the highest potential for failure (Bransom 1991, Deitrich 1989, Burroughs 1984). As part of the previous work, a number of assumptions have necessarily been made about the subsurface conditions in headwalls.

Few studies have specifically addressed subsurface conditions in high risk headwalls, either from a geotechnical or geohydrological perspective. Yet these sites are of primary concern to many land managers due to their failure risk and the associated potential to do significant damage to downstream values. This study was designed to gain some fundamental understanding of the processes of subsurface flow in headwalls, and evaluate whether it would be feasible to construct a mathematical model of these processes for prediction of piezometric levels during extreme storm events. The objectives of the study can be stated as follows:

1) To intensively instrument and monitor subsurface-flow and precipitation conditions on a headwall having characteristics of a site with a high potential of landslide failure.

2) To investigate the relative significance of macro-porosity and matrix flow in routing water through the subsurface on steep slopes in the forest environment.

3) To develop a mathematical model for prediction of piezometric levels in headwalls that requires a minimum of data inputs.

4) To test the usefulness of the groundwater model for classification of sites on the basis of failure potential.

5) To characterize the geotechnical and geohydrologic properties of the soil found in the headwall.

In order to meet the objectives in a field study, two headwalls in the central Oregon coast range were selected. The two sites were instrumented with well points, tensiometers, and tipping bucket rain gages. The sites were monitored during the winters from 1992 through 1995.

The body of this work will include a development of the theory of ground-water flow and review of the literature pertaining to subsurface conditions on steep slopes. Characteristics of the sites will be discussed in the context of the issues surrounding slope stability. The results of the monitoring effort will be presented, as will the results of the development of a groundwater model. A discussion of the previous topics will follow, with conclusions drawn from the field study, and the monitoring and modeling efforts.

2. LITERATURE REVIEW

The direction, magnitude, and timing of groundwater flow has implications for geotechnical, geohydrological, and geomorphological investigations. Common areas of problem analysis in these disciplines include: stability of natural slopes and earth structures, water supply and aquifer recharge, fate and transport of solutes, landform genesis, and subsurface contribution to stream channel runoff. To understand the mechanics of subsurface flow requires an understanding of both the fluid, its properties and constituents, and the media in which flow is being investigated.

This review will begin by summarizing key points of groundwater flow theory including fluid potential, Darcy's Law, hydraulic conductivity, and flow in saturated and unsaturated porous media. Following an introduction to groundwater flow theory, a summary of several techniques for characterizing subsurface flow, with advantages and disadvantages of each method, will be presented. The review will end with a discussion of the development of mathematical models and their use in analyzing fluid flow through porous media.

2.1 Groundwater Flow Theory

Knowing the relative energy state of a fluid in a porous media is a necessary and sufficient condition for predicting movement of that fluid. The energy state of a fluid in a porous media can be analyzed by applying the concept of fluid potential

(Hubbert 1940, Freeze and Cherry 1979, Hillel 1982, Jury et. al. 1991). Subsurface water moves as a result of potential gradients in the flow field. Potential is a quantity, measurable at every point in the flow system, whose properties are such that flow always occurs from regions of higher potential to regions of lower potential, as the system tends toward equilibrium (Hubbert 1940). Potential gradients that will induce groundwater flow include thermal, electrical, and chemical gradients (Freeze and Cherry, 1979). However, for most hydrogeological flow regimes they are considered minor, relative to total mechanical potential gradients, discussed below. The meaning of potential at a point can be can be understood by considering the total energy of a unit of fluid, relative to a reference state. Consider a unit mass (of unit volume) of fluid in a flow field. The potential possessed by the fluid has classically been expressed in terms of the amount of work per unit quantity of pure water necessary to "move" that fluid from the reference state to the state at the point of interest (Hillel 1982, Jury et. al. 1991). The work, W_z , required to raise a unit mass of fluid from the reference elevation, z_0, to elevation z is given by

$$W_z = mgz \tag{2.1}$$

where m = mass of the unit of fluid (M)
g = acceleration of gravity (L/T^2)
z = elevation relative to z_0, termed the elevation head (L)

Similarly, the work, W_v, required to bring the unit mass from the velocity at the reference state, v_0, to velocity, v, is given by

$$W_v = \frac{1}{2} m v^2 \tag{2.2}$$

where v = velocity at the point of interest relative to v_0 (L/T)

Finally, the work, W_p, required to move the unit mass from the reference pressure, P_0, usually taken as atmospheric pressure, to the pressure P, is given by

$$W_p = \int_{P_0}^{P} \frac{m}{\rho}\, dP \tag{2.3}$$

where P_0 = pressure at the reference state (M/LT^2)
P = pressure at the point of interest (M/LT^2)
ρ = density of the fluid (M/L^3)

The potential, or total mechanical energy <u>per unit mass</u> of fluid relative to the reference state, is

$$\Phi = gz + \frac{v^2}{2} + \int_{Po}^{P} \frac{dP}{\rho} \tag{2.4}$$

The velocity potential for most groundwater flow problems is much less than the gravity potential and the pressure potential, due to low groundwater velocity. For velocity potential less than unity, the square of the velocity term further reduces the relative contribution to total potential. The velocity potential term is often eliminated from the expression for total potential, and Equation 2.4 can then be reduced to

$$\Phi = gz + \int_{P_0}^{P} \frac{dP}{\rho} \tag{2.5}$$

For incompressible fluids where density, ρ, is not a function of the hydrostatic pressure, P, we can write

$$\Phi = gz + \frac{1}{\rho}\int_{P_0}^{P} dP \tag{2.6}$$

or, evaluating the integral

$$\Phi = gz + \frac{(P - P_0)}{\rho} \tag{2.7}$$

The hydrostatic pressure at a point is given by

$$P = \rho g h_P + P_0 \tag{2.8}$$

where h_P = distance from free fluid surface to point of measurement, termed the pressure head (L)

Substituting this into Equation 2.7 gives

$$\Phi = gz + \frac{(\rho g h_P + P_0) - P_0}{\rho} = g(z + h_P) \tag{2.9}$$

Defining the hydraulic head, H, as the sum of elevation head, z, and pressure head, h_P, Equation 2.9 becomes

$$\Phi = gH \tag{2.10}$$

Equation 2.10 says that the fluid potential at any point is the product of the hydraulic head and the acceleration of gravity, where potential is the energy per unit mass of fluid, and hydraulic head is the energy per unit weight of fluid.

2.1.1 Saturated Flow and Darcy's Law

The concept of potential is useful in understanding what drives groundwater flow; groundwater flows in response to gradients in potential between points in the flow field. Empirical evidence provides an understanding of groundwater velocities and discharges. For laminar flow conditions, the rate of water flow through sands was shown to be proportional to the difference in hydraulic head between two points (as given by potential theory), and inversely proportional to the distance between the two points (Darcy, 1856). When combined with a proportionality constant that takes into account properties of both the fluid and the porous media, Darcy's Law states that

$$q = -K \frac{\Delta H}{\Delta l} \tag{2.11}$$

where q = specific discharge (L/T)
ΔH = difference in hydraulic head between two points (L)
Δl = distance between the two points (L)
K = hydraulic conductivity (L/T)

The negative sign in Equation 2.11 is necessary as the hydraulic head decreases in the direction of flow, ie. $\Delta H < 0$. In differential form Darcy's Law is stated as

$$q = -K \frac{dH}{dl} \tag{2.12}$$

The term *dH/dl* is defined as the hydraulic gradient and is a measure of how rapidly the potential changes with distance.

The flow distance between two points in a porous media is greater than Δl due to the pore structure of the media. For a given cross-sectional area, A, the effective flow area is the product of A and the porosity, n. The increase in the flow path that results from interference of solids is termed the tortuosity factor of the media. The average component of velocity, v, in the l direction is given by

$$\frac{q}{n} = v = -\frac{K}{n}\frac{dH}{dl} \qquad (2.13)$$

As stated previously, the hydraulic conductivity, K, is a proportionality constant that reflects properties of both the fluid and the porous media. Hydraulic conductivity of soil and rock varies over as many as ten orders of magnitude or more (Domenico and Schwartz, 1990). The principle factors affecting hydraulic conductivity include (Lambe, 1951):

1) size of soil particles;
2) void ratio, or porosity, of soil;
3) shape and arrangement of pores;
4) properties of the fluid;
5) degree of saturation of the media.

The first three factors are seen to be properties of the porous media, and their effect on hydraulic conductivity are best understood by introducing another conductivity parameter termed the intrinsic permeability of a media. The intrinsic permeability, k, is a function of the properties of the porous media alone and is related to hydraulic conductivity by

$$k = K\frac{\mu}{\gamma} \tag{2.14}$$

where k = intrinsic permeability (L^2)
μ = dynamic viscosity of the fluid (M/LT)
γ = ρg, defined as the unit weight of the fluid (M/L^2T^2)

When Equation 2.14 is substituted into Equation 2.13, average linear velocity of groundwater is

$$v = -\frac{k\gamma}{\mu n}\frac{dH}{dl} \tag{2.15}$$

Use of a media based conductance factor is valuable in analysis of multiphase flow systems where the behavior of different fluids in the flow system is being modeled.

For most cases of one dimensional flow, it is sufficient to use Darcy's Law in the form given in Equation 2.13. However, the general form of the equation for flow in three dimensions is

$$\mathbf{v} = -\mathrm{K}\,\nabla \mathrm{H} \tag{2.16}$$

where

$$\nabla H = \frac{\partial H}{\partial x}\boldsymbol{i} + \frac{\partial H}{\partial y}\boldsymbol{j} + \frac{\partial H}{\partial z}\boldsymbol{k}$$

All these forms of Darcy's Law thus far have implicitly assumed that K is independent of direction. For anisotropic material, K is a second order tensor and the general form of Darcy's Law becomes

$$\begin{bmatrix} v_x \\ v_y \\ v_z \end{bmatrix} = - \begin{bmatrix} K_{xx} & K_{xy} & K_{xz} \\ K_{yx} & K_{yy} & K_{yz} \\ K_{zx} & K_{zy} & K_{zz} \end{bmatrix} \begin{bmatrix} \frac{\partial H}{\partial x}\boldsymbol{i} & \frac{\partial H}{\partial y}\boldsymbol{j} & \frac{\partial H}{\partial z}\boldsymbol{k} \end{bmatrix} \tag{2.17}$$

For the case where the coordinate axes are taken to be coincident with the principal directions of anisotropy, the off diagonal elements of the conductivity tensor are all zero and Darcy's Law for anisotropic media becomes

$$v_x = -K_x \frac{\partial H}{\partial x} \tag{2.18a}$$

$$v_y = -K_y \frac{\partial H}{\partial y} \tag{2.18b}$$

$$v_Z = -K_z \frac{\partial H}{\partial z} \tag{2.18c}$$

The different forms of Darcy's Law presented can be used to analyze flow in a wide variety of geohydrological situations. Flow velocities, flux, and determination of conductivity are possible by applying Darcy's Law in the form appropriate for the field or laboratory conditions being analyzed.

2.1.2 Unsaturated Flow

It has been established that saturated flow results from potential gradients in the flow field, that flow occurs in the direction of decreasing potential, and that flow rate is proportional to properties of the fluid and the porous media, and to the magnitude of the potential gradient. In fact, the same principles apply to unsaturated flow. However, the governing equations must be modified to account for the functional dependence of hydraulic conductivity on potential in unsaturated media.

2.1.2.1 Surface Tension and Capillarity

At an interface between fluids such as water and air, molecules of each fluid experience an unbalanced force compared to molecules of either fluid away from the interface. Molecules at the interface experience a net force into their respective fluid because of the lower density of like molecules on the outside of the fluid (Jury et. al., 1991). As a result of the unbalanced force, molecules at the surface require extra energy to remain at the interface. This extra energy per unit surface area is defined as the surface tension, σ.

In addition to molecular bonds and other cohesive forces that attract fluid molecules to one another, adhesive forces attract molecules to other substances, such as the attraction of soil particles for water. The combined effect of surface tension and adhesion result in the phenomenon of capillarity. Small diameter glass "capillary" tubes demonstrate that adhesion forces between the glass and water cause the water to rise in the tubes and form a meniscus (Holtz and Kovacs, 1981). The pressure difference across a meniscus is proportional to the surface tension of the fluid and inversely proportional to the radii of the meniscus, as given by Laplace's capillary equation (Hillel, 1982):

$$\Delta P = -\sigma\left(\frac{1}{R_1} + \frac{1}{R_2}\right) \qquad (2.19)$$

where ΔP = pressure drop across the meniscus (M/LT^2)
σ = surface tension of fluid (M/T^2)
R_1,R_2 = principle radii of curvature of a point on the meniscus (L)

When the pressure outside the fluid is atmospheric pressure, and taking the reduced radius $R = 2R_1R_2/(R_1+R_2)$, Equation 2.19 can be written

$$P = -\frac{2\sigma}{R} \qquad (2.20)$$

Where the static gage pressure above a free fluid surface is given by

$$P = -h_c \rho g \tag{2.21}$$

where h_c is the height above the free surface at the point of interest, the height of capillary rise is given by substituting Equation 2.21 into Equation 2.20:

$$h_c = \frac{-2\sigma}{\rho g R} \tag{2.22}$$

Equation 2.21 shows that pressure decreases linearly with height above a free surface, and is sub-atmospheric (negative gage pressure). Thus, in soils where a free surface is present, a capillary zone develops. This zone is sometimes referred to as the capillary fringe or the tension saturated zone, and can represent a significant quantity of water. In sands, the capillary fringe can extend from 3 to over 15 cm above the free surface, while in clay soils the height can exceed 10 m (Holtz and Kovacs, 1981).

2.1.2.2 Matric Potential and Soil Water Retention

The potential of water in a three phase soil system has been termed the capillary pressure, or matric potential, ψ, and is equivalent to h_c when expressed in head units (units of length). As a soil drains after some input of water has occurred, the volumetric water content, θ, decreases and ψ becomes larger, or more negative. The amount of water retained by a soil at low values of ψ is primarily a function of the capillary effect and the pore size distribution, and is strongly affected by soil structure (Hillel, 1982). At high values of ψ, water retention is due primarily to adsorption and is affected less by structure and more by texture and specific surface of the soil material. A critical value of ψ exists at which the largest pores in the media will suddenly drain. This value is termed the air entry value, ψ_a. The value of ψ_a is typically small for coarse-textured soils and well aggregated soils. Because coarse soils often have pores that are more uniform in size, the air-entry phenomenon may be exhibited more distinctly than in fine-textured soils (Hillel, 1982).

The functional relationship between ψ and θ is typically determined experimentally and represented graphically. Such a plot is termed the soil-moisture characteristic curve for the media, and is essential in solving many unsaturated flow problems. Figure 2.1 shows a hypothetical soil moisture characteristic curve.

2.1.2.3 Hysteresis

When the soil-moisture characteristic curve obtained by wetting an initially dry soil is compared to the curve obtained by desorption of an initially saturated soil, the two may have similar form but generally are not identical. The difference between the two curves results from the phenomenon of hysteresis (Haines 1930, Philip 1964). This effect has been attributed to several causes (Hillel, 1982):

1) geometric non-uniformity of individual pores;
2) contact angle effect which results in larger radius of curvature in an advancing meniscus than in a receding one, meaning a given θ will exhibit a greater ψ in desorption than in sorption;
3) entrapped air which reduces the θ value at any given ψ for a wetting soil;
4) shrink-swell processes in some soils which results in changes in soil structure.

The two curves described above are called the main wetting curve and main draining curve respectively. If either the wetting or draining process is reversed while between end points of the appropriate curve, branches join the two curves and are called scanning curves, or secondary wetting or draining curves. Higher order curves occur as soils drain and re-wet, resulting in a complex soil-moisture characteristic function (Figure 2.1).

2.1.2.4 Unsaturated Hydraulic Conductivity

As ψ increases during drainage and the larger, most conductive pores drain, the connectivity of flow paths is reduced. Reduced connectivity results in an increase in flow path length. The increase in flow path length, and the higher resistance to flow through smaller pores are the two factors that act to reduce hydraulic conductivity in unsaturated media. At matric potential values greater than the air-entry value the hydraulic conductivity, K, decreases abruptly, and continues to decrease with increasing ψ as the conductive portion of a soils cross-sectional area decreases. Like the soil-moisture characteristic curve, a $K(\psi)$ vs ψ relationship can be determined

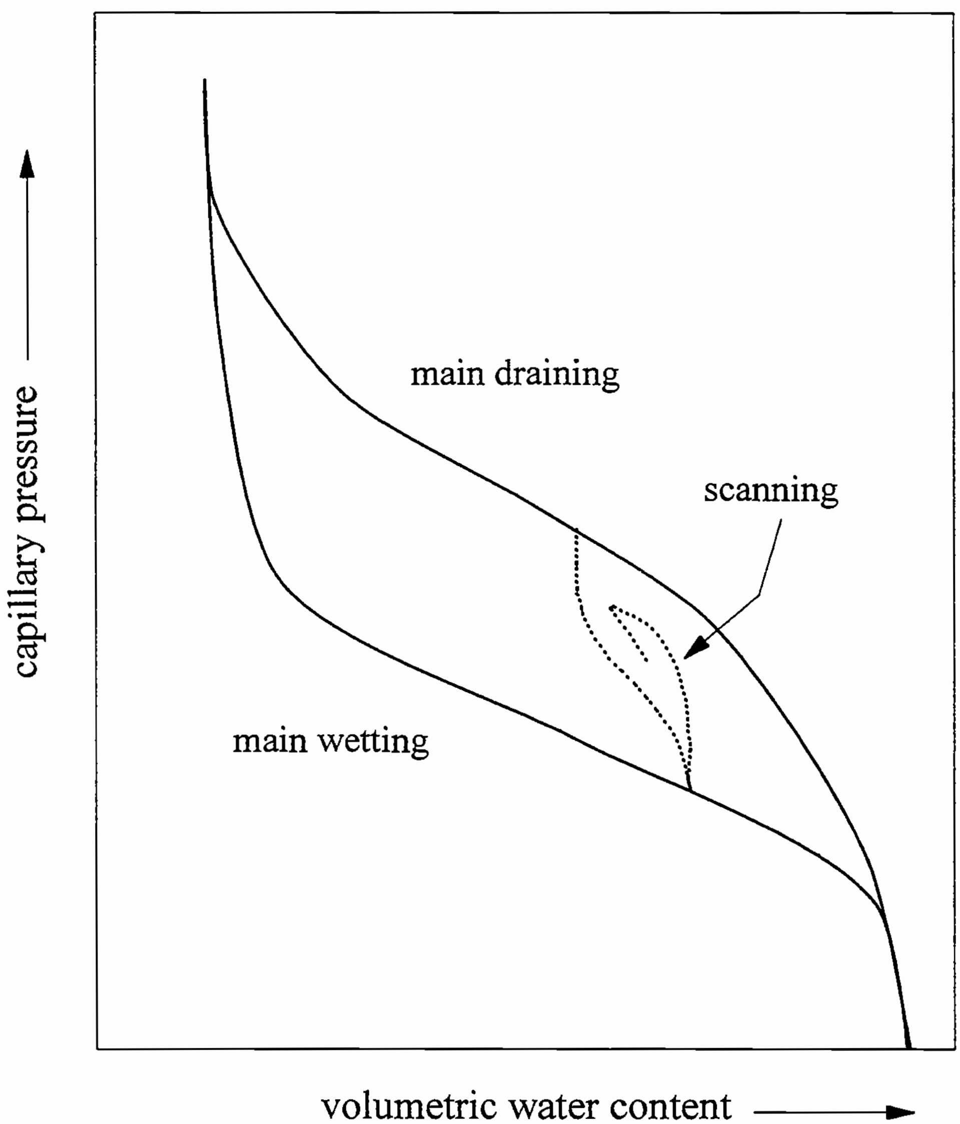

Figure 2.1 Hypothetical soil moisture characteristic curve showing main draining, main wetting, and scanning curves.

experimentally, and is similarly necessary for solution of most unsaturated flow problems.

Some functional relationships have been proposed that allow estimation of unsaturated conductivities, including that of Brooks and Corey (1966). The method of Brooks and Corey (1966) uses parameters obtained from capillary tension-desaturation data for a media to determine $K(\psi)$ for any value of ψ. The expression for $K(\psi)$ relative to the saturated conductivity K_s is

$$\frac{K(\psi)}{K_s} = \begin{cases} \left(\dfrac{\psi_a}{\psi}\right)^{\eta} & (|\psi| > |\psi_a|) \\ 1 & (|\psi| \leq |\psi_a|) \end{cases} \tag{2.23}$$

where $\eta = 2 + 3\lambda$ (1/L)

The two parameters η and λ are pore-size distribution indices. The parameter λ is the absolute value of the slope of the logarithmic plot of effective saturation, S_e, vs. ψ, (Figure 2.2) where effective saturation at any value of θ is given by

$$S_e = \frac{\theta - \theta_r}{\theta_s - \theta_r} \tag{2.24}$$

where θ_r = residual water content (L^3/L^3)
θ_s = saturated water content (L^3/L^3)

A media having uniform pore sizes would have a larger value of λ than would a media with a greater pore size distribution. The parameter η is the absolute value of the slope of the logarithmic plot of relative conductivity, $K(\psi)/K_s$ vs. ψ. Brooks and Corey (1966) report that for typical porous media, the value of λ was approximately 2; from the relationship between the two pore size indices, a value of η of 8 is typical for soil or porous rock. Highly structured soils have lower values of η, while unlithified sands may have values of η as high as 15.

Other techniques for estimating the unsaturated conductivity function include the Gardner method (1958), the Mualem method (1976), and the van Genuchten and Nielson method (1985). The Mualem, and van Genuchten and Nielson methods are similar to the Brooks and Corey method, in using the effective saturation parameter. The van Genuchten and Nielson function is given by

$$K(\theta^*) = K_s\,\theta^{*^{1/2}}\,[1 - (1 - \theta^{*^{1/m}})^m]^2 \tag{2.25}$$

where $\theta^* = [1 + (\alpha\psi)^n]^{-m}$
$m = 1 - 1/n$
α, m, n = empirical parameters dependent on the porous media

The Gardner method is an exponential decay function of the form

$$K(\psi) = K_s \exp\,[\alpha\,\psi] \tag{2.26}$$

where α = parameter dependent on the porous media.

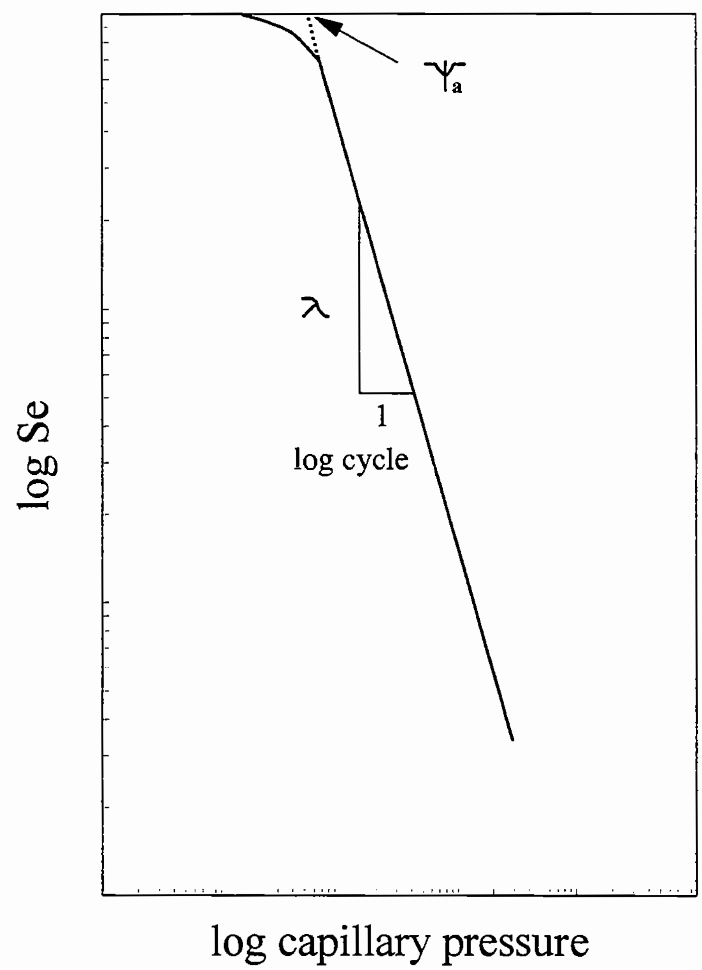

Figure 2.2 Effective saturation as a function of capillary pressure head, showing the Brooks and Corey pore-size parameter, λ, and the air-entry value, ψ_a.

The principle drawback of the Gardner method is that it fails to take into account the ability of the capillary fringe to conduct water at or near the saturated conductivity, even though fluid in the zone is under tension. As evident by Equation 2.26, the conductivity drops below K_s as soon as ψ is non-zero. A modification of the function has been proposed to correct this (Rijtema, 1965) and has the form

$$K(\psi) = \begin{cases} K_s \exp(\alpha(\psi - \psi_a)) & (|\psi| > |\psi_a|) \\ K_s & (|\psi| \leq |\psi_a|) \end{cases} \tag{2.27}$$

Use of conductivity relationships derived from desaturation data of porous media can eliminate the need to experimentally determine the unsaturated conductivity function, which can be a tedious process. However, use of such a relationship must be validated to ensure appropriate use in solving flow problems.

2.1.2.5 Richards Equation

When a porous media is not fully saturated, Darcy's Law as presented in Section 2.1.1 can not be applied directly, as K is now a function of the degree of saturation of the media. When Darcy's Law is written with K as a function of matric potential, ψ, and combined with the continuity equation, the result is known as the matric potential form of Richards equation (Richards, 1931). Alternatively, Richards equation can be expressed with conductivity as a function of water content. The water content form of Richards equation is a second-order nonlinear partial differential equation called a Fokker-Planck equation and can typically only be solved by numerical methods. In terms of matric potential, Richards equation for vertical flow is

$$C(\psi)\frac{\partial\psi}{\partial t} = \frac{\partial}{\partial z}\left[K(\psi)\left(\frac{\partial\psi}{\partial z} + 1\right)\right] \tag{2.28}$$

where $C(\psi) = d\theta/d\psi$ (1/L)

Equation 2.28 can be solved given two boundary conditions and an initial condition, assuming that $C(\psi)$ and $K(\psi)$ are known.

We have seen that the flow of fluid through a porous media is dependent on properties of both. Groundwater flow results from potential gradients in the flow field, with flow from regions of higher potential to regions of lower potential. The same principles apply to saturated and unsaturated flow conditions, yet the equations describing flow must take into account the fact that hydraulic conductivity is a function of matric potential for unsaturated flow conditions, and solutions depend on a knowledge of the unsaturated conductivity function. Next, we will review methods of investigating subsurface flow, with particular attention to the study of hillslope hydrology.

2.2 Characterizing Subsurface Flow

Characterizing subsurface flow on steep natural slopes can provide insight into the stability of such sites, as well as hillslope contribution to stream channel runoff. Subsurface flow has been defined as that part of precipitation that infiltrates the surface soil and moves laterally through the upper soil horizons toward the stream as ephemeral, shallow, perched groundwater above the main groundwater level (Chow, 1964). In many cases, such as where an impermeable layer is found near the ground surface, there may be no distinction between subsurface flow and a deeper, main groundwater aquifer. Such is the case in many small steep mountain drainage basins that maintain shallow soil mantles and are underlain by tight bedrock formations.

Researchers often disagree about the timing, mechanics, and magnitude of subsurface flow from slopes (Beasley, 1976). Widely different opinions are held concerning the contribution of subsurface flow to runoff and storm hydrographs. Hewlett and Hibbert (1965) considered subsurface flow velocities too low to contribute much volume to direct runoff. Sidle (1985) concluded that the rapid response of subsurface water to precipitation is greater than can be explained by vertical infiltration of rainfall, and proposed that rapid interflow through discontinuous macropores and pipes is a likelihood. Under such conditions, rapid movement of water to the stream is possible.

Some of the disagreement surrounding the movement of subsurface flow may arise from the different methods by which flow and flow conditions are measured, and the resulting interpretation of subsurface flow processes. It is the purpose of this review to investigate different methods of monitoring and measuring subsurface flow, and to draw conclusions regarding the advantages and disadvantages of their application to various hillslope hydrology problems. No attempt will be made to report the results and conclusions of the individual studies other than as they relate to the methods of monitoring and measuring subsurface flow.

For the purpose of this discussion, the methods of studying subsurface flow will be classified into four categories. Three of the techniques are field based while the fourth comprises a suite of techniques that includes physical and theoretical modeling. The four techniques can be categorized as follows:

1) Piezometry and tensiometry;
2) Tracer movement;
3) Interception;
4) Subsurface flow modeling.

It is important to point out that these methods can, and frequently do, overlap in a particular study, as suggested above, and are not exclusive of one another. For example, tracer studies may rely on piezometers as injection points, and interception for recovery of samples. Information regarding the hydraulic head profile in an aquifer, as determined by piezometry can be used in mathematical models to determine hydraulic properties of the media (the so-called "inverse problem").

Further, this list is not exhaustive, but includes the techniques most commonly employed.

2.2.1 Piezometry and Tensiometry Studies

Nearly all investigations of saturated hillslope groundwater flow include the use of piezometry as a tool. Sidle (1985) monitored shallow groundwater levels piezometrically on two steep, unstable, forested headwalls in coastal Alaska using a typical piezometer installation. The piezometers were 2.3 cm I.D. polyvinyl chloride (PVC) pipe with perforations drilled in the lower 12 cm. The perforated sections were covered with fine-mesh screen and packed in coarse silica sand at the base of the well hole. A bentonite plug was used between the organic and mineral horizons during backfilling of the augured hole to prevent inflow. Figure 2.3 shows a schematic diagram of a typical slotted standpipe piezometer and the components of hydraulic head at the point of measurement. The piezometer is used to measure the pressure head at the base of the instrument. A total of nineteen piezometers were installed in the soil mantle down to bedrock near the longitudinal axes of the two headwalls. Water level fluctuations were monitored by a battery powered scanning recording system described by Holbo et al. (1985). Capacitive probes in each piezometer monitored water levels, which were recorded hourly in a centrally located analog recorder. Extra circuits were used for calibration piezometers. Harr (1977) made use of a similar recording system in two piezometer grids designed to evaluate

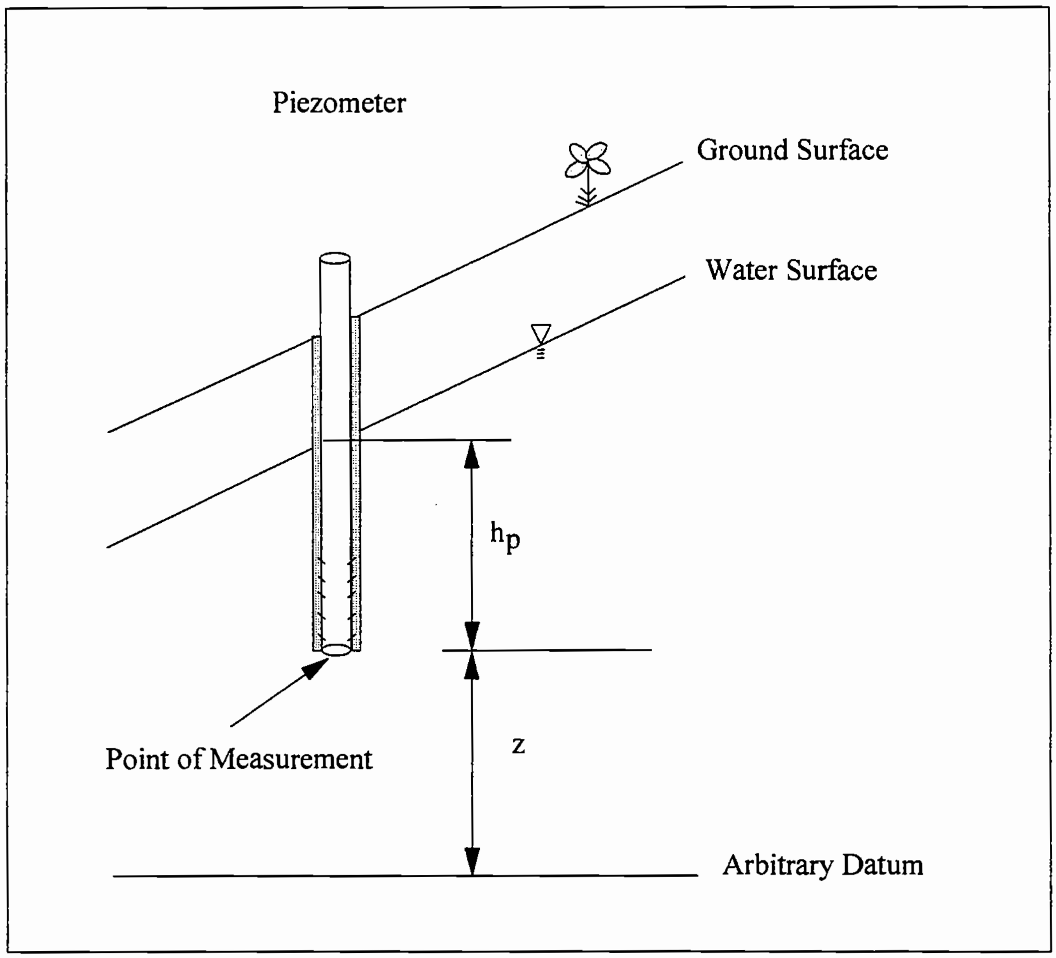

Figure 2.3 Schematic diagram of a piezometer showing components of hydraulic head at point of measurement.

water flux in soil and subsoil on the H.J. Andrews Experimental Forest. Crest gauges that record maximum water level between readings are often used in piezometers when continuous monitoring is not feasible.

Wilson and Dietrich (1987) monitored flow in soils and bedrock of headwalls to examine the role of topography in controlling the hydrologic response of hillslopes to rainfall. Piezometers were also used to determine hydraulic conductivity of the soil mantle and the bedrock using the standing head conductivity test (O'Rourke et al. 1977). Swanston and co-workers (1988) monitored water levels in inclinometer access tubes in a study of progressive hillslope deformation.

The most significant limitation of piezometry occurs in cases where significant unsaturated flow occurs in the subsurface flow regime. Water entry into piezometers will occur only when the soil surrounding the piezometer is saturated and positive gage pressures exist. Under conditions of unsaturated flow, tensiometer plots such as those used by Harr (1977) are a more appropriate means of determining magnitude and direction of water flux in soils. Tensiometers consist of a water filled tube terminating in a porous cup that is placed in hydraulic contact with the soil. Tension exerted on the water column as the device equilibrates with the soil water can be measured with a vacuum gage, manometer or pressure transducer. Figure 2.4 shows a schematic diagram of a typical tensiometer and the components of hydraulic head at the point of measurement. A tensiometer measures the capillary pressure at the tip of the instrument.

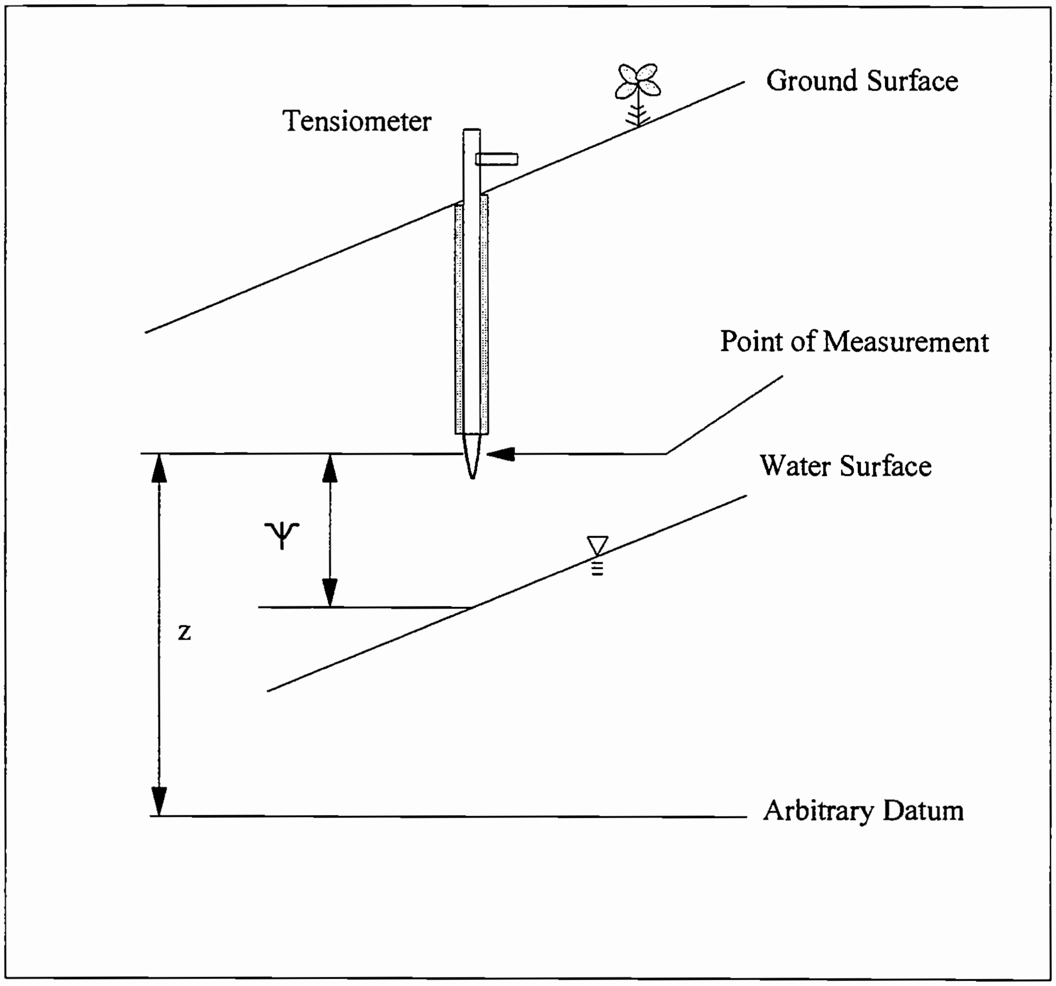

Figure 2.4 Schematic diagram of a tensiometer showing components of hydraulic head at point of measurement.

Tensiometer data was used by Harr (1977) in a two-dimensional analysis of water flux. Conductivity was determined for transient unsaturated conditions by the empirical method of Brooks and Corey (1966), discussed in section 2.1.2.4. Water fluxes in the vertical and downslope directions, as determined from the tensiometer data were summed to obtain the resultant flux. Flux angle was also determined. In this manner, magnitude and direction of flow in the unsaturated zone can be estimated.

Knowledge of piezometric head and pore water pressures in soil and bedrock are important inputs to models of subsurface flow and slope stability models. Piezometry techniques can be an efficient means of generating the necessary information. Much of the advantage of piezometry would seem to lie in the ease of construction and wide array of recording devices available to monitor water levels. Maximum height devices are inexpensive, yet often lack the precision and accuracy of pressure transducers or other electronic monitors, and provide a limited record in time. On the other hand, electrical and mechanical malfunction is not uncommon for transducers and data-loggers. Nearly all the studies discussed reported some equipment failure during the study. Harr (1977) concludes that an electronic water level monitoring and recording system has the advantage of eliminating frequent site visits and the cumulative damage to sensitive forest soils that may occur.

A distinct advantage of the method is the opportunity to characterize soil hydraulic properties in situ under appropriate hydraulic conditions. Sidle (1985) used the piezometer recovery technique of Bouwer (1978) to estimate saturated conductivity. Reiter (1991) analyzed slug test data in piezometers using the Hvorslev method (1951) to estimate hydraulic conductivity in situ, in a study of subsurface flow from a hillslope through a riparian zone. Slug tests were conducted by inserting PVC pipes into the piezometers to suddenly change the water level. Measurements of water level recovery were used to determine K values. Several piezometers were excluded from the test because the water table was below the bottom of the pipe.

The use of soil samples for laboratory analysis of hydraulic properties often results in estimates of conductivity quite dissimilar to estimates made by piezometer methods on the same site. Higher estimates from field determinations are thought to better reflect the presence of macropores and pipes (Megahan and Clayton 1983, Reid et al. 1988). Other in situ techniques, such as the tension infiltrometer, can be used to determine both saturated and unsaturated hydraulic properties.

Combined use of piezometers and tensiometers would appear to offer good opportunity for characterizing subsurface flow under a wide range of geohydrologic conditions and flow regimes, including highly transient saturated and unsaturated flow.

2.2.2 Tracer Movement Investigations

Tracer movement studies make use of compounds that are expected to move through the porous media by advection in the fluid, with little adsorption or decay. Tracer compounds that have been used in investigations of subsurface flow include salts, fluorescent dyes and radioactive compounds. Analysis of flow characteristics can be made by collection of water samples and/or soil samples, and can involve field based or laboratory analyses, or a combination of both.

The use of piezometers as input points in a tracer study was demonstrated by Megahan and Clayton (1983). Sodium chloride solution (6M NaCl) was injected into piezometers located 1.5, 3, and 6 m directly up-slope of a roadcut face. The roadcut face was selected as the sampling point rather than piezometers downslope of the injection point due to concerns that flow paths may be influenced by root channels and bedrock irregularities such that downslope piezometers would not be in a position to accurately sample flow velocities. In this manner, sampling could take place along the entire roadcut face, and the most hydraulically efficient path determined.

Water samples were collected at the roadcut face and tested for initial occurrence of the tracer by adding a 0.1 M $AgNO_3$ solution and looking for a precipitate of AgCl. Subsequent samples were collected for laboratory analysis of Na^+ and Cl^-, and time to peak tracer concentration was determined. This information was used to estimate flow velocities assuming a straight line flow path. The same assumption was used along with piezometric head data to calculate hydraulic conductivity. Laboratory determination of hydraulic conductivity resulted in average values one order of magnitude lower than field estimates.

In analyzing forest harvest techniques and snowmelt runoff timing, MacDonald (1987) used a sodium bromide tracer (NaBr) in simulated snowmelt. Water samples collected at a downstream weir were analyzed by ion chromatography.

Tracer concentrations were determined in soil, litter, and foliage samples to estimate retention.

Factors influencing choice of tracer include: cost, ease of use and site characteristics, among others. Cation exchange capacities of soils will influence the choice of ion. Adsorption and dispersion of the tracer can adversely affect results. Fluorescent dyes, commonly used in tracer studies, can be strongly adsorbed by both clay and organic matter, and may be decolorized by these substances as well (Atkinson, 1978). Advantages of dyes include the characteristic spectrum of absorption and fluorescence, and the relative ease in making concentration measurements.

Applying results of tracer movement investigations to in situ conductivity estimates and determination of flow velocities is uncertain. The choice of tracer travel time, whether from start of rise or center of mass of the concentration curve, influences velocity calculations. Without knowledge of the actual flow path length, velocity calculations, and conductivity determined by the Darcy equation, will be only rough approximations.

2.2.3 Interception

Investigations that fall under this heading typically involve intercepting part or all of the flow from an exposed soil profile. This method is appropriate for investigating intergranular flow and flow through structural voids (matrix flow), as well as studying macropore and pipe flow.

In an early interception study, Whipkey (1965) constructed a trough system on a 40% slope designed to intercept and collect water seepage from major textural layers in a soil profile. After excavating a trench to a flow-impeding layer, a series of troughs were mortared to the profile face. Plastic sheeting was placed so as to direct flow from the horizon above into the trough. Areas surrounding the gutters were packed with pea-gravel to ensure good hydraulic contact with the face. Water was routed through the gutters to collecting drums equipped with stage recorders to monitor the level of accumulated throughflow (Atkinson, 1978). Wooden skirting lined with plastic sheeting protected the trough system and profile face. Rainfall was simulated with an upright sprinkler system. Water was applied to an area 3.7 m wide in order to reduce water movement toward dry soil beyond the boundaries of the test plot. Multiple-unit tensiometers were installed to make hydraulic head measurements during wetting and draining of the plot. By comparison, Mosely (1982) applied water to a width equivalent to that of the collector trough. As a result, lateral flow in the soil reduced the interception volumes. In addition, where unsaturated conditions were encountered, water flowing down the face was often reabsorbed. Whipkey (1965) never measured seepage volumes over 16% of the water applied, suggesting lateral flow or deep percolation losses that were unaccounted for.

Beasley (1976) prepared a contour map of the subsurface drainage area by determining depth to a dense stratum of kaolinitic clay. In this manner, the location of interception trenches was based on a knowledge of drainage patterns. Similarly, Troendle (1985) used seismic survey to evaluate soil layering pattern for trench location in his study of subsurface flow.

Trenching also provides an opportunity to map subsurface flow routes. Tsukamoto and Ohta (1988) used trenching in order to make a pipe network investigation of their study slopes. Slope gradient averaged 35%. Pipes were mapped and instrumented, and an attempt was made to separate pipeflow from soil matrix flow. The ratio of pipe flow to total runoff from the profile ranged from 0.855 to 0.995. Ziemer and Albright (1987) collected flow from individual pipes, overland flow, and colluvial wedges in metal flashing driven into trench faces. Water was routed into upright PVC stand-pipes. Drainage holes were drilled into the stand-pipes and a laboratory calibration between stage and discharge was determined. Pressure transducers in each container were read at 10-minute intervals by a four-channel digital data logger, and stage data was written to an Erasable Programmable Read Only Memory (EPROM) chip. Pipe flow volumes represented proportions of total flow similar to those reported by Tsukamoto and Ohta (1988).

Interception studies have the advantage of being able to distinguish flow from either natural or imposed pedogenic layers. Also, it is possible to observe flow through pipes and estimate their contribution to discharge apart from matrix flow. These studies can be conducted with either natural or artificial rainfall, and can be equipped with manual or automatic recording systems. The most serious disadvantage of the method concerns the effect of an artificial free face on the hydraulic potential at the exposure surface, and distortion of the flow net behind it. In order for water to leave the soil at the face, the capillary pressure head must exceed atmospheric pressure. Inevitably, saturation of the face results in a saturated wedge of soil behind it. Hence, only saturated throughflow is measured. A second disadvantage of creating an exposure is the distortion of the hydraulic potential flow net (Atkinson 1978, Knapp 1973). When saturation behind the free face exists, unsaturated natural throughflow is directed outward, around the pit, and the contributing area is narrower than the exposure. When the slope above the pit is saturated, lower potential at the pit face results in flow being directed to the exposure, and the contributing area is wider than the face. Many of the problems mentioned can be avoided or corrected by use of additional instrumentation such as tensiometers and piezometry to analyze hydraulic potential and map contributing area.

2.3 Subsurface Flow Modeling

Investigation of hydrologic systems frequently makes use of modeling techniques in order to simplify the system under consideration and provide predictive capabilities. Use of subsurface flow models in hillslope hydrology typically provides a simplified version of reality yet, if properly constructed, can be useful predictive tools for insight to the subsurface flow regime. However, the validity of the predictions depends in part on how well the model approximates field conditions (Wang and Anderson, 1982).

Modeling approaches commonly employed include physical modeling of a natural flow system, (e.g. physical aquifer models, laboratory hillslope models, electric circuit models of groundwater flow), and mathematical modeling of flow. Mathematical models can be generally classified as deterministic or probabilistic models, and analytical or numerical in character.

In many cases field measurements of the groundwater system are combined with theoretical modeling techniques in order to determine characteristics of the flow system, such as the hydraulic head distribution, or flux. Even in cases where direct measurements of hydraulic head are made, extrapolation over great distances is frequently required in order to characterize the subsurface flow regime between known points. Any approximation of the distribution of groundwater characteristics can potentially be improved by use of calibrated and verified mathematical models. Such models can be based on either exact analytical solutions or approximate numerical techniques (Freeze and Witherspoon, 1966). Analytical solutions are limited by an inability to handle anisotropy, heterogeneity, and complex site geometry encountered in most natural hillslopes. Numerical methods, on the other hand, may require simplifying assumptions whose validity may be uncertain. Solutions of nonlinear equations describing groundwater flow are usually approximated numerically, although linearizing techniques are employed that allow analytical solutions to be obtained.

Most modern numerical modeling studies have utilized finite difference, or finite element techniques. The finite element method has several advantages over the finite difference techniques for hillslope hydrology problems (Beven, 1977). These include:

1) complex geometries are more easily approximated;
2) boundary conditions described by differential equations are more easily handled;
3) the method can handle variations in hydraulic conductivity and anisotropy in the flow region; and
4) there is a great deal of flexibility in varying the density of the mesh of elements where rapid or important changes occur.

For these reasons, the finite element method is commonly used when attempting to model natural hillslope hydrologic flow regions, however, as will be discussed, results of finite element modeling are not always superior to simpler models.

It is the purpose of the next portion of the review to summarize the literature wherein mathematical techniques of groundwater modeling have been applied to hillslope investigations, and to evaluate the methodology by which they were developed and applied. The review will begin with an investigation in which five subsurface flow models were used to simulate a hillslope drainage hydrograph, as well as transient water table position. A second section will provide an overview of models that employ probabilistic techniques to model subsurface hillslope hydrology, including stochastic rainfall-runoff models.

2.3.1 Characteristics of Typical Forested Hillslopes to be Modeled

Subsurface flow is likely to be a significant portion of runoff from watersheds where surface soils have high permeability, and subsoils have high hydraulic conductivity. Soil profiles in forested watersheds are frequently characterized by highly permeable organic surface horizons, subsurface roots, decayed root channels, animal burrows and other structural features that provide a highly permeable medium for water movement (Aubertin, 1971). This array of features is often referred to as a macropore network, and flow in the network is termed macropore- or pipe-flow. The response time of pipe flow to precipitation, under certain hydraulic conditions, is considered to be much greater than that of matrix flow. Results of numerous subsurface flow investigations conclude that direct application of the concepts of saturated and unsaturated Darcian flow under conditions of both matrix and pipe flow may not be valid due to non-laminar flow (Sloan et al. 1984, Mosley 1982, Whipkey 1965).

A number of deterministic methods of representing turbulent subsurface flow have been attempted. Barcelo and Nieber (1982) coupled pipe flow hydraulic equations with the Richards equation to model pipe flow and matrix flow separately. The inability to accurately define the heterogeneous pipe network is a limiting factor in this approach (Sloan and Moore, 1984). A second approach is to modify Darcy's equation to accommodate turbulent flow with addition of a second-order term (Whipkey, 1967). Many of these modifications are developed from laboratory data, and apply only to specific porous media conditions. Therefore, general application of such modifications to highly permeable, shallow forest soils may be unrealistic (Whipkey,1967).

2.3.2 Development and Testing: A Comparison of Five Models

One investigation provides an opportunity to evaluate the performance of five mathematical models in simulating subsurface flow. A review of the work presented by Sloan and Moore (1984) is valuable, as it results from the use of the same data set in testing all five models.

2.3.2.1 The Models

Sloan and Moore (1984) describe five subsurface flow models of varying complexity. All are considered deterministic conceptual models. The models are: a two-dimensional finite element model, a one-dimensional finite element model, a kinematic wave flow model, and two storage models. The kinematic and Boussinesq simple storage-discharge models are based on a water balance in which the entire hillslope under consideration acts as the control volume. The mass continuity equation is expressed in mixed finite difference form. The kinematic model assumes the water table has constant slope along the length of the sloping soil mass, and the hydraulic gradient is equal to the slope of the impermeable underlying bed. The Boussinesq storage model also assumes the water table has a constant slope but considers the hydraulic gradient to be equal to this slope value. Equations that relate drainable volume of water stored in the saturated zone to soil depth, volumetric water content, and hill-slope and water table slope can be substituted into the mass continuity equation and solved iteratively for angle of the water table, and values related to discharge at successive times.

The models range in degree of mathematical sophistication from the storage models, to the two-dimensional finite element model. Input requirements vary from model to model, but all are physically based and measurable. The finite element models are based on Richards equation of flow in saturated and unsaturated porous media, that itself is derived from Darcy's equation and the mass continuity equation (see Section 2.1.2.5). Model parameters, which are functions of soil water pressure head h, include volumetric water content, $\theta(h)$, specific water capacity, $C(h)$, (slope of the θ vs. h curve), and unsaturated hydraulic conductivity $K(h)$. These parameters were estimated utilizing empirical functional relationships proposed by Verma and Brutsaert (1971) that are determined from soil water characteristic curves. The two-dimensional form of the Richards equation is reduced to the one-dimensional model by assuming no flow normal to the hillslope gradient. For both finite element models the finite element procedure was applied to the space domain, and a fully implicit backward finite difference scheme was used for the time domain.

The kinematic wave model used in this investigation is described in detail by Beven (1981). The model is a linear kinematic wave equation for approximation of saturated subsurface flow that assumes that flow lines are parallel to an impermeable bed and that the hydraulic gradient equals the slope of the bed. In a later paper Beven (1982) allowed the saturated water content, θ_s, and saturated conductivity, K_s, to vary with depth.

The two storage models, the kinematic wave model and the one-dimensional finite element model each require a coupled model to account for vertical flow from the unsaturated zone to the saturated zone during wetting and drying events. A piston flow approach described by Beven (1982) was used with the kinematic wave model for simulating the movement of wetting and drying fronts. The remaining models assumed an input rate to the saturated zone to be a function of the volume of water stored in the unsaturated zone and the unsaturated conductivity, assuming the entire unsaturated zone could be considered homogeneous.

2.3.2.2 Boundary Conditions

Boundary conditions for the models were defined to approximate conditions on a hillslope with an impermeable bed, that were also consistent with the assumptions inherent in the models. The boundary conditions were either Neumann (specified flux) type, or Dirichlet (known head) type. The upper slope vertical boundary was considered to be a no-flow boundary while the lower face was a seepage boundary for all five models.

2.3.2.3 Hillslope Conditions

Sloan and Moore (1984) tested the five models using published drainage discharge data from a soil trough investigation (Hewlett and Hibbert, 1963). A 0.92 m x 0.92 m x 13.72 m concrete-lined trough was constructed on a 40% slope and filled with recompacted C-horizon forest soil. The trough was instrumented with piezometers, tensiometers, and nuclear moisture-meter access tubes. Water was applied with overhead sprinklers and the trough was allowed to drain. Discharge was measured with a water level recorder in a tank in the base of the trough. Initial hillslope conditions for the models were based on the assumption that steady state discharge existed before drainage of the soil profile began. This was approximated in the models by providing a precipitation input rate of 2.1 mm per hour, until steady state conditions were attained. Drainage of the profile began after steady state conditions were attained.

Because the soil was mixed and compacted in the trough, the role of macro-pore flow could not be evaluated. However, the data provided the opportunity to test the ability of the five models to simulate matrix flow in a steeply sloping soil mass, and to compare the simulation results.

2.3.2.4 Model Testing Results

With the exception of the kinematic wave model, the hillslope drainage hydrograph was fairly accurately simulated by the models. However, none of the models correctly predicted extended high flows that were observed during the drainage period spanning 1000-3000 minutes. During this period predicted water table levels dropped rapidly. Because the original data reported by Hewlett and Hibbert (1963) did not adequately define transient water table positions, the two-dimensional finite element model was used as a standard to evaluate the other models.

Steady state water tables for the two finite element models and the models based on the kinematic wave assumption show good agreement in the upslope and midslope positions. Different boundary conditions at the seepage face result in differences in water table position and slope in the lower slope. The Boussinesq storage model predicts a water table like that of the finite element models in the lower slope position but deviates from the predictions in the mid- and upper-slope positions. At a drainage time of 1000 minutes the one-dimensional finite element and kinematic storage models are in good agreement with the two-dimensional finite element model prediction in the upper slope. The kinematic wave model predicts a much higher water table at this time, due to overestimation of input from the unsaturated zone, rather than violation of the kinematic assumption.

While the models performed reasonably well overall, the finite element models were more accurate for $0 < t < 1000$ minutes, while the storage models were better predictors for $5000 < t < 50{,}000$ minutes. In addition, the finite element models required extensive computer resources and CPU time while the requirements of the other models were relatively small.

2.3.2.5 Conclusions of the Model Comparisons

Results of the simulations reveal the important role of the infiltration models coupled with the flow models. The infiltration models overestimated vertical input from the unsaturated zone early in the drainage simulation. The piston drying front model used with kinematic wave model produced the most unsatisfactory results. Sloan and Moore (1984) conclude that simple subsurface flow models that make assumptions consistent with the physical processes can be as effective as more sophisticated models, e.g. the one- and two-dimensional finite element models, in predicting hillslope discharge and the extent and position of the saturated zone. A principle conclusion of the work is that the kinematic storage model, when coupled with the simple infiltration model assuming gravity drainage in the unsaturated zone, gave the best overall performance for this particular data set. In addition, the more complex models may not be a good standard against which to judge the simpler models because their inherent assumptions may be similarly limiting.

An additional conclusion is that if macropore flow and soil matrix flow both contribute to the hydrologic response of steeply forested watersheds, the finite element models based on Richards' equation would be expected to simulate flow poorly due to violation of assumptions of diffusion-type flow inherent in the model. Because of the limitations imposed by the soil trough experimental design, this conclusion needs to be tested independently.

The ability to accurately predict subsurface flow characteristics using flow models relies, in part, on the quality of the field data and the degree to which the model accurately approximates field conditions. In many ways a mathematical model is no better than the least certain simplifying assumption. Rigorous testing and verification of models is a necessary condition for their use in subsurface flow investigations.

2.4 Statistical Modeling of Subsurface Flow on Steep Hillslopes

The stochastic nature of many hydrologic processes has long been recognized. As a consequence, much work has been done utilizing statistical techniques to develop rainfall-runoff models for prediction of stream flows and, more recently, to analyze groundwater flow and distribution of soil hydraulic properties (Bakr et. al. 1978, Andersson and Shapiro 1983, Gomez-Hernandez and Carrera 1994).

Germann and Beven (1981) used regression analysis to describe water movement in saturated macropores. The predictive models from the regression analysis were compared to the theoretical capillary bundle model of Childs (1969). The regression coefficients compared closely to the theoretical value, for two very different sets of field experiments. Reddi and Wu (1991) analyzed piezometric levels on steep hillslopes using a simplified lumped-parameter model. An uncertainty model based on the first-order, second moment method was used to estimate uncertainty in moisture contents of the unsaturated zone, and piezometric levels in terms of uncertainties in the input parameters. Bayesian updating was formulated and observed piezometric levels used to update parameter values.

2.4.1 Stochastic Rainfall Analysis

Results of many rainfall modeling efforts suggest that antecedent precipitation is often a strong variable in prediction of either stream runoff volume (Istok and Boersma, 1986), or groundwater levels in steep hillslopes (Sidle, 1986). Local and regional models of groundwater levels based on antecedent rainfall conditions have been developed for use in predicting landslide hazard (Crozier and Eyles, 1980). A development of a general antecedent precipitation index is presented. A discussion of the application of such an index to subsurface flow analyses will follow.

2.4.2 Antecedent Precipitation Index, API

Cumulative storm precipitation volume and cumulative storm runoff volume have been shown to be highly correlated (Hewlett et al. 1977, 1984; Bren et al. 1987). Yee (1975) determined that 48 hour cumulative antecedent rainfall was highly correlated with piezometric levels in his study of soil and hydrologic factors affecting slope stability. One shortcoming of cumulative precipitation as a predictor of either runoff volume or groundwater levels is that precipitation occurring early in the storm is given the same weight as precipitation that occurs late in the storm.

Fedora (1987) developed a simple rainfall-runoff model that decayed the residual effect of precipitation observations through time. He described an antecedent precipitation index, API, used in predicting stream discharge that weighted early precipitation less heavily than late precipitation, to account for the diminished effect of the early precipitation on instantaneous runoff. A recession coefficient, C, was obtained from a stream hydrograph for a period when no precipitation fell. The coefficient, C, is simply the ratio of discharge at time t to discharge at time t-1. This coefficient is raised to a variable power related to the length of time before runoff was to be estimated. Assume precipitation, p, to be given on the basis of some time interval t. The weighted precipitation, p_n', for any time interval before an arbitrary time zero is given by

$$p_n^{\prime} = p_n \times C^{n} \tag{2.29}$$

where C is the recession coefficient, and n is the number of time intervals before time zero. The API is then obtained by summing the weighted precipitation values from the beginning of the precipitation event to time zero. The form of the equation for API is

$$API = p_0 + p_{-1}^{\prime} + p_{-2}^{\prime} + p_{-3}^{\prime} + \ldots + p_n^{\prime} \tag{2.30}$$

Substituting Equation 2.30 into Equation 2.31, API is given by

$$API = p_0 + p_{-1} \times C + p_{-2} \times C^2 + p_{-3} \times C^3 + \ldots + p_n \times C^n \qquad (2.31)$$

Factoring out the recession coefficient, C, we have

$$API = p_0 + C \times \left\{ p_{-1} + p_{-2} \times C + p_{-3} \times C^2 + \ldots + p_n \times C^{(n-1)} \right\} \qquad (2.32)$$

The term inside brackets in Equation 2.33 is simply the value of API at time t_{-1}. Therefore, the general equation for API can be written as

$$API_t = p_t + API_{t-1} \times C \qquad (2.33)$$

The API model is used by first determining the appropriate value of C. Then, for n time periods, the value of p' is determined. API is then determined by using equation 2.33 starting at time zero. API can then be correlated to stormflow, whether stream discharge or piezometric levels.

2.4.3 Use of API in Runoff, Subsurface Flow and Slope Stability Modeling

Fedora (1987) used the API he developed in regression analysis of stream flow for a number of watersheds in the Oregon coast range. The analysis suggested that the best linear regression models result from transforming stream discharge by the square root function, and using API and watershed area as independent variables.

One persistent problem with the models was hysteresis. The models over-predicted discharge on the rising limb of the hydrograph, and under-predicted discharge on the falling limb. Predicted peak discharges were typically in close agreement with observed peaks.

Borehole inclinometers were used in a study to measure progressive hillslope deformation by Ziemer (1984). The author regressed measurements of borehole inclination on a variable describing antecedent precipitation. The independent variable in the regression analysis was obtained by summing the daily API values over the time period between borehole surveys, if the API value exceeded some threshold value. This threshold was established on the basis of a fraction of the maximum daily API value observed during the study for a given recession coefficient (Fedora's C). The coefficient of determination between displacement of the borehole and the API variable was maximized by calculating a series of regressions with different values of the recession coefficient and threshold value.

The study sites were within two different geologic formations. One set of inclinometer tubes was located in soils derived from unmetamorphosed sedimentary sandstones and mudstone, while others were placed in soils derived from metamorphic schists. Of the original 17 tubes, 9 yielded data of sufficient duration and quality to use in the regression analysis. For the schist sites the best models all resulted from a recession coefficient of 0.99 and an API threshold of zero. The best models for the sandstone sites resulted from different combinations of recession coefficients and threshold values. In order to select a global model to describe borehole movement as a function of the API variable for the sandstone sites, regression variances were investigated. The combination of recession coefficient and API threshold that resulted in a minimum sum of variances for the site models was selected as the best global model. Based on the sum of regression variances for the sandstone sites, the best model was derived from a recession coefficient of 0.99 and an API threshold of zero, the same as for the schist sites.

In a later study Ziemer and Albright (1987) used API to investigate a relationship between discharge in soil pipes and antecedent precipitation. The calculation of API differed in this study in that the recession coefficient was raised to a power that was the time interval over which individual precipitation measurements were made. This value ranged from 0.04 days to 0.5 days. Again, coefficient of determination of the regression was maximized by fitting a series of models with various values of time interval. The smaller the value of the time interval, the more sensitive was the index to short-term rainfall intensities. In addition, each regression series was repeated using one of several lag times. The lag time was defined as the time difference between the hydrograph component (start, peak, trough, end) and the associated API value. Time lags varied from zero to 0.5 days, and were used to determine if there was a delay in the time of precipitation input and hydrograph response. For the 7 storms analyzed, use of a non-zero time lag did not result in model improvement. Pipes were classified as either large or small discharge pipes. For both classes, the API variable produced significant regressions for both the storm peak discharge and within storm trough hydrograph components. For the peak component of the hydrograph, the time interval producing the best model was 0.25 days for the large pipes, and 0.5 days for the small pipes. This result suggests that once a storm is underway and the hydrograph is rising, flow from large pipes is more responsive to short-term rainfall intensities than is that from small pipes.

Crozier and Eyles (1980) developed an antecedent excess rainfall index, similar to the API of Fedora, to be used in conjunction with soil water balance calculations to identify threshold conditions for landsliding. These thresholds were used to assess the probability of landslide occurrence. The API was calculated as the sum of the daily excess rainfalls (runoff) multiplied by an decay factor (Fedora's C) raised to the n'th power where n is the number of days before day zero. The API was determined on a 10 day antecedence basis. A running soil water balance is used with the API to assess soil water status. Linear threshold envelopes are delineated on plots of landslides and associated daily rainfalls versus the soil water indices, that separate sliding from non-sliding conditions.

Sidle (1986) developed an empirical model from 40 storms in coastal Alaska that predicts soil mantle saturation as a fraction of soil depth, using antecedent precipitation characteristics. Regression analysis was done to determine the best model using maximum one-hour rainfall intensity, antecedent 2-day rainfall, and total storm precipitation. The resulting model explained 84% of the variability in piezometric response.

2.5 Advantages and Disadvantages of Mathematical Modeling

Mathematical modeling can be a means of synthesizing the results of field subsurface flow investigations to gain predictive capabilities. Freeze, (1978) however, lists several limitations of physically based mathematical models of subsurface flow, that warrant consideration. These include limitations due to: the assumptions of the theoretical developments; lack of correspondence between models and reality; scarcity of data; and limitations of the calibration procedures.

Site characteristics will strongly affect the use of a particular model. For example, Burroughs (1984) suggested that strongly converging flow lines and a hyperbolic flow section commonly observed in small depressions, can present very difficult conditions for use of kinematic wave methods in modeling efforts. As previously mentioned, combined macropore and soil matrix flow can limit the ability of finite element models based on Richards equation to simulate flow, due to violation of assumptions of diffusion-type flow inherent in the model.

Statistical methods have the advantage of describing the uncertainty in parameters, and models may have wider application than deterministic models. Disadvantages of statistical methods include large data requirements, frequently complex mathematical construction, and potential for misinterpretation and misuse of results.

When the physical problem at hand can be adequately represented by a mathematical one, the opportunity for improved understanding of subsurface flow processes exists. Enhanced computer capacity has made relatively rapid solution of flow equations possible. What remains, once a solution is obtained, is proper interpretation of the results in terms of the physical problem (Freeze 1978).

2.6 Summary of Field Methods and Modeling Techniques

Investigations of hillslope subsurface hydrology can be undertaken by the methods discussed herein. Table 2.1 summarizes some advantages and disadvantages of piezometry, tensiometry, tracer movement studies, interception and mathematical modeling. These categories of methodology frequently overlap, yet each can provide unique information for solution of specific problems. Certainly, the nature of the flow problem, as well as site characteristics, must guide the selection of appropriate monitoring techniques.

Table 2.1 Summary of some advantages and disadvantages of various methods of monitoring and modeling subsurface flow.

Method	Advantages	Disadvantages
Piezometry	-characterize soil hydraulic properties in situ -relatively low cost of start-up, maintenance -equip with manual or automatic recorders	-unable to monitor unsaturated conditions -prone to equipment malfunction or non-reading
Tensiometry	-characterize unsaturated zone conditions -relative simple instruments -ease of installation	-high maintenance required -sensitive to diurnal temperature fluctuations -potential for poor hydraulic contact in coarse media
Tracer Movement	-ease of use -typically low cost -accurate concentration measurements possible	-some compounds susceptible to adsorption, retention, decolorization -lab analysis costs variable -sample contamination concerns
Interception	-measure flow by pedogenic horizon -flow visualization -separate matrix and macropore flow -equip with manual of automatic recorders	-catches only saturated throughflow -distorts hydraulic potential flow net -variable contributing area depending on moisture conditions behind face
Mathematical Modeling	-mathematical expression of physical problems -predictive capabilities -rapid solutions of complex problems -ability to quantify uncertainty	-simplifying assumptions often required -lack of correspondence with reality -intensive input requirements -solutions typically not exact

3. STUDY AREAS

Two headwalls in the central Oregon coast range were selected for instrumentation and monitoring of groundwater response to precipitation. Both sites are small zero-order basins, have moderately heavy forest cover, and are steeply sloping. The climate regimes are similar for both sites, with high winter precipitation and warm, dry summers. The geology of the two sites is markedly different. A description of the study site in the Alsea River basin will be emphasized, as it was the primary source of data analyzed in this study.

3.1 Location

The two sites are located approximately 30 km from one another on opposite sides of the central Oregon coast range (Figure 3.1). Site 1 is located on the east side of the coast range, in the McDonald Research Forest, managed by the College of Forestry at Oregon State University. The site is located at the SE¼,SE¼,S8, T11S,R5W Willamette Meridian, in Benton County Oregon. Site 2 is on the west side of the coast range, at the headwaters of a tributary of Honey Grove Creek in the Alsea River basin. It is under jurisdiction of the Bureau of Land Management (BLM) and is located at NE¼, NW¼,S33,T13S,R7W Willamette Meridian, in Benton County Oregon.

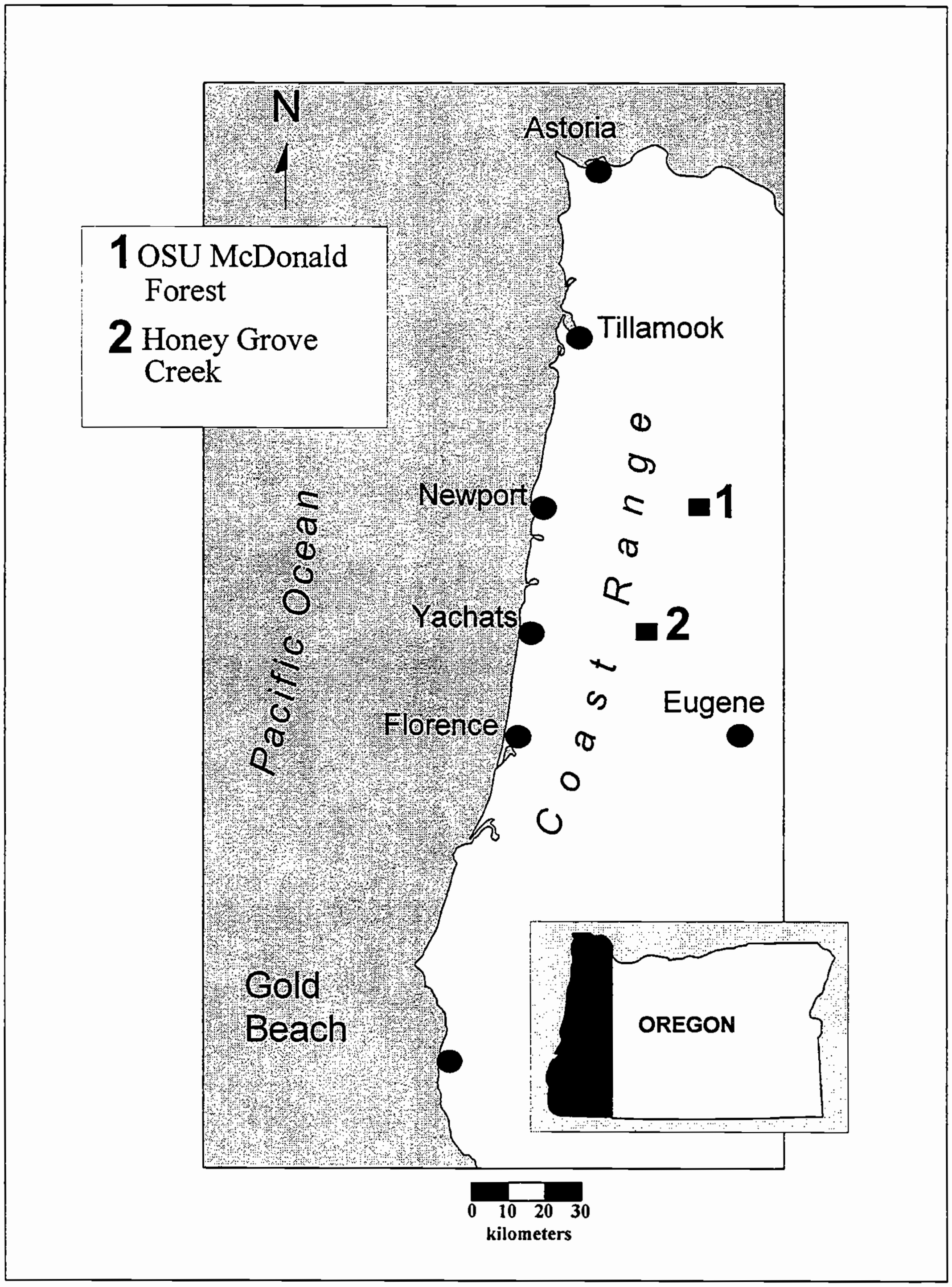

Figure 3.1 General study area location in the central Oregon Coast Range.

3.2 Geology

The central coastal mountains of Oregon are geologically young, and characterized by high relief (150 - 600 m). The mountains are composed primarily of Cenozoic marine sedimentary and volcanic rocks. Steep slopes (40% - 100%) and narrow valleys are common throughout the range. The Oregon coast is an active margin where the Juan de Fuca plate is being subducted under the North American plate. This convergence, thought to have begun 30 million years ago, has caused uplift of the coastal mountains (Baldwin, 1981). Since uplift of the coast range began, the drainage network has been actively downcutting, draining the region to the Pacific Ocean to the west, and to the Willamette River Valley to the east. Large rivers have cut through uplifting rock, giving way to new valley and ridge terrain features.

3.3 Climatic Regime

The region's climate is dominated by marine air masses from the Pacific Ocean. A Mediterranean type climatic regime prevails, with a dry season extending from approximately May through September, and a wet season from October through April. Average annual precipitation ranges from 150 to 300 cm, mostly in the form of rain (NOAA Climatological Data - Oregon). Snowfalls commonly occur, but persist only at higher elevations. Prolonged periods of freezing temperatures are rare.

3.4 Vegetation

The region supports extensive forests consisting primarily of Douglas-fir (Pseudotsuga menziesii), western hemlock (Tsuga heterophylla), and western redcedar (Thuja plicata) as the primary overstory softwoods. Bigleaf maple (Acer macrophyllum), vine maple (Acer circinatum), and red alder (Alnus rubra) are common hardwood species. Numerous brush, fern and forb species occupy the understory.

3.5 Site Characteristics

A description of typical soils found in the region of each site follows. The information presented was taken from the appropriate soil survey report prepared by the United States Department of Agriculture, Soil Conservation Service. Results of testing and classification of soils found on the sites by this investigation are reported in Chapter 5, Results. Topographic features and vegetative characteristics reported in the following sections are based on work done by this investigator.

3.5.1 Site 1 Characteristics

The first study site selected is a steeply sloping (60%) headwall, has a North-North-East aspect (45°), and is approximately 365 m above mean sea level. Soils were mapped as the Price-Ritner Complex 30-60% slopes (USDA, Soil Conservation

Service Benton Co., OR Soil Survey, 1970). The Price series is classified as a fine, mixed, mesic Dystric Xerochrept in the USDA system. In the Unified Soil Classification System (USCS) the Price series has a ML surface soil and a MH subsoil. The Ritner series is classified as a clayey-skeletal, mixed, mesic Dystric Xerochrept in the USDA system. The USCS designation is GM surface soil and a GM subsoil. The complex consists of deep, well-drained soils formed in colluvium and residuum weathered from basic igneous rocks. The underlaying formation is the Siletz River Volcanics, consisting of early Eocene basalt flows, tuffs, and brecias (Baldwin, 1981). Surface soils are gravelly silty clay loam with subsoils gravelly silty clay loam, gravelly silty clay, and very cobbly silty clay. The type profile is underlain by fractured basalt at 1.25 m. On the study site, however, bedrock was determined to be at approximately 3.7 m depth. Furthermore, the headwall was divided into two distinct soil types. On one side of the headwall centerline, the soils were typical Price-Ritner. On the other side of the centerline, the soil consisted of colluvial gravels with very few fines.

Overstory vegetation on the site is Douglas-fir (Pseudotsuga menziesii) in the 150 year age class. Hardwood species include bigleaf maple (Acer macrophyllum), and red alder (Alnus rubra). Shrubs include salal (Gaultheria shallon), and sword fern (Polystichum munitum).

Instrumentation of this site was undertaken on the basis of preliminary field reconnaissance and the estimate of soil depth given in the soil survey. The extremely deep soils, and the mixed nature of the soil as described above, made placement of wells and tensiometers very difficult. This fact, combined with equipment malfunctions resulted in very little useful data gathered at this site.

3.5.2 Site 2 Characteristics

The second study site selected is a steeply sloping (60%) headwall having a South aspect (160°), and is approximately 305 m above mean sea level. Figure 3.2 shows the topographic characteristics of the site. The underlaying bedrock is the Flournoy Formation (Baldwin, 1981). This formation is composed of massive, rhythmically bedded micaceous and arkosic sandstone and sandy siltstone. Soils overlaying bedrock are colluvial deposits or residual soils weathered from near-surface sedimentary rock. Many soils on the steepest slopes are formed from colluvium, and frequently are thin and stony, exhibiting a relatively homogeneous profile due to transportation and thorough mixing (Pierson, 1977).

Soils are mapped as the Digger-Apt complex 37 - 60% slopes (USDA, Soil Conservation Service Alsea Area, OR Soil Survey, 1973). However, no evidence of the Apt clay soil was observed on the study site. The characteristics of the site soil fit closely with those of the Digger gravely loam, dissected, 50 - 75% slopes. This soil series is classified as a loamy-skeletal, mixed, mesic Dystric Eutrochrept in the USDA classification, and SM or GM in the USCS. The soil consists of well drained, moderately deep soils formed in alluvium and colluvium weathered from sandstone. They are gravelly loam mixtures, underlain by sandstone at approximately 1 m

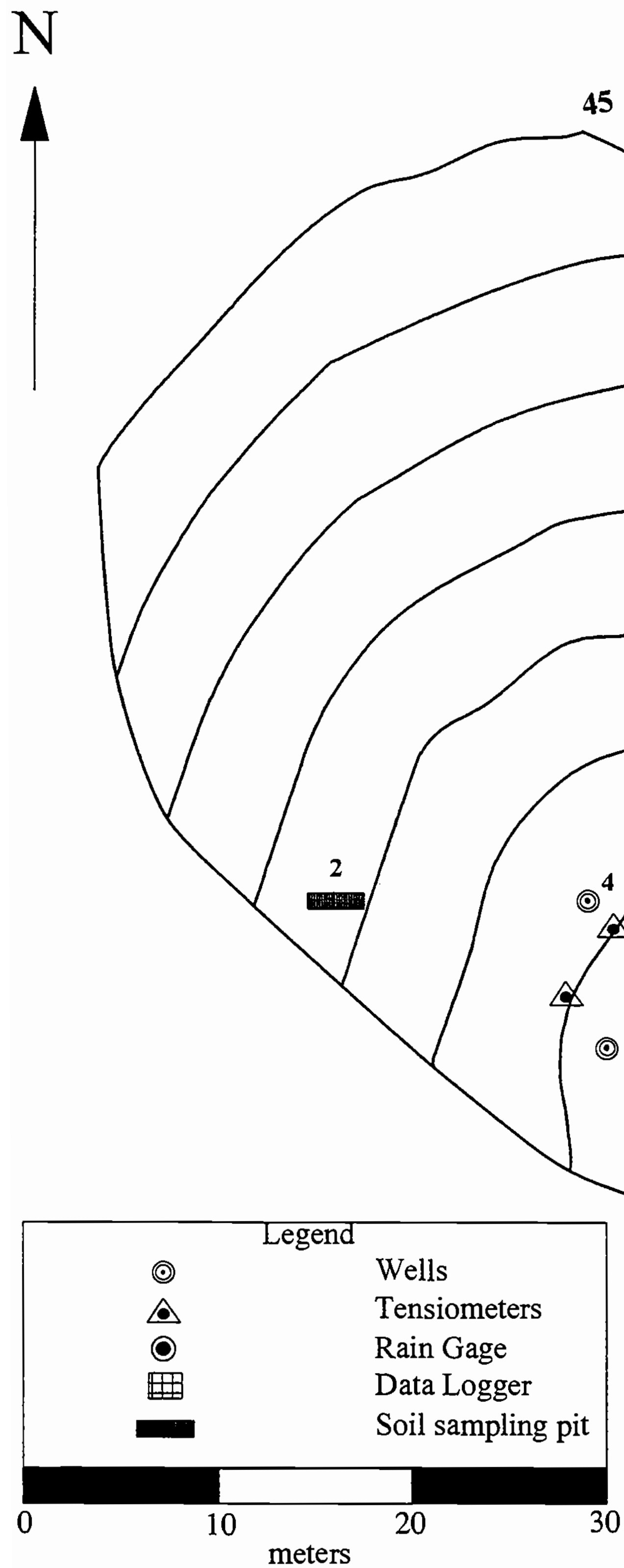

Figure 3.2 Topographic map of study site 2, the Honey Grove Creek headwall.

depth. Soils on the instrumented portion of the site are derived from colluvium and ranged from 1 m to nearly 2 m in depth. Figure 3.3 shows a schematic diagram of a longitudinal cross-section of the headwall showing elevations of the tips of three well points used in analysis of piezometric response to precipitation, and the soil depth above bedrock for the three wells.

Overstory vegetation on the site is Douglas-fir (Pseudotsuga menziesii) in the 30 year age class, bigleaf maple (Acer macrophyllum), vine maple (Acer circinatum), and red alder (Alnus rubra). The shrub layer is composed primarily of dense salal (Gaultheria shallon), and sword fern (Polystichum munitum).

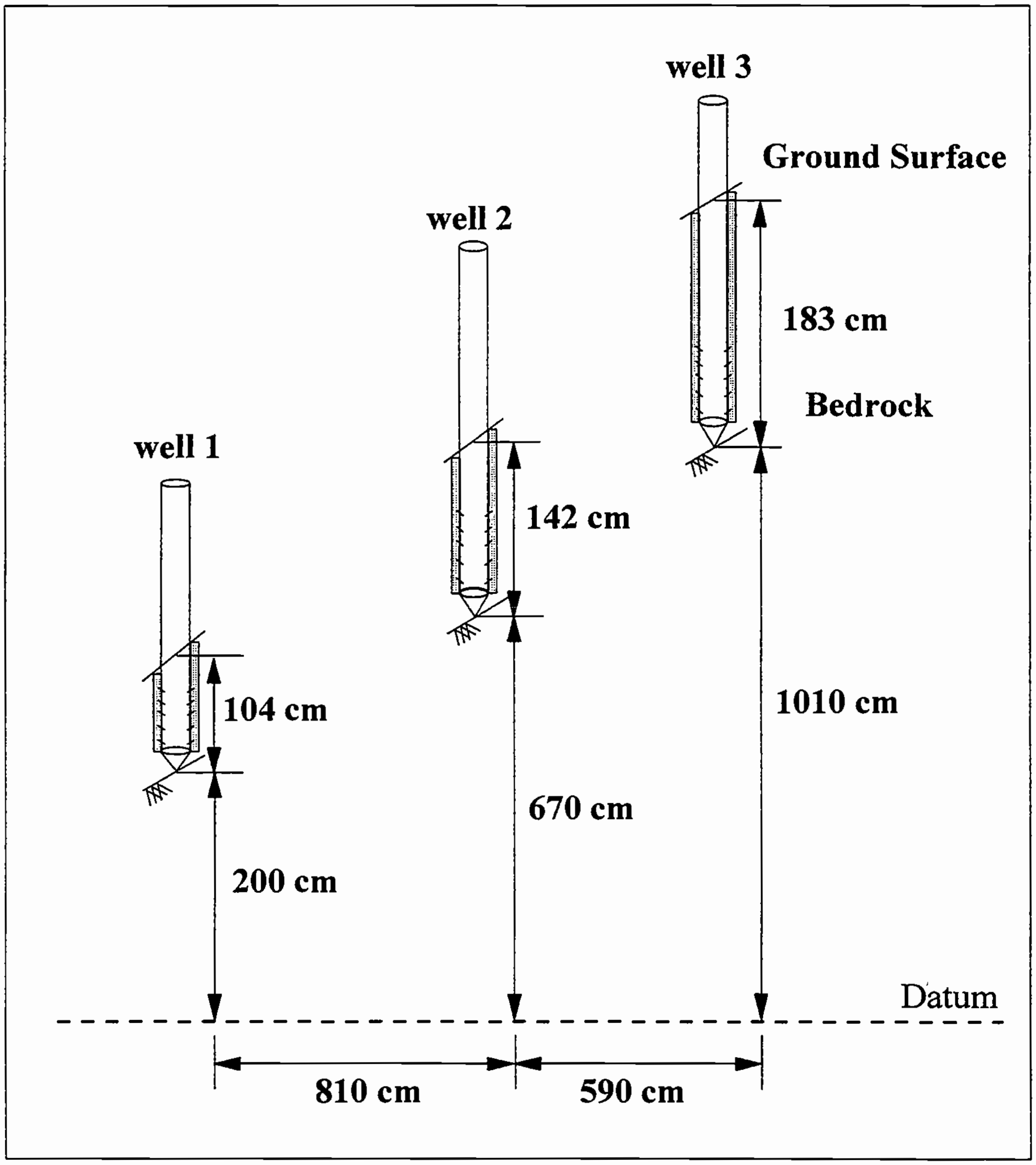

Figure 3.3 Schematic diagram of a longitudinal cross-section of site 2 showing elevations of well points 1-3 relative to bedrock at the toe of the headwall, and soil depth above bedrock. Not to scale.

4. MATERIALS AND METHODS

The two forested headwalls were selected for study of hillslope groundwater response to natural precipitation input. The study was designed to monitor saturated and unsaturated conditions in the soil before, during, and after winter storms.

Increases in pore-water pressure in hillslope materials as a result of rainfall is recognized as a leading cause of rapid, shallow landslides and debris avalanches (Pierson 1977). An understanding of slope stability processes requires an under-standing of the pore-water pressure distribution in the hillslope. This requires some knowledge of the groundwater flow system, which in turn is dependent on the soil and geological characteristics of the site under consideration.

Because groundwater plays such an important role in the stability of steep slopes, it was the intent of this study to investigate the mechanisms by which water is routed to channels, through and over hillslopes. A component of the study was designed to quantify saturated throughflow at the lower end of the instrumented slopes, and to determine the relative importance of macropore flow in routing of subsurface water. In addition, we wished to test the feasibility of developing a simple predictive groundwater model with minimal data requirements. Such a model would allow estimates to be made of the entire subsurface hydrographic response, and/or peak pore-water pressures, for given antecedent moisture conditions and precipitation input.

4.1 Site Selection Criteria

The primary consideration in selecting study sites for monitoring was use of representative forested sites having moderate to high slope failure potential. In addition, sites having minimal upslope disturbance such as roads and other land management activities were desired. Practical considerations included shallow to moderately deep soils to minimize difficulties associated with installation of instruments, and accessibility during inclement weather.

A number of sites on Forest Service land in the Oregon coast range were considered. However, constraints on development of a research site in or near Habitat Conservation Areas established to protect the Northern Spotted Owl were prohibitive. Sites on Oregon State University's McDonald Research Forest were investigated and Site 1 was determined to meet most of the selection criteria. Personnel of the Bureau of Land Management were instrumental in identifying an area having a number of locations that satisfied the selection criteria on land managed by that agency. Following field reconnaissance of the area, the Honey Grove Creek site in the Alsea River Basin was selected as Site 2. Figure 3.1 shows the location of this study site.

4.2 Field Instrumentation

Following site selection, field instrumentation was undertaken during the Spring of 1991. The instrumentation scheme consisted of a installing a series of well points, a grid of porous cup tensiometers, and tipping bucket rain gages. In addition, an attempt was made to dig a trench at the downslope end of the headwall, exposing the soil profile to down to bedrock, in order to intercept and measure flow in macro-pores. Soil water pressure head and capillary tension head were measured with electronic pressure transducers, and data logged on automatic data-logging equipment.

A number of site constraints and technical difficulties at Site 1 during the first winter monitoring season led to the decision to abandon further work there. As a result, the instrumentation scheme was repeated at Site 2 during the summer of 1992. More detailed analyses of soil properties and site conditions, including topographic mapping, was undertaken at Site 2.

4.2.1 Piezometry

Standard piezometry makes use of open standpipes, that typically are constructed from PVC or steel pipe. The piezometers have a number of holes or slots cut through the pipe at the lower end to allow water to enter and exit. The slotted end is typically screened to prevent inflow of fine soil material, and plugging of the holes. The piezometers are placed in the ground via a borehole and the screened portion backfilled with a silica sand. Bentonite clay is then used to seal the lower end of the pipe from surface inflows, and the native material replaced to the surface. Water flows in and out of the pipe, with measurement of the pressure head being made by any number of methods, including pressure transducers, electrical resistance, and floats. Various techniques allow continuous head measurement while others are maximum head recording only.

One shortcoming of these instruments is that in order to measure a change in head, the piezometer must experience a change in volume of water inside the pipe an amount given by

$$\Delta V = \frac{\pi D^2}{4} \Delta h \tag{4.1}$$

where ΔV = change in volume in the piezometer (L^3)
D = inside diameter of piezometer (L)
Δh = change in height of water inside the piezometer (L).

In formations with low saturated conductivity, the lag time between a change in head in the formation, and the change in volume in the piezometer can be significant (Hvorslev 1949, 1951). Furthermore, significant head loss across the screened portion of the piezometer can affect the timing and magnitude of the head measurement. For these reasons a well point design that minimizes time lag and head loss would be beneficial from the perspective of accurately and precisely determining the timing and magnitude of changes in head.

For this study, a well point was designed that eliminated the need to have a volume change in order to read a change in head. The wellpoint (Figure 4.1) has six ports that lead into a threaded central chamber. The six ports were packed with fiberglass batting to prevent inflow of fines. The threaded chamber holds the pressure transducer diaphragm at the same level as the ports. A small volume of water is required to exert hydrostatic pressure on the transducer diaphragm, however, no water need enter the body of the piezometer. This decreases the lag time between pressure head change in the formation and sensing of that change by the instrument.

Well points were constructed of a steel point welded to 5 cm O.D. by 2 m length of Schedule 40 steel pipe. The 2 m length of pipe was threaded at the opposite end to accept 1.5 m extension sections that were added as required by soil depth. Wellpoints were installed by driving the sections into the ground using a 40 kilogram drive hammer. The wellpoints were driven until resistance was too great to gain additional depth. On Site 1, average depth of placement of five wells was 2.5 m, significantly short of bedrock in all cases. On Site 2, 8 wells were installed to bedrock at depths from 1 to 2 m. At this site resistance to driving was minimal until bedrock was encountered, at which time advancement of the wellpoint was negligible. Transducers were mounted in the end of a 2.5 cm O.D. PVC pipe sleeve with only the threaded nipple exposed at the lower end through an end cap. This allowed isolation of the atmospheric reference port and the electrical cables from any water that may enter the well casing through the central chamber threads. Furthermore, this design had the distinct advantage that the transducer assembly could be easily removed from the well casing. Such a need could arise from electrical or mechanical malfunction of the transducer, or in order to use the transducer in a different

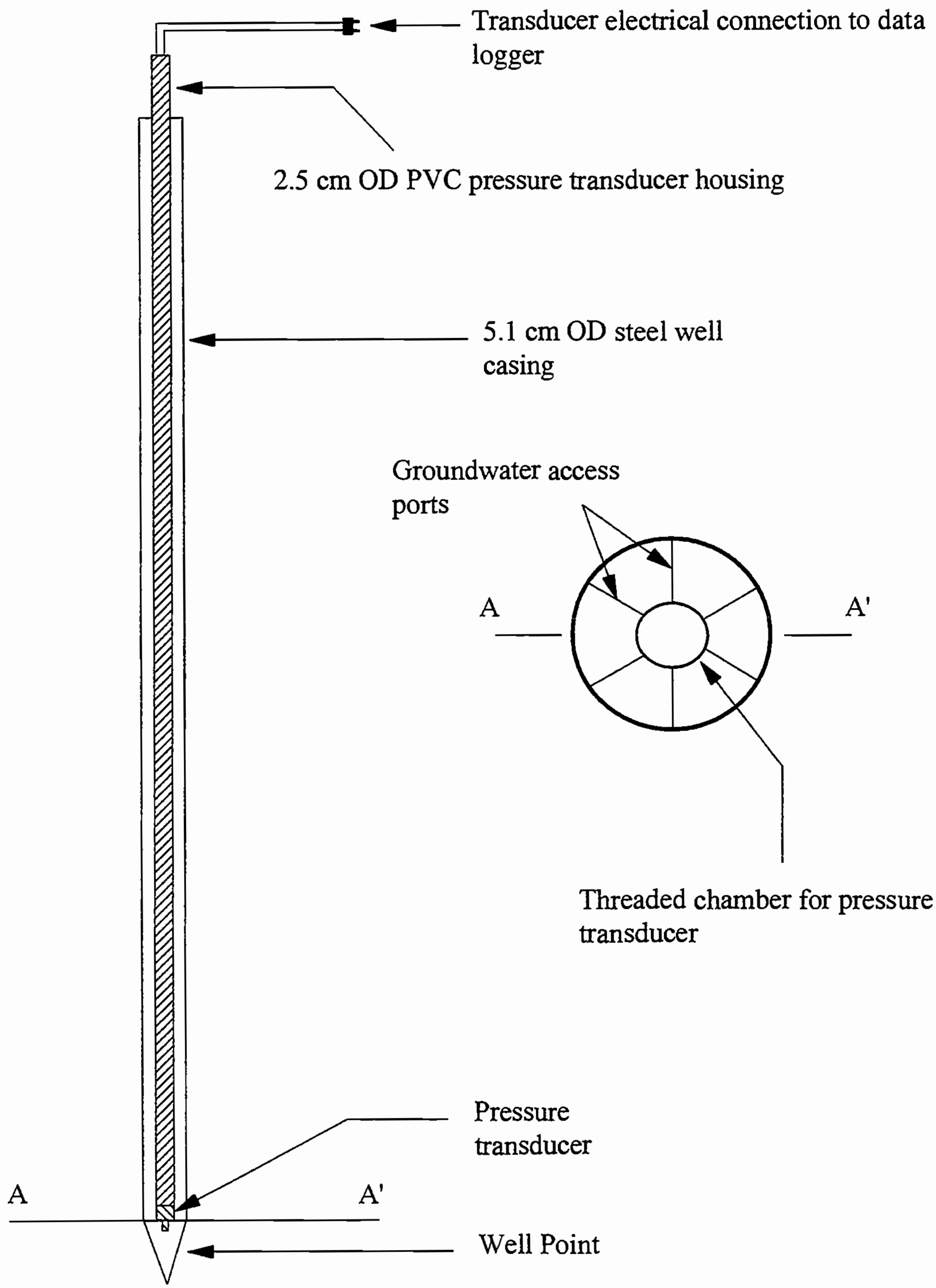

Figure 4.1 Schematic diagram of well point and pressure transducer assembly. Not to scale.

location. Length of the PVC pipe sleeve was determined by the length of the steel well casing.

Early in the monitoring period, a transducer failed due to water leakage through the joint between the PVC pipe and the end cap. In this case the voltage readings from the transducer were obviously erroneous. The transducer was replaced and the joint was sealed by injecting glue into the joint with a fine tipped syringe. No further problems with this configuration were encountered.

4.2.2 Tensiometry

In order to quantify hydraulic conditions in the unsaturated zone, porous cup tensiometers were installed. The tensiometers selected were Soil Moisture Corp. porous cup tensiometer with reservoir filling caps. These tensiometers consist of a clear hollow plastic body, 2.2 cm O.D., 1.9 cm I.D., terminating in a threaded fitting to which a porous cup is attached. Near the top of the tensiometer body a threaded fitting holds the pressure measuring device. Nine porous cup tensiometers were installed on Site 2.

A circular thin-walled steel insertion tube was used to remove a soil core slightly smaller in diameter than the tensiometer body, to the desired depth. Tensiometers were then placed in the bore hole and pushed lightly into the bottom of the hole to establish good hydraulic contact with the soil. The hole was then backfilled and the surface soil compacted around the tensiometer to prevent inflow.

The nine tensiometers on Site 2 were installed at various depths. Figure 3.2 shows the location of the instruments. Each instrument in a row up and down slope was installed at a uniform depth. Depth increased across slope from right to left looking upslope, from 30.5 cm below the soil surface on the right, to 45 cm down the centerline, to 61 cm on the left line. Tensiometers were outfitted with a reservoir top to facilitate filling of the tube. Tensiometers were equipped with electronic pressure transducers mounted to the tensiometer body, and connected to the data logger.

No tensiometer installation was possible on Site 1 due to the nature of the soil material. Porous cups repeatedly were broken during installation attempts, and successful installations failed to equilibrate with soil water tension due to the coarse nature of the material.

4.3 Soil Excavation and Sampling

The soil profile at each site was exposed at a location below the instrumented portion of the slope. This excavation was intended to provide soil samples for soil index property and strength testing, as well as provide a means of intercepting and observing saturated flow through the slope. On the basis of preliminary investigation of soil depth, and review of the Benton County Soil Survey, excavation was undertaken on Site 1 to expose the soil profile to bedrock. At a depth of approximately 1 m, the ability to excavate with hand tools became severely limited due to the high dry strength of the soil. A depth probe was used to determine the depth to bedrock, but no highly resistant layer that could be interpreted to be bedrock was encountered. The decision was made to use a portable soil and rock drill to conduct a subsurface investigation. Bedrock was encountered at approximately 4 m in two bore holes. At Site 2, the soil profile was exposed down to bedrock, at 1 m depth, using hand tools.

4.3.1 Soil Testing

Soil samples from Site 2 were collected for laboratory analyses. Disturbed samples were taken for determination of index properties and for strength tests of remolded samples. Relatively undisturbed samples were also collected in thin walled steel Shelby tubes for strength tests, and small cores for hydraulic property testing. Samples for index properties and strength tests were collected from soil sampling pits 1 and 2 shown in Figure 3.2. Samples for hydraulic properties were collected from sampling pits 3 and 4 shown in the same figure.

4.3.1.1 Index Properties

Index properties of the soils were determined using standard laboratory procedures. Tests included soil classification (Unified Soil Classification System, USCS), dry unit weight, specific gravity of soil solids (ASTM D 854), and Atterberg Limits (ASTM D 4318).

Mechanical grain size analysis was conducted to determine a typical soil particle size distribution curve for the soil (ASTM D421-58,D422-63). Sieve sizes used in the analysis were U.S. Standard sieve numbers 4 (4.75 mm), 10 (2.00 mm), 20 (850 μm), 40 (425 μm), 60 (250 μm), 100 (150 μm), and 200 (75 μm mesh). No particle settling (hydrometer) analysis on material finer than the number 200 sieve was conducted. The rationale for this decision was that properties of the fines other than size distribution controls engineering behavior of the soil. Information about the behavior of the fines is obtained by the Atterberg tests previously described, among others.

4.3.1.2 Effective Strength Parameters

Strength testing was done on the undisturbed core samples and reconstructed samples using the disturbed material. Specimens were recompacted to field density and water content for triaxial testing. Multi-stage consolidated-undrained (CU) triaxial tests with pore-pressure measurements, and consolidated-drained (CD) triaxial tests were conducted to determine effective strength parameters angle of internal friction, ϕ', and cohesion, c'. Not all samples were subjected to the same range of confining pressures during the consolidation and shear phases of the tests. Two tests were conducted at confining pressures between 34.5 and 276 kPa. Three tests were conducted at confining pressures between 3.4 and 34.5 kPa. Two additional tests were conducted at confining pressures that were subsets of the two full ranges given. Standard geotechnical testing procedure has employed high confining pressures during triaxial testing of soil materials. However, shallow soils on steep slopes in the forest environment typically experience low in situ vertical confining stresses. In a study of strength parameters of headwall soils in forest environments, Bransom (1991) determined the average overburden stress at bedrock was 12.8 kPa at field moisture levels, excluding the weight of vegetation. This value increased to 15.5 kPa assuming fully saturated conditions. Morgan (1995) concluded that strength tests should be conducted within the range of field stresses to account for a nonlinear strength envelope.

A minimum of two confining pressures, and a maximum of five, were used in the multi-stage tests. During each shear phase, the stress path was monitored in real time. This allowed determination of the point of failure, which was considered to have occurred when stress paths reached a point of tangency with a unique line known as the K_f line. Effective strength parameters ϕ' and c' were then determined using equations relating the parameters to the slope and intercept of the K_f line (Morgan 1995, Holtz and Kovacs 1981).

4.3.2 Soil Hydraulic Property Testing

Field and laboratory work was undertaken with soils from Site 2 to characterize the soil hydraulic properties. The work was delayed until after monitoring to minimize disturbance to the site. Soil samples were collected for laboratory determination of soil moisture characteristic curves and hydraulic conductivity.

4.3.2.1 Soil Moisture Characteristic Curves

A slide hammer and cutting ring tool was used to collect relatively undisturbed soil cores from three depths in a profile on the instrumented portion of the hillslope. Soil cores were used for laboratory testing of the functional relationship between matric potential, ψ, and volumetric moisture content, θ. This relationship, called a soil moisture characteristic curve, is specific to a particular porous media, though general forms of these curves are applicable to classes of media. Only the main draining curves were constructed. In order to determine the degree of hysteresis present in the media the main wetting curve must also be determined. Many analyses of subsurface flow rely on use of the main draining curve, with the effects of hysteresis unaccounted for.

Tests were conducted using the hanging water column procedure of Jury et al. (1991). For the desorption tests, samples were saturated by placing them in a shallow pan of water and allowing them to fully saturate. Samples were then mounted in a Soil Moisture Corp. tempe pressure cell, with filter paper at each end, and a saturated porous disk at the base of the sample. The pressure cell was then placed in a ring stand. A reservoir of water was attached to the lower half of the pressure cell using tygon tubing. The level of the pressure cell was set above the reservoir at 5, 10, 20, 30, 50, and 75 cm. Tensions of 100 and 200 cm of water were applied using a vacuum pump. The soil samples were allowed to reach equilibrium at each tension head, were weighed and placed back in the ring stand, and the sample raised to the next tension level. Equilibrium times for the low tension tests ranged from two to four hours, with higher tensions allowed to equilibrate up to twenty-four hours.

After completing the desorption phase, the soil was oven dried at 105° C. Water contents at each head level were then determined from the respective wet sample weight and the oven dried weight, and expressed as volumetric water content, volume of water as a fraction of total sample volume.

4.3.2.2 Hydraulic Conductivity

Desaturation data from the laboratory tests was used to estimate the hydraulic conductivity function using the method of Brooks and Corey (1966). The necessary parameters are λ, the absolute value of slope of the logarithmic plot of effective saturation vs. matric potential, and η, given by the relationship

$$\eta = 2 + 3\lambda \tag{4.2}$$

and ψ_a, the air-entry value for the media. Residual water content, θ_r, was estimated from the soil moisture characteristic curve. The air entry value, ψ_a, was determined from the linear portion of a log-log plot of effective saturation, S_e, vs. ψ (Figure

2.2). ψ_a is the value of ψ that corresponds to an S_e of 1. The hydraulic conductivity function was then calculated using the Brooks and Corey method given by equation 4.3.

$$\frac{K(\psi)}{K_s} = \begin{cases} \left(\dfrac{\psi_a}{\psi}\right)^{\eta} & (|\psi| > |\psi_a|) \\ 1 & (|\psi| \leq |\psi_a|) \end{cases} \tag{4.3}$$

The magnitude of saturated conductivity, K_s, was estimated by inversing, using observed hydraulic head data to estimate parameter values.

4.4 Macropore Flow Measurement

During excavation of the trench at the lower end of each headwall, numerous large diameter pores (1-10 cm) were observed throughout the soil profile. Many of the large pores appeared to be old root channels, while others may have resulted from animal activity, or piping related to subsurface flow. Widely referred to as macropores, large pores are believed to be common in forest soils and are thought by many researchers to be important in routing large quantities of water very quickly through hillslopes under certain hydraulic conditions (Aubertin 1971, Beven et al. 1982). In order to quantify the hydraulic role of macropore flow on the study sites in this investigation, the interception method was employed.

As previously mentioned, the interception technique has the undesirable effect of altering the moisture and energy conditions in the hillslope behind the exposed soil by introduction of a flow barrier. In order for water to flow through the soil at this location the soil water pressure must be at least equal to atmospheric pressure. This can result in the buildup of water behind the face until a sufficient increase in head occurs for water to flow through the face. In addition, the upslope area contributing flow to the face can either increase or decrease depending on the moisture conditions behind the face. If the soil behind the face is near saturation, the contributing area to the face can decrease as the potential gradient can be away from the face. If the soil water is at high tension behind the face, the contributing area can increase as the gradient in potential is directed toward the face (Atkinson, 1978). No other field method, however, affords the opportunity for direct observation of quantity and timing of macropore flow. Other methods may allow analysis of the role of macropore flow by inference from other measurements.

Flow gages were constructed based on the design of Ziemer and Albright (1987) to measure the magnitude and rate of macropore flow from the trench face. The gages were constructed of 15 cm I.D. by 1 m length PVC pipe sealed on the bottom, and having a line of irregularly spaced 0.65 cm diameter holes drilled through the pipe wall. A half section of 2.5 cm I.D. PVC pipe was attached to the inside of the larger pipe to serve as a sleeve for a pressure transducer used to determine stage. Flow measurements are made via a stage-discharge rating curve determined for each gage. Water was to be routed from a macropore, or series of macropores, to a gage by driving pipe or flashing material into the soil and directing the opposite end to the gage opening.

4.5 Pressure Transducers

The pressure transducers used in the study were ICSensors Company Model 115, 4 - 20 mA two wire devices. They are solid state, temperature compensated and have $\pm 0.5\%$ accuracy. Transducers with a range of 0 - 34 kPa gage pressure were used with the wellpoints. Transducers with a range of 0 - 200 kPa absolute pressure were used with the tensiometer and for atmospheric pressure reference. The devices were calibrated in the laboratory either by submersion under a positive head of water (0 - 34 kPa transducers) or by a hanging water column in both tension and positive head (0 - 200 kPa transducers) over a range of pressures from 0 - 150 cm of water. The transducer output current was passed through a resistor to produce voltage readings for data logging.

Transducers were originally calibrated by taking voltage readings directly across the resistor for each individual device. It was later observed that a different voltage reading resulted at the same pressure head when the devices were connected to the data loggers. Recalibration of all devices was subsequently done with all transducers connected to the data logger that was to be used in the field.

4.6 Data Logging

Wellpoint and tensiometer transducers at each site were connected to a Campbell Scientific, Inc. 21X, 16 channel Data Logger. On Site 2 a Campbell Scientific, Inc. AM416 Multiplexer was used to expand the 21X channel capacity to accommodate 8 wells, 9 tensiometer and 1 atmospheric reference transducer. The data loggers were housed in fiberglass boxes and set some distance to the side of the instrumented site under cover of a nearby tree. Electrical cable was run from the instruments to the data loggers and was housed in 4 cm O.D. ABS pipe laid across the ground surface to protect the cable from weather and animal activity. The transducer and data logging system was powered by three 12 Volt batteries, one powering the data logger, and two in parallel powering the pressure transducers. Switches were wired in to power up the transducers just prior to being queried, in order to increase battery life.

The data loggers were programmed using the PC208 Datalogger Support Software (Campbell Scientific, Inc.). Transducers were queried at user specified time intervals. Each transducer was scanned 15 times at the designated time interval. Time intervals ranged from 15 minutes during storm events to greater than 2 hours between events. Output was the average voltage reading and standard deviation of the voltage readings for each channel. Data was recorded on a Campbell Scientific, Inc. SM192 Storage Module.

4.7 Precipitation Measurements

Each site was instrumented with an RG40 Sierra Misco Tipping Bucket Rain-gage. Precipitation passes through a debris screen on a funnel, enters a collection orifice and fills a calibrated tipping bucket assembly. When the bucket assembly tips, a momentary closure of a reed switch sends a signal to a data logger. The second bucket in the assembly is then positioned to receive precipitation. Water is discharged through orifices in the bottom of the gage housing.

The factory gage calibration of 0.025 cm precipitation per tip was verified prior to installation in the field. Gages were bolted to a flat steel plate that had a collar welded to the underside. A 1.3 cm O.D. by 2 m long steel pole was driven into the ground approximately 1 m, and the collar on the plate was bolted to the top of the pole. Adjustable legs on the gage allowed it to be leveled. The gage was placed near the center of the instrumented portion of the site (Figure 3.2).

The gages were equipped with a Omni-Data International, Inc. Model DP101 one channel time of event recorder. The DP101 uses a Erasable Programmable Read Only Memory (EPROM) chip for data storage. The DP101 prescale factor can be set to record data to the EPROM chip each 2^0 to 2^7 events. This feature allows the user to increase chip storage capacity, at the cost of data resolution. A prescale factor of 1 was used throughout this study to give the highest data resolution. Chip capacity for a prescale factor of 1 is 50 cm of precipitation. Chips were checked regularly and changed as necessary. The DP101 was housed in a water-tight container with electrical wiring between the container and the gage enclosed in electrical conduit.

4.8 Analysis of Piezometric Response to Precipitation

A two part analysis of the piezometric response to precipitation was undertaken following the monitoring period. Phase one involved development of a set of regression equations for prediction of hydraulic head based on antecedent precipitation, using the API variable (described in Chapter 2) as the independent term in the model. The second phase included development of a mathematical groundwater model based on mass-balance considerations, to serve as a comparison to the API model. A version of the kinematic storage model described in Chapter 2 was developed.

4.8.1 Antecedent Precipitation Index Model of Hillslope Pressure Head

As suggested in previous sections, groundwater modeling efforts typically face a high degree of uncertainty regarding soil hydraulic properties, and the associated difficulty in obtaining quality data about these properties. In view of this, an effort was made to develop a simple model of predicting pressure head that did not require intensive soils data. Because rainfall is the driving mechanism for hillslope groundwater rise, it seems reasonable that there should exist some quantifiable relationship between the time-history of precipitation input, and the resulting subsurface hydrograph. In order to investigate this relationship, the correlation between pressure head in the piezometers, and simple cumulative antecedent precipitation for a series of time intervals between 6 and 96 hours was tested. It was determined that the highest correlation coefficient occurred for the majority of storms using the 72 hour antecedent cumulative precipitation.

In order to properly weight antecedent precipitation to account for the diminishing effect on groundwater level of an increment of rainfall with time, an antecedent precipitation index (API) was tested for correlation with pressure head. In contrast to simple cumulative precipitation described above, the API is a decayed cumulative precipitation index. The procedure for developing the API variable was outlined in Chapter 2. The correlation coefficient between pressure head and API was maximized by varying the recession coefficient, C, determined from the recession limb of the groundwater hydrograph. The API was then used as an independent variable in regression analysis of piezometric levels in each of the wells for the extreme storm events.

4.8.2 Kinematic Storage Model of Hillslope Hydraulic Head

A version of the mass balance model previously described as the kinematic storage model (Sloan and Moore, 1984), was developed for prediction of hydraulic head. The kinematic storage model is based on the kinematic assumption, that the hydraulic gradient is equal to the slope of the impermeable (no flow) base of the control volume. The topographic conditions at Site 2 suggest that converging subsurface flow is likely. It is difficult to develop the kinematic storage model to determine hydraulic head analytically for cases of converging flow due to non-linearity of the hydraulic head function. However, hydraulic head determined by the planar hillslope model used by Sloan and Moore (1984) can be scaled to account for converging flow under certain conditions. A schematic diagram of a hillslope with converging flow is shown in Figure 4.2.

For the planar hillslope case, the mass continuity equation is expressed in mixed finite difference form, and hydraulic head at the outlet of the control volume is calculated explicitly at the end of each time period. Figure 4.3 shows idealized representations of the hillslope with terms used in the kinematic storage model. With reference to Figure 4.3, the mass continuity equation has the form

$$\frac{S_1 - S_0}{t_1 - t_0} = iL - \frac{(q_1 + q_0)}{2} \tag{4.3}$$

where S is the drainable volume of water in the saturated zone, t is time, i is the rate of water input to the saturated zone from the unsaturated zone, q is the discharge from the hillslope per unit width, given by $q=Hv$ where $v= K_s \sin \alpha$, and H is the saturated thickness normal to the slope at the outlet. Subscripts 0 and 1 refer to the beginning and end of a time period, respectively. The drainable volume of water in the saturated zone, S, is given by

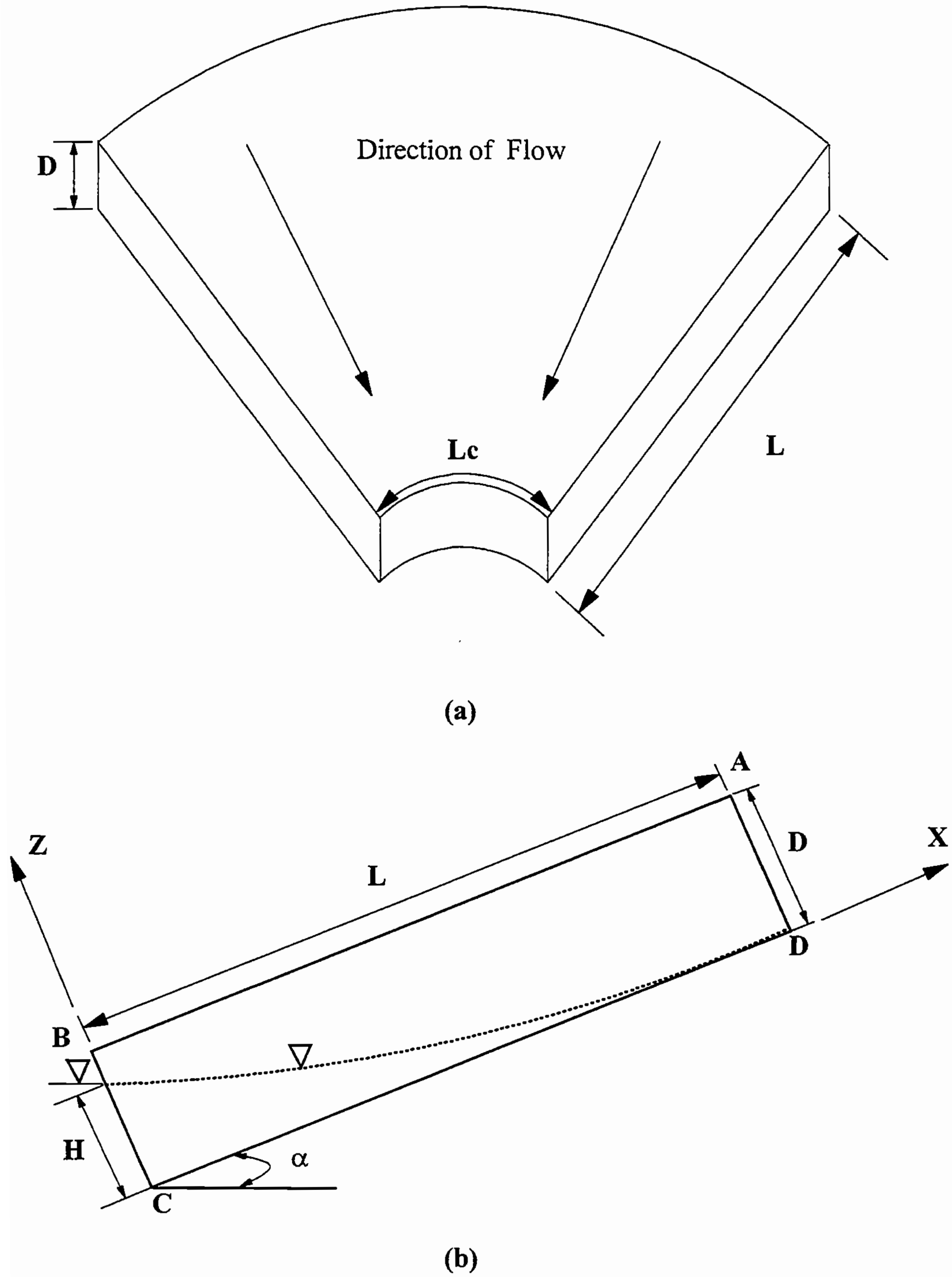

Figure 4.2 Schematic diagram of the idealized hillslope with converging flow: (a) three-dimensional block perspective; (b) longitudinal profile showing non-linear water table.

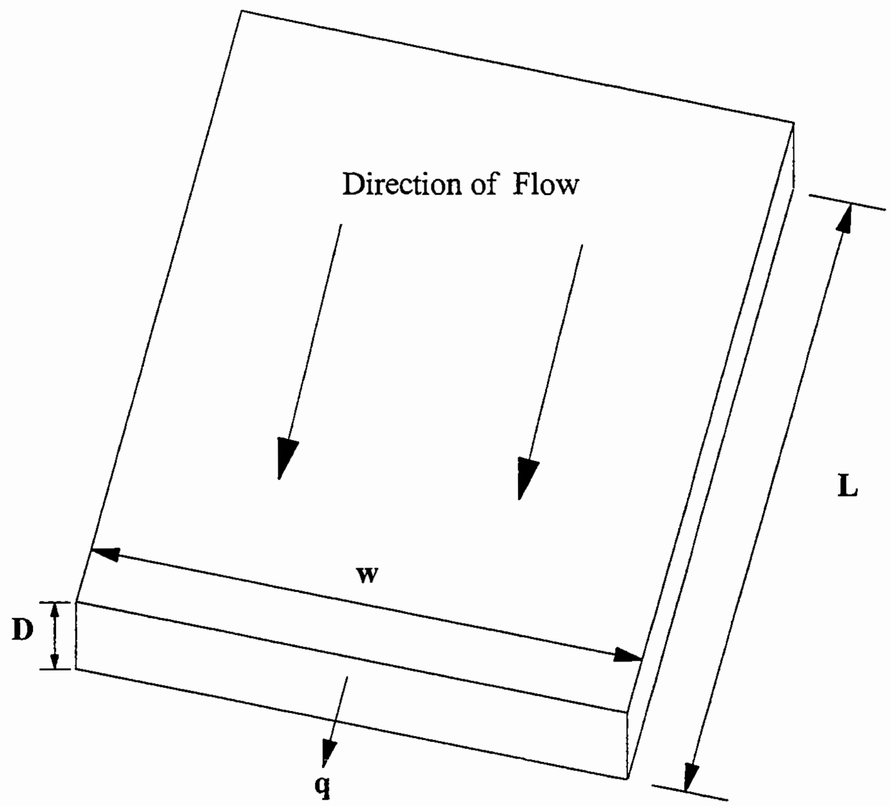

(a)

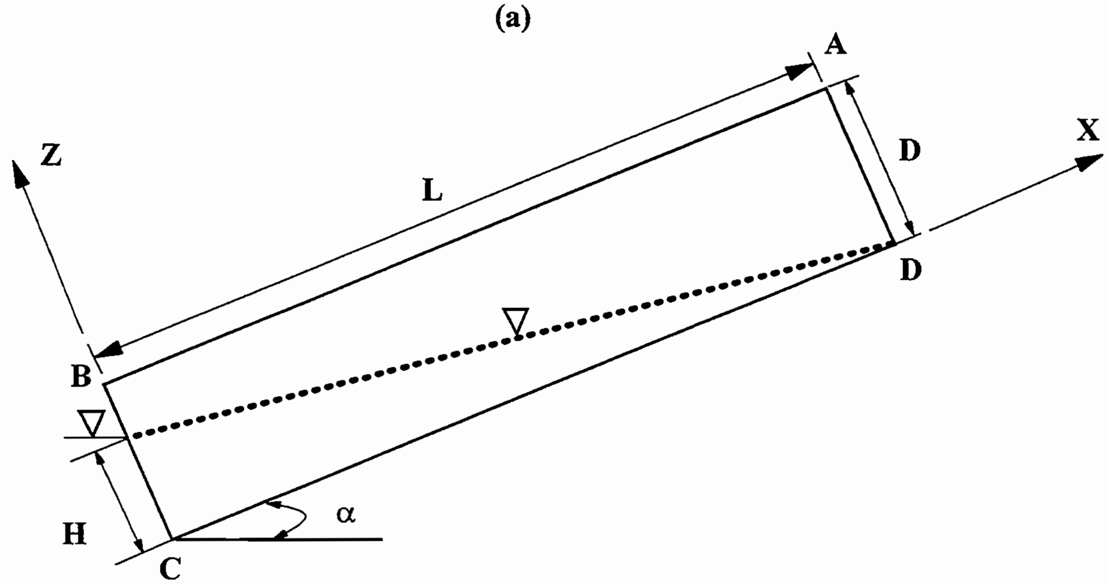

(b)

Figure 4.3 Schematic diagram of the idealized planar hillslope used in development of the kinematic storage model: (a) three-dimensional block perspective; (b) longitudinal profile showing linear water table.

$$S = \frac{H \theta_d L}{2} \tag{4.4}$$

where θ_d is the drainable porosity of the soil.

Substituting Equation 4.4 into Equation 4.3, and solving for hydraulic head, H, gives

$$H_1 = \frac{2\, i\, L\, \Delta t + (\theta_d L - v\, \Delta t)\, H_0}{\theta_d L + v\, \Delta t} \tag{4.5}$$

Vertical input of water to the saturated zone from the unsaturated zone, i, is considered to be equal to the unsaturated hydraulic conductivity corresponding to the average volumetric water content of the unsaturated zone. For cases where gravity dominates flow, as is typically the case in steeply sloping soils, the hydraulic gradient normal to the slope is unity, and this is a reasonable assumption (Sloan and Moore, 1984). This assumption, then, gives

$$i = K(\theta_u) \tag{4.6}$$

where θ_u is the average volumetric water content of the unsaturated zone. This treatment also assumes that the entire unsaturated zone can be treated as a homogeneous unit in terms of the soil moisture characteristic functions. As with the hydraulic head, average water content is modeled using mass balance considerations. The average water content at the end of any time interval is calculated as

$$\theta_{u1} = \frac{\left[\theta_{u0} U_u + L \Delta t (r - i)\right]}{U_u} \tag{4.7}$$

where r is the precipitation rate, and U_u is the total volume of the unsaturated zone given by

$$U_u = L\left(D - \frac{H}{2}\right) \tag{4.8}$$

4.8.2.1 Model Boundary Conditions

With reference to Figure 4.3, boundary conditions for the control volume are given by the following expressions:

Boundary CD, DA

$$\frac{\partial H}{\partial z} = 0 \ , \ z = 0 \ , \ 0 < x < L \tag{4.9a}$$

$$\frac{\partial H}{\partial x} = 0 \ , \ x = L \ , \ 0 < z < D \tag{4.9b}$$

Boundary BC

$$H = h_z \ , \ x = 0 \ , \ 0 < z < H \tag{4.10a}$$

$$\frac{\partial H}{\partial x} = 0 \ , \ x = 0 \ , \ H < z < D \tag{4.10b}$$

where h_z is the elevation head

Boundary AB

$$- K(\theta) \frac{\partial H}{\partial z} = r \cos \alpha < K_s \ , \ z = D \ , \ L_s < x < L \tag{4.11a}$$

$$H = h_z \ , \ z = D \ , \ 0 < x < L_s \tag{4.11b}$$

where L_s is the length of the seepage face along Boundary AB.

4.8.2.2 Scaling Hydraulic Head for Converging Flow

To account for converging flow, hydraulic head determined using the planar hillslope model was scaled by the ratio of the arc length of the outlet of the control volume (L_c in Figure 4.2) to the width of the rectangular control volume (w in Figure 4.3). That is, hydraulic head for the converging case, H_c, is given by

$$H_c = H \frac{L_c}{w} \tag{4.12}$$

where H is the hydraulic head determined by the planar hillslope model.

The values of L_c and w were obtained from the topographic map of Site 2 (Figure 3.2). For this relationship to be strictly valid it is necessary that the magnitude of i, the input from the unsaturated zone to the saturated zone, and precipitation, r, be small, relative to the magnitude of v, the Darcy velocity of saturated flow. This is because the planar representation of the hillslope does not take into account the decreasing input area in the downslope direction, and the resulting increase in volume of water input per unit area. If, in fact, the magnitude of i and r are small relative to v, the unsaturated zone model described by Equations 4.6 - 4.8 can be uncoupled from the saturated zone model. In this case precipitation, r, is input directly to the saturated zone. Preliminary runs of the full model described by Equations 4.6 - 4.11 were used to determine whether it was reasonable to disregard i, and utilize the relationship given by Equation 4.12.

4.8.2.3 Model Parameter Estimation

The equations described above, hillslope parameters, and soil hydraulic property characteristic data were coded in FORTRAN and the model run using precipitation data from several of the largest storm events observed during the monitoring period. The unknown parameters were saturated hydraulic conductivity, K_s, and θ_{u0}, the initial value of average volumetric water content for the unsaturated zone. Several methods of estimating drainable porosity, θ_d, were used, as described below.

Figure 4.4 shows a hypothetical soil moisture characteristic curve. Several volumetric water contents are labeled: $\theta_{saturation}$ is the water content at saturation, $\theta_{average}$ is an average water content, and $\theta_{field\ capacity}$ is the water content remaining in a unit volume of soil after downward gravity drainage has ceased. The first method of estimating drainable porosity was the method of Bear (1972), shown in Figure 4.4(a). This technique considers the drainable porosity to be the difference between the water content at saturation and at field capacity. This method would seem to overestimate the value of drainable porosity for cases when the soil profile is not initially fully saturated, or when the profile does not fully desaturate between storms. Therefore, a modification of the Bear method was deemed necessary.

The modified Bear method is shown in Figure 4.4(b). This method assumes a hydrostatic state in the soil profile, with a capillary pressure of zero at the soil - bedrock interface, increasing (more negative) linearly with elevation, z, above bedrock. The degree of desaturation is then calculated as a function of soil depth, and used as an estimate of drainable porosity.

The third technique was based on observations from the piezometer response to precipitation. A given amount of rainfall would be expected to produce a rise in the piezometric surface in indirect proportion to the porosity of the soil, e.g. 1 cm of rainfall producing a change in water level in the soil of 10 cm suggests a porosity of approximately 0.10. Therefore, by comparing the depth of precipitation to the rise in piezometric surface, an estimate of the active porosity can be made. Data from

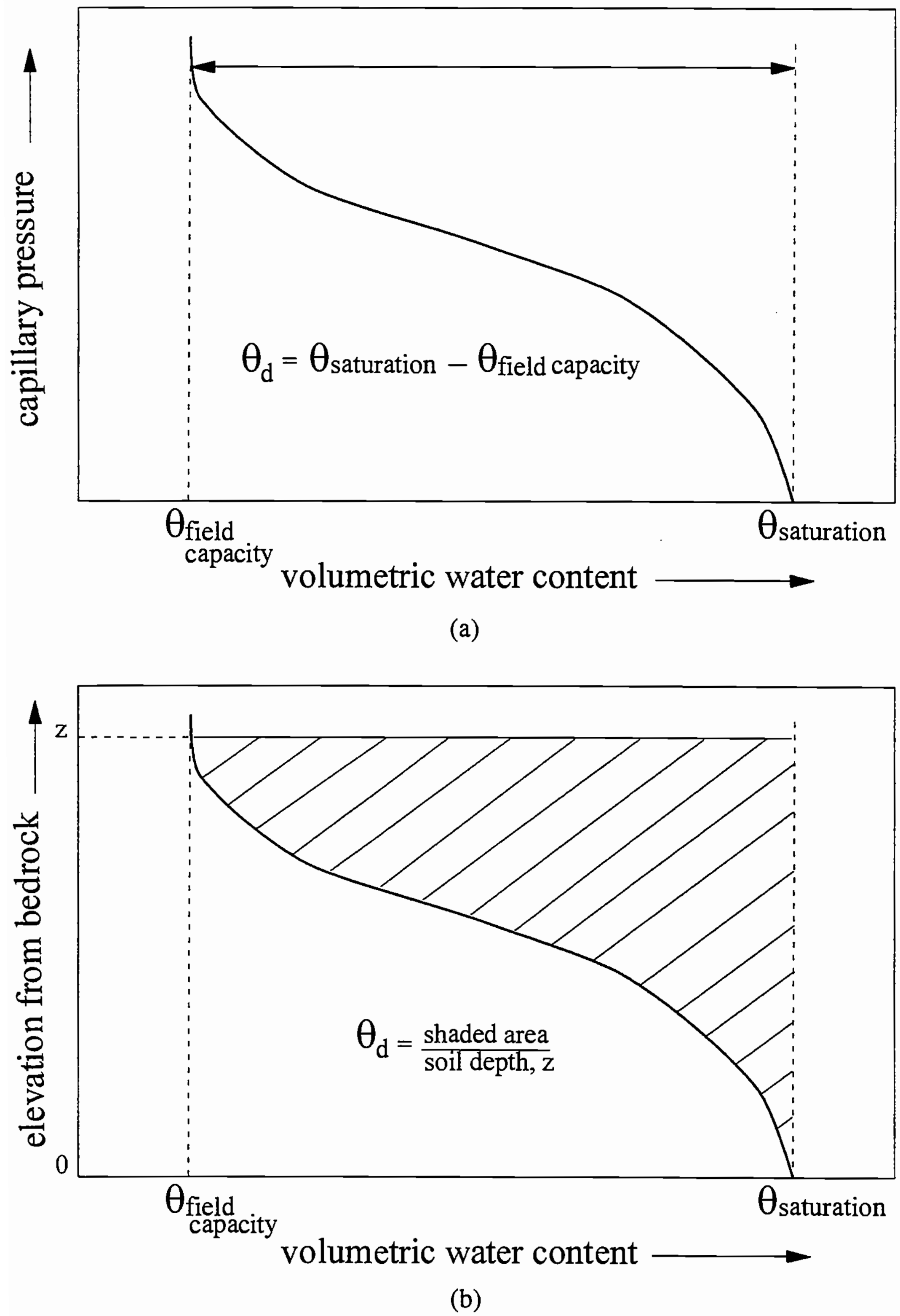

Figure 4.4 Hypothetical soil moisture characteristic curve showing two methods of estimating drainable porosity, θ_d: (a) Bear (1972); (b) modified Bear.

the piezometers on the margins of the headwall were used in this analysis to minimize the effects of converging flow.

During early model runs it was observed that values of i were typically three orders of magnitude less than v, suggesting that use of Equation 4.12 was appropriate.

After reformulating the model to consider just the saturated flow component, results of model runs were compared to observed hydraulic head data. The value of saturated conductivity was adjusted until a model run produced a hydrograph of hydraulic head versus time that was considered a "best-fit" with the observed data for a storm. Criteria for determining a best-fit included agreement with the magnitude and timing of the rising limb of the observed hydrograph, magnitude and timing of the peak hydraulic head, and magnitude of recession limb head values.

4.9 Piezometric Response and Slope Stability

The piezometers used in the investigation determine the pressure head at bedrock at the base of each instrument. The absolute magnitude of pressure head at a point is an important variable for slope stability analyses. However, in order to make valid comparisons about the effect of pressure head on stability from point to point on a slope, the important parameter is some form of a ratio of pore-pressure to soil depth, where pore-pressure is the product of pressure head and the unit weight of water. A common slope stability model will be presented to show the role this relationship has in a stability analysis. It is not within the scope of this work to conduct a full slope stability analysis, but rather the purpose of this exercise is to illustrate the results of the piezometric monitoring in the context of slope stability.

If the slope under consideration is at least one order of magnitude longer than the soil is deep, the one-dimensional infinite slope model can be used to determine the factor of safety against sliding for a given set of hillslope conditions (Morgenstern et al., 1978). The study sites satisfy this criteria, therefore an infinite slope analysis is deemed appropriate. Figure 4.5 shows a schematic diagram of a hillslope with the forces acting on an idealized slice of the infinite slope. An expression for the factor of safety for the slope can be derived as follows, with reference to Figure 4.5.

The weight of the slice on a unit width basis is given by

$$W = \gamma D b \tag{4.13}$$

where γ = unit weight of soil (M/LT^2)

The total normal force, N, is the sum of the effective normal force N', and the force due to pore-water pressure, U. N' is calculated as the difference between N and U. The total normal force is given by

$$N = W \cos\beta \tag{4.14}$$

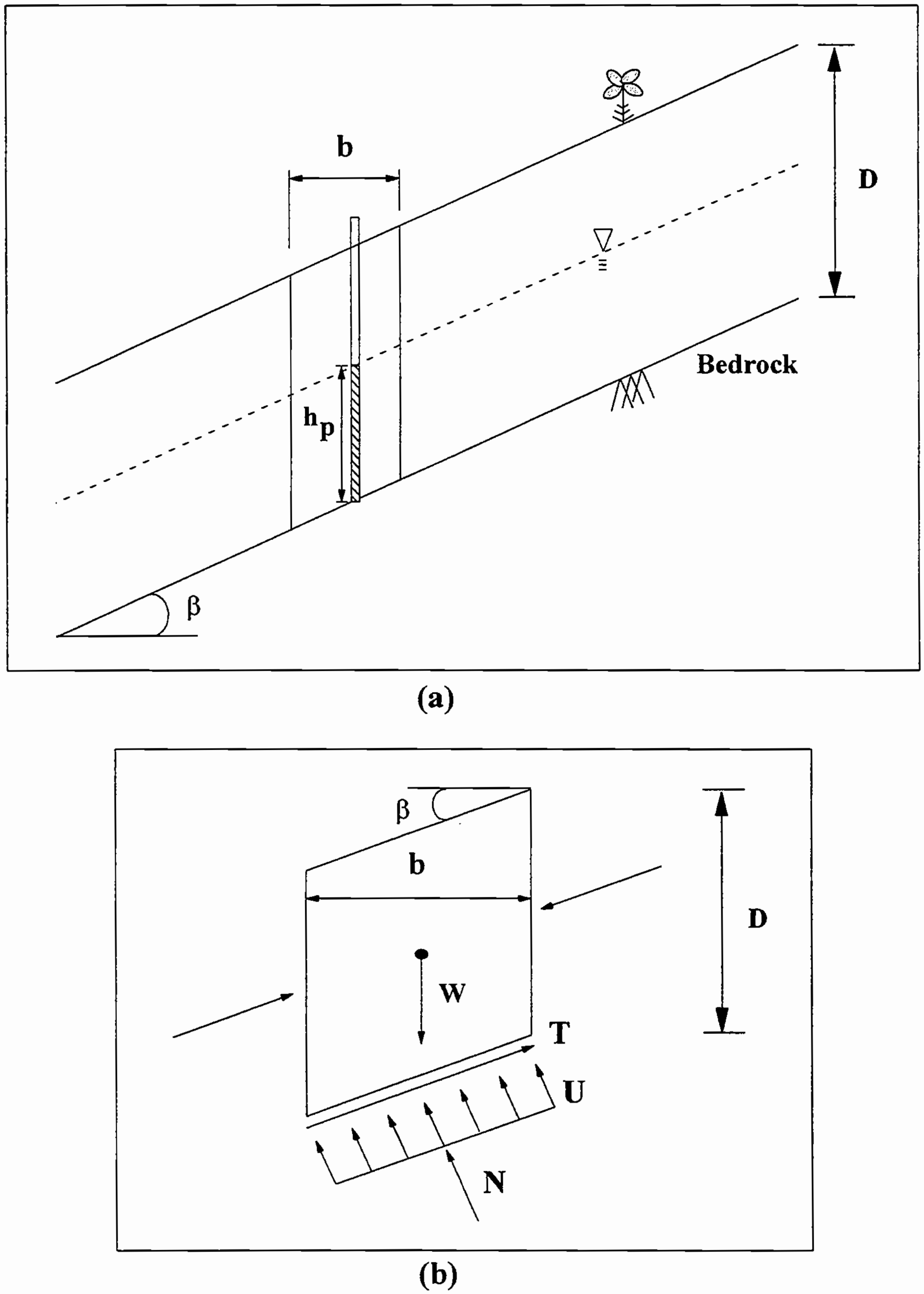

Figure 4.5 Schematic diagram of a hillslope showing terms used in development of the infinite slope model for factor of safety: (a) hillslope with piezometer; (b) free-body diagram of a representative section.

and the force due to the pore-pressure is

$$U = \gamma_w h_p b \sec\beta \tag{4.15}$$

therefore

$$N' = \gamma D b \cos\beta - \gamma_w h_p b \sec\beta \tag{4.16}$$

where γ_w = unit weight of water (M/LT^2)

The shear force, *T*, acting on the base of the slice is

$$T = W \sin\beta \tag{4.17}$$

so the shear stress acting on the base is

$$\tau = \frac{T}{A} \tag{4.18}$$

where *A* is the area of the base of the slice. The shear stress, then, is

$$\tau = \gamma D \sin\beta \cos\beta \tag{4.19}$$

The soil strength, S, (the "available" shear stress on the failure plane) in terms of effective strength parameters, is given by the Mohr-Coulomb equation (Holtz and Kovacs, 1981):

$$S = c' + \sigma' \tan\phi' \tag{4.20}$$

where c' = effective cohesion
σ' = effective normal stress
ϕ' = effective angle of internal friction

The effective normal stress, σ', is given by

$$\sigma' = \frac{N'}{A} \tag{4.21}$$

where A is the area of the base of the slice.

The effective stress at the base, then, is

$$\sigma' = \gamma D \cos^2\beta - \gamma_w h_p \tag{4.22}$$

The factor of safety for the slope, FS, is equal to the ratio of soil strength on the failure plane to the applied shear stress on the failure plane.

$$FS = \frac{S}{\tau} \tag{4.23}$$

Substituting the appropriate terms, and rearranging gives

$$FS = \frac{c'}{\gamma D} \sec\beta \operatorname{cosec}\beta + \frac{\tan\phi'}{\tan\beta}\left[1 - \frac{\gamma_w h_p}{\gamma D}\sec\beta^2\right] \tag{4.24}$$

The factor of safety is seen to be dependent on three dimensionless ratios, $(c'/\gamma D)$, $(\tan\phi'/\tan\beta)$, and $(\gamma_w h_p/\gamma D)$. The last of these ratios expresses the relationship between the magnitude of pore-pressure at a point and the overburden stress at that point. This relationship has been called the pore-pressure ratio, r_u (Bishop and Morgenstern, 1960). Results of the piezometric monitoring will be used to evaluate this parameter on the hillslope during storm events.

5. RESULTS

Due to the complex geologic and soil conditions at Site 1 in the McDonald Research Forest, limited data was gathered. Several wellpoints installed on this site regularly recorded no measurable groundwater response to precipitation. In wells that did show a response, pressure head measurements were small (on the order of 10-20 centimeters of water). No tensiometers could be placed in the soil due to the cobbley nature of the material. Repeated equipment malfunctions limited the precipitation data to several small storms. Attempts were made to use precipitation records from the nearest known precipitation gaging station. However, results suggested that significant timing errors were present due to the distance between the sites. It did not seem reasonable to extrapolate precipitation timing or quantities from the gaging site to the instrumented site for use in analyzing groundwater response.

Drilling revealed that bedrock was on the order of 4 m depth, far beyond the reach of hand installation of our well points. Two 2.5 cm OD PVC piezometers such as those described in previous sections were installed to bedrock in bore holes, in order to gain some idea of depth of flow on the site. However, during the course of the two winters following installation, measurements of depth to water in the piezometers using an electrical resistance device were unsuccessful. The fine grained native material may have been compacted or sealed during drilling, preventing flow into the piezometers.

A number of clay lenses, and bedrock fractures were observed in cores obtained during the drilling operation. These features suggest that significant flow may occur through the fractures, with only localized buildup of perched water tables in the soil. In addition, results of the geologic investigation suggested that the direction of dip of bedrock may be normal to the slope rather than parallel, raising the possibility that flow is directed toward the opposite side of the ridge.

As a consequence of the difficulties in obtaining data as outlined above, the presentation of results will focus on data obtained from the Honeygrove Creek site in the Alsea River basin (Site 2). A more thorough instrumentation, and analysis of soils, was conducted on this site.

5.1 Soil Testing

Soils on Site 2 were collected and tested for some index properties, and strength parameters by researchers from a related field study (Morgan, 1995). Additional index properties including particle size distribution and soil classification, and soil hydraulic properties were determined as part of this subsurface flow investigation.

The results of the soil tests from Site 2 are presented in the following section. Soil index properties, strength parameters, and hydraulic properties are given.

5.1.1 Soil Index Properties

Table 5.1 shows the index properties of the soils tested (Morgan, 1995). Two samples were used for determination of index properties of the soil, a disturbed sample and an undisturbed sample. Specific gravity of soil solids was determined to be approximately 2.68 for the sandstone derived soils. The average unit weight of the soil was determined to be 13.25 kN/m^3. The soil is a non-plastic, silty-sand mixture classified as SM in the Unified Soil Classification System (USCS).

Table 5.1 Soil index properties and USCS classification.

Index Property	Undisturbed Sample	Disturbed sample
$G_s^{(a)}$	2.68	2.69
$\gamma_d^{(b)}$ (kN/m^3)	13.1	13.4
$LL^{(c)}$ (%)	45.4	41.9
$PL^{(d)}$ (%)	33.3	31.2
$I_p^{(e)}$ (%)	12.1	10.7
USCS Group	SM	SM

(a) : specific gravity of soil solids
(b) : dry unit weight
(c) : liquid limit
(d) : plastic limit
(e) : plasticity index

5.1.2 Soil Effective Strength Parameters

Table 5.2 shows the effective strength parameters obtained from triaxial tests of soil samples (Morgan, 1995). The type of test, consolidated-undrained (CU) or consolidated-drained (CD), and confining pressures used are given for each specimen. Six remolded samples and one undisturbed sample were tested.

The average value of ϕ' for the remolded samples was 29.3° (standard deviation 2.30°), and the average value of c′ was 5.6 kPa (standard deviation 1.2 kPa). For the tests conducted at low confining pressures (3.4 - 34 kPa) the average ϕ' was 29.7° (standard deviation 0.55°), and the average c′ was 4.4 kPa (standard deviation 0.24 kPa). The undisturbed sample had the highest ϕ', 32.5°, and a c′ value of 5.2 kPa.

5.1.3 Soil Hydraulic Properties

Soil samples were collected for determination of the soil moisture characteristic curve, porosity, and the hydraulic conductivity function. Samples were collected from three depths in the soil profile: 0-10 cm, 51 cm, and 107 cm. Data from the two sub-soil layers were combined following the laboratory testing because of similarity. Figure 5.1 shows the main draining moisture characteristic curve for surface soil and sub-soil. Figure 5.2 shows the plots of effective saturation, S_e, versus capillary pressure. Plots of effective saturation versus capillary pressure were used in determination of the hydraulic conductivity parameters λ and η. Figure 5.3

shows the hydraulic conductivity function derived from the soil property data. The magnitude of saturated hydraulic conductivity was determined by calibration of the kinematic storage model.

Table 5.2 Effective strength parameters for remolded and undisturbed samples.

Specimen	Test Type	Effective Confining Pressures (kPa)	ϕ' (degrees)	c' (kPa)
Remolded Samples				
1	CU	34.5,69,138, 207,276	31.9	4.1
2	CU	34.5,69,138, 207,276	30.7	7.3
3	CU	3.4,6.9,13.8 24,34.5	29.1	4.2
4	CU	138,207	29.1	5.9
5	CU	3.4,6.9,13.8 24,34.5	30.2	4.7
6	CU	24,34.5	29.9	6.2
7	CD	3.4,6.9,24	24.1	6.9
Undisturbed Sample				
1	CU	3.4,6.9,13.8 24,34.5	32.5	5.2

Calculations from data obtained during the hydraulic property tests suggest that the soil has somewhat lower dry unit weight than reported by Morgan (1995), for soils on the same site. The results of these tests are given in Table 5.3.

Table 5.3 Hydraulic and index properties of Site 2 soil samples.

Property	Surface Soil	Sub-Soil
γ_d (kN/m^3)	12.4	12.7
$n^{(a)}$	0.53	0.52
$\lambda^{(b)}$ (1/cm)	0.29	0.34
$\eta^{(c)}$ (1/cm)	3	3
$\psi_a{}^{(d)}$ (cm)	3	8

(a): porosity
(b),(c): hydraulic conductivity function parameters
(d): air-entry pressure

5.2 Precipitation Measurements

Measurement of precipitation on both sites was complicated by equipment failure. Both mechanical problems and natural interferences resulted in periods when no precipitation data was obtained. On several occasions the precipitation data loggers were found to be inoperative due to an undetermined malfunction. The DP101 data loggers entered what is normally a user initiated procedure known as a

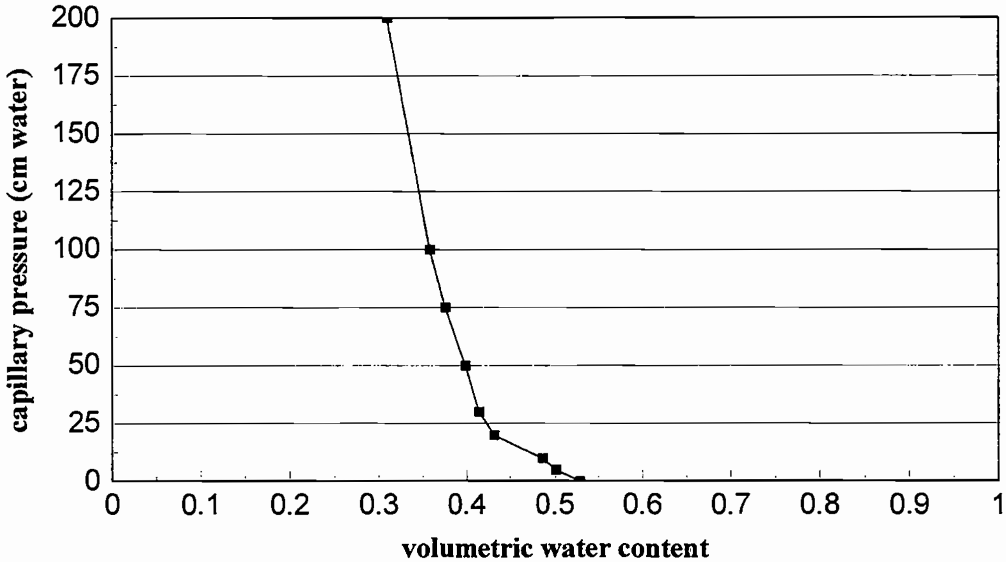

(a)

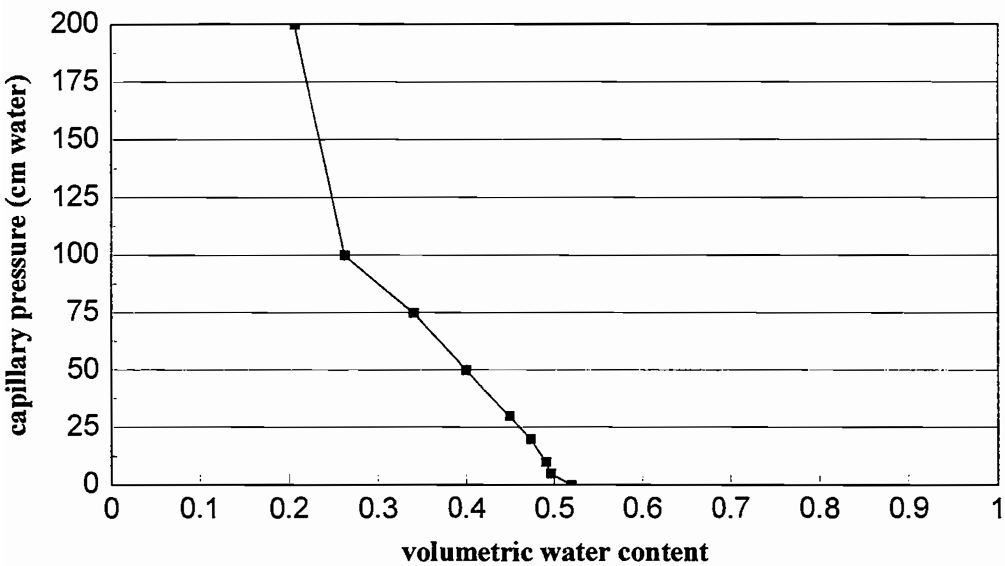

(b)

Figure 5.1 Soil moisture characteristic curves for Site 2: (a) surface soil; (b) sub-soil.

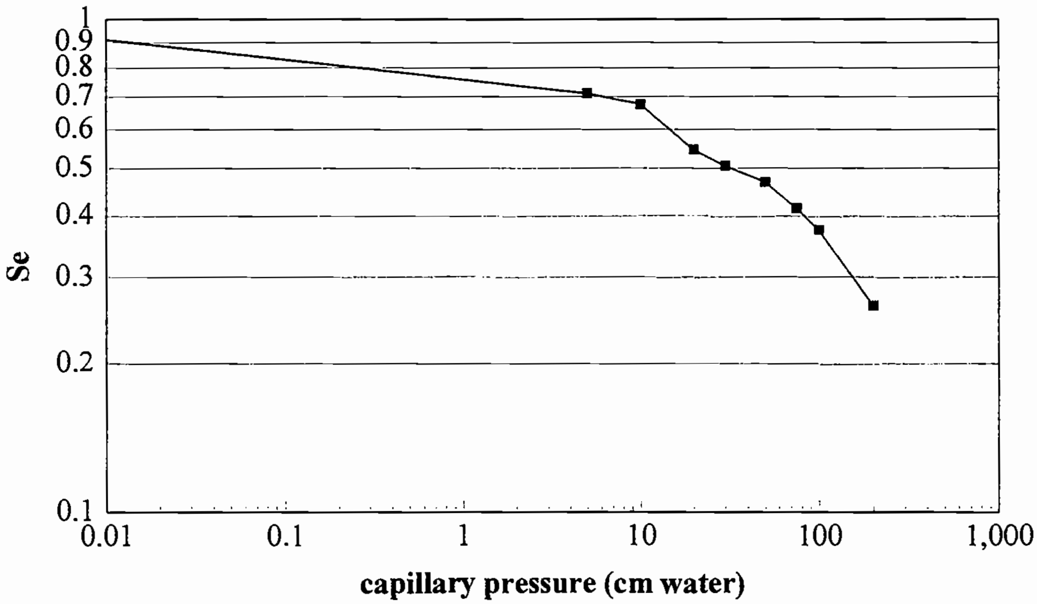

(a)

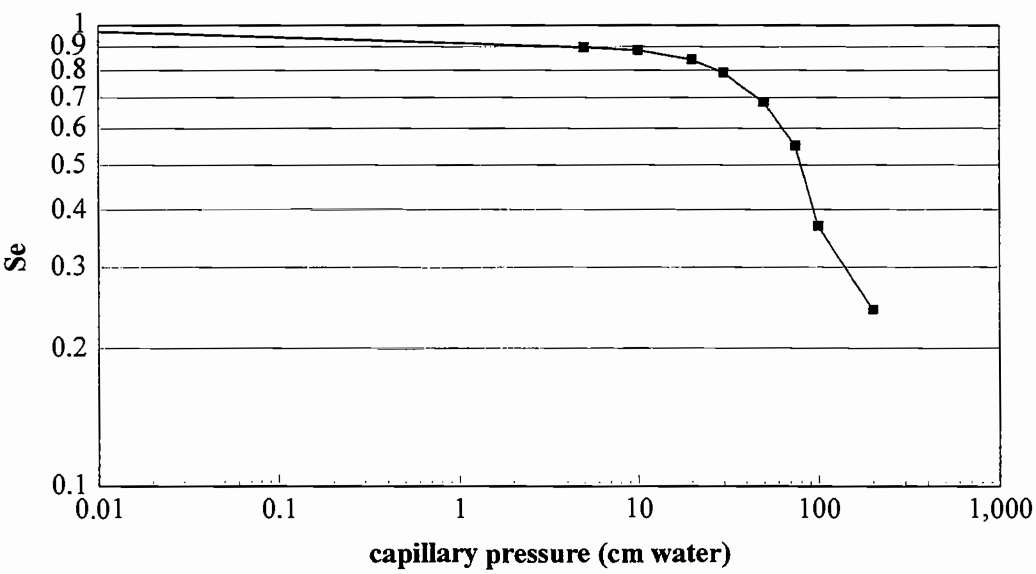

(b)

Figure 5.2 Effective saturation, Se, versus capillary pressure for Site 2:
(a) surface soil; (b) sub-soil.

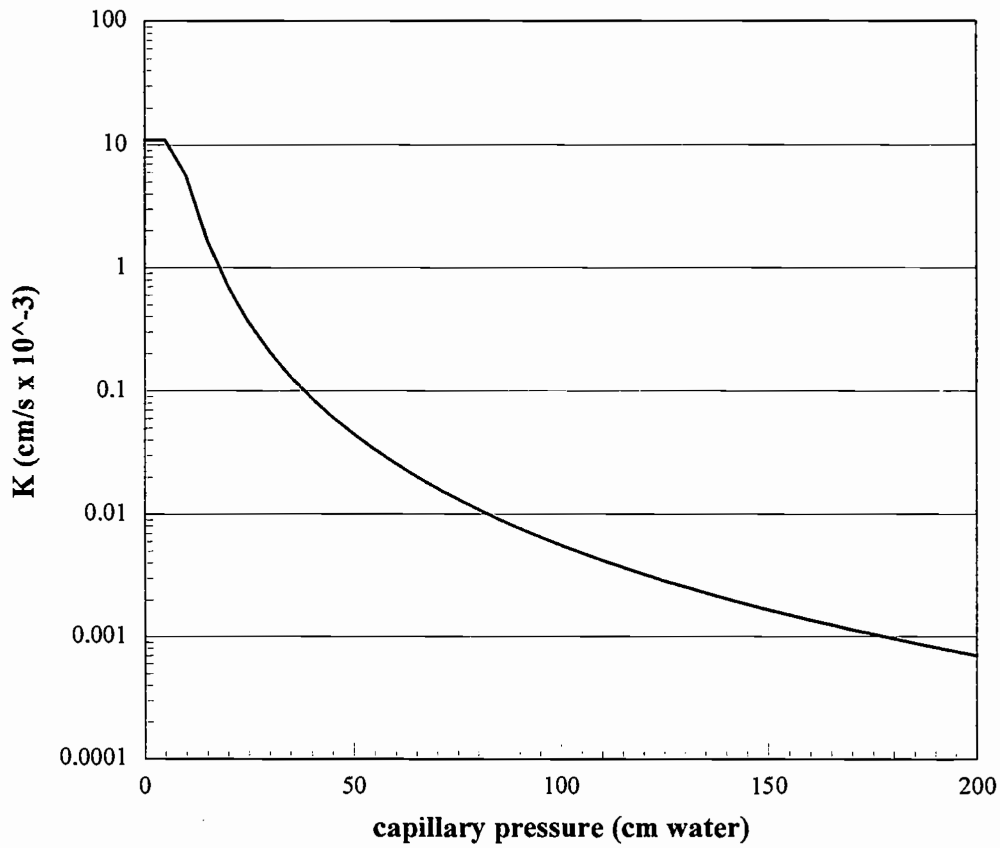

Figure 5.3 Hydraulic conductivity function for Site 2 soil.

long data dump during which the data logger counts down from the last recorded data value. Although desiccant packets were used in the DP101's, two data loggers appeared to malfunction due to the presence of moisture inside the case. Returning the devices to the laboratory for several days to dry out restored full function.

The tipping bucket rain gages were also subject to mechanical malfunction. The tipping bucket mechanism of one gage would occasionally stick in one position and fail to tip back the other direction. The loss of data from this problem was extensive. Further, the funnels on top of the gages are susceptible to plugging with falling needles and leaves from nearby vegetation, and required regular cleaning. Finally, the magnet used in the sensor mechanism came unglued from the gage, and was lost, late in the winter of 1995. As this coincided with the end of monitoring, it did not affect data collection. After the first field monitoring season, the problems with precipitation measurement equipment were reduced, and good data were obtained.

Table 5.4 shows characteristics of the five largest storm events recorded during the monitoring period. The temporal distribution of precipitation, and cumulative precipitation, for these select storm events is shown with the corresponding well and tensiometer response plots in the following sections. Hourly precipitation values are represented by bars and cumulative precipitation is shown as a line on these plots. These storms represent the most extreme events observed during the monitoring period. Table 5.4 shows the total precipitation, the duration, average rainfall intensity, and maximum rainfall intensity for each of the storms. Two distinct rainfall periods of Storm 3 are given separately in Table 5.4.

Table 5.4 Total precipitation, duration, average intensity, and maximum intensity for the five extreme storm events.

Storm	Date	Total Precipitation (cm)	Duration (hr)	Average Intensity (cm/hr)	Maximum Intensity (cm/hr)
1	3/14-3/17 1993	12.6	100	0.13	0.71
2	2/22-2/24 1994	10.7	54	0.20	0.46
3-1	11/29-11/30 1994	1.3	12.5	0.10	0.18
3-2	11/30-12/1 1994	2.8	8.5	0.33	0.43
4	12/15-12/17 1994	5.3	39.5	0.13	0.76
5	1/12-1/14 1995	6.7	82	0.08	0.33

In order to investigate the relationship between rainfall and piezometric response, correlation analysis between cumulative antecedent precipitation and pressure head for several wells was carried out. Cumulative rainfall for different periods of antecedence were determined and correlated to pressure head in a moving sum fashion. In the majority of events tested, the highest average correlation coefficient for the wells occurred at 72 hour cumulative precipitation. In order to take into account the declining effect of early precipitation on piezometric response, an antecedent precipitation index was developed. Using this construction, precipitation data was used as an independent variable in regression analysis of piezometric response. Results of this analysis are included with piezometry results.

5.3 Tensiometry

Nine tensiometers installed on Site 2 were used to monitor unsaturated conditions in the soil. Operational difficulties with the instrumentation limit the quantitative value of the data. However, timing of the movement of the wetting front, and relative differences in magnitude of capillary pressure head can be observed from plots of tensiometric response. Figure 5.4 and 5.5 show relative tensiometer response during Storm 2. Figure 5.4 shows the relative response for tensiometers at three depths across slope on contour. Figure 5.5 shows relative response up and down the centerline of the headwall, for a uniform depth in the soil (46 cm).

5.4 Piezometric Response

The five storm events that produced the greatest groundwater response in the eight wells was the basis of the analysis of piezometer response. The wells along the center line of the headwall recorded much greater pressure heads than those along the margin of the headwall. Results from three of the four wells along the centerline of the headwall will be reported; data from the fourth well is suspected of containing

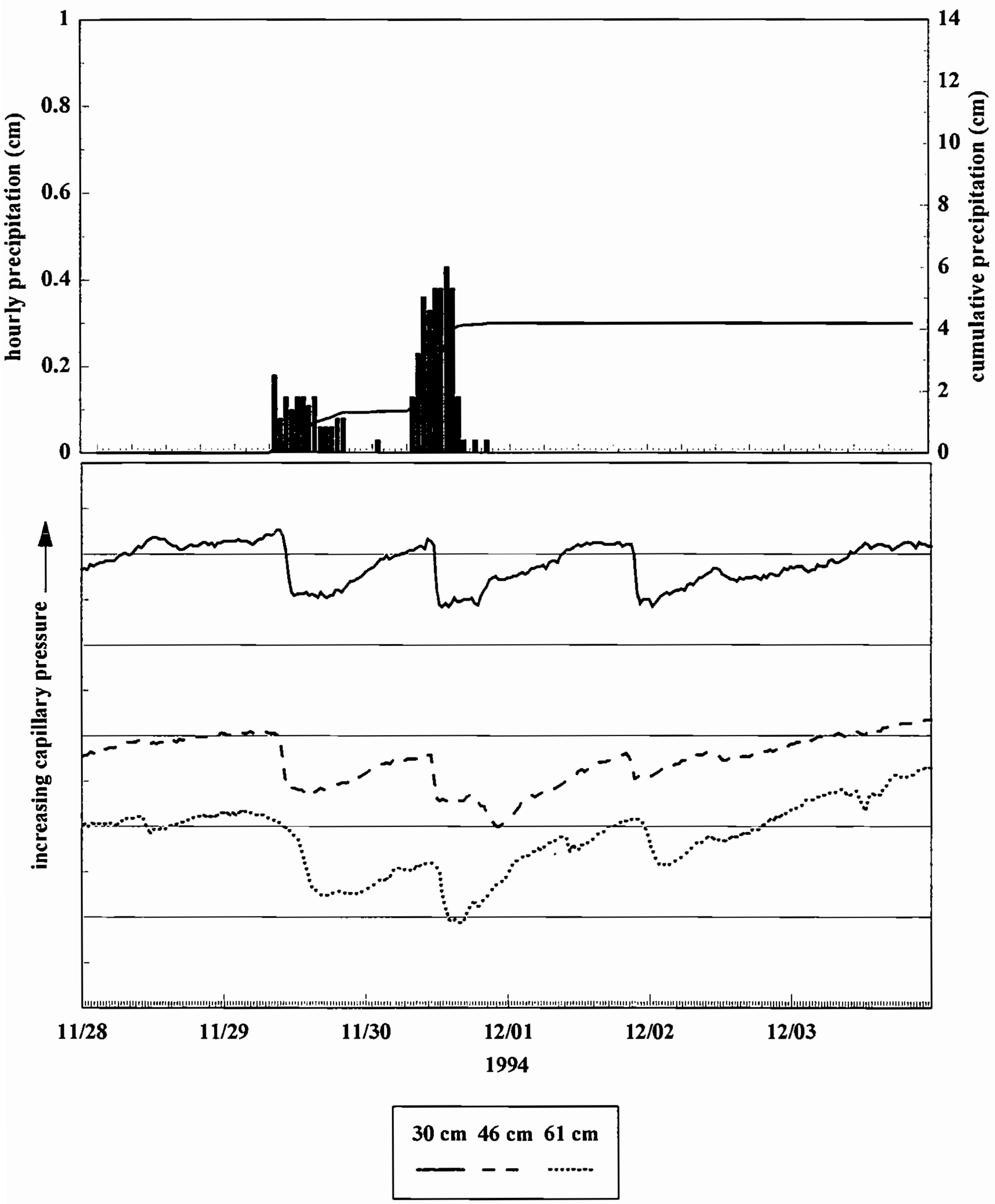

Figure 5.4 Relative tensiometric response at 3 depths on contour during Storm 3.

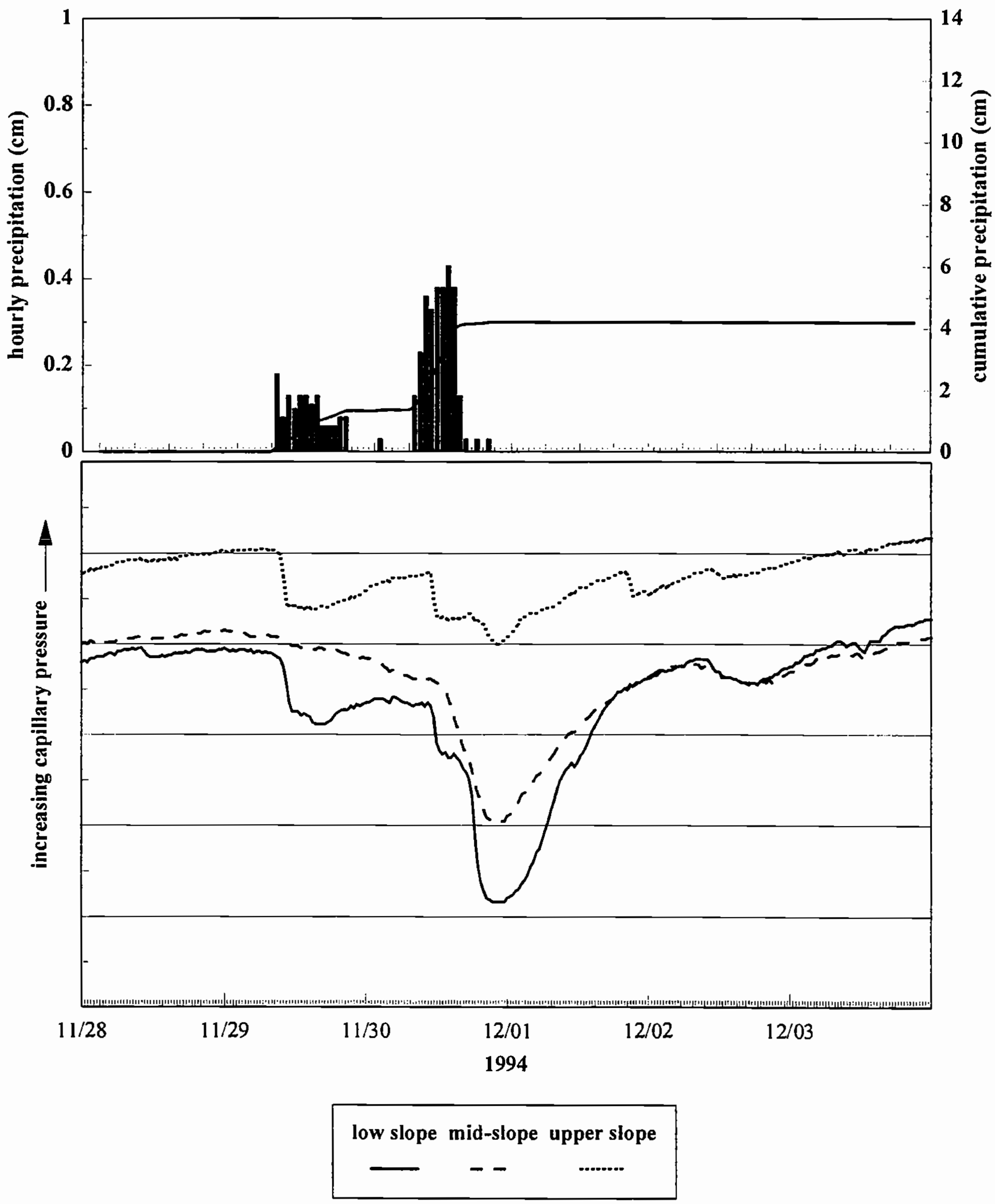

Figure 5.5 Relative tensiometric response at 46 cm depth and variable slope position during Storm 3.

errors due to pressure transducer malfunction resulting from water entry. Wells 1, 2, and 3 are numbered consecutively starting at the downslope position, just above the free face at the constriction in the headwall (Figure 3.2).

A series of plots are presented that show the well response to a short duration, moderate to high intensity storm (Storm 2), and long duration storms of low (Storm 4,5) and moderate intensity (Storm 1). Figures 5.6 - 5.10 show precipitation and pressure head plots for the five largest storms from March, 1993 through January 1995. Pressure heads are measured relative to bedrock at the base of each well.

5.4.1 Results of Antecedent Precipitation Index Analysis

Antecedent Precipitation Index (API) analysis was done for the five major storm events presented in Table 5.4. The correlation coefficient between pressure head and API was maximized by varying the hydrograph recession coefficient, C. The recession coefficient is simply a decay coefficient, calculated as the ratio of pressure head at time t to pressure head at time t-1 for values of pressure head on the recession limb. It was determined that the value of C that maximized the correlation coefficient was not the same for all wells, nor was it a constant for all storms. However, "best" values of C varied over a small range, from 0.985 to 0.995. A C value of 0.990 was selected as representative of the data set and used to calculate API using Equation 2.34 for the five storms.

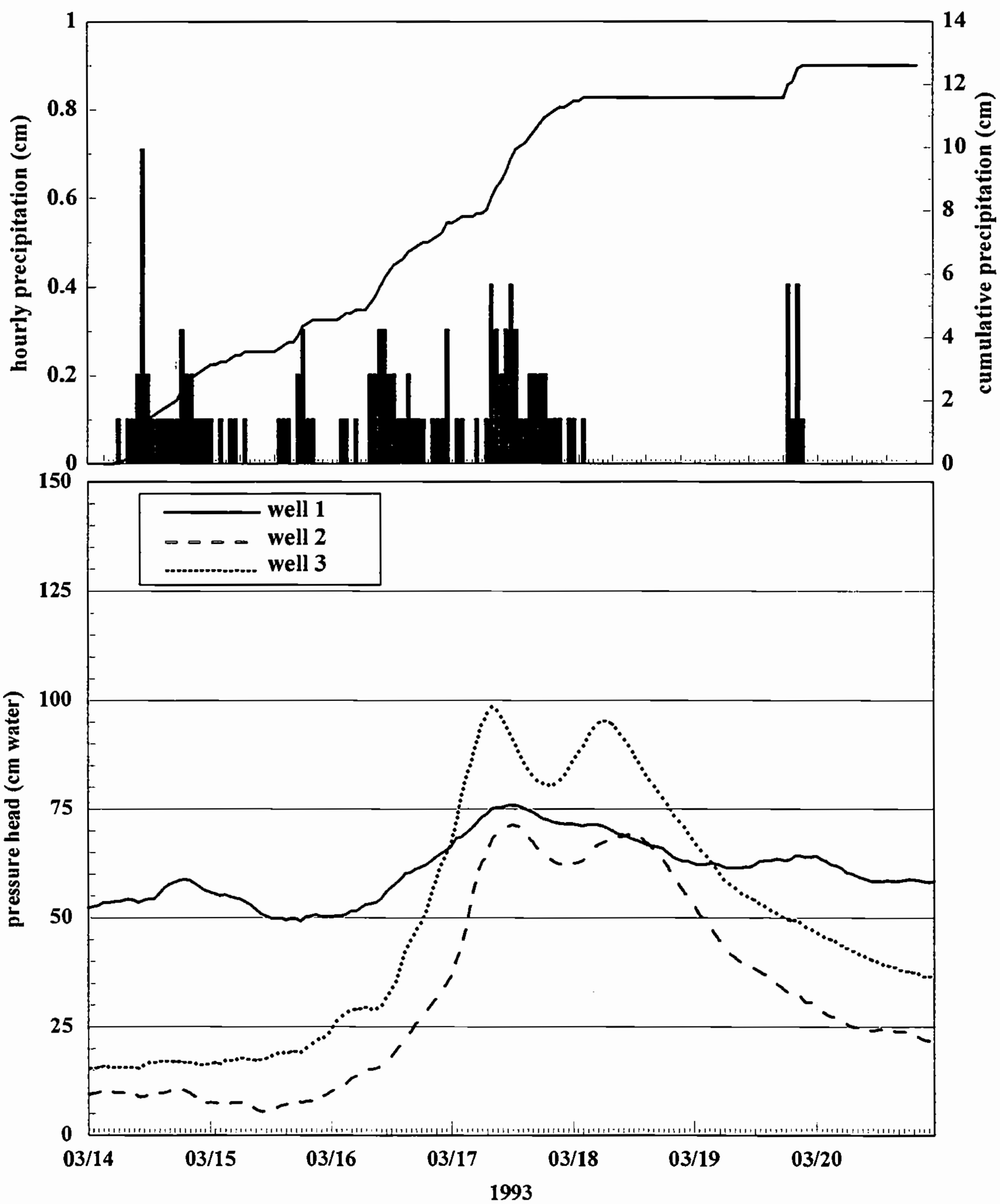

Figure 5.6 Observed pressure head at wells 1-3 during Storm 1.

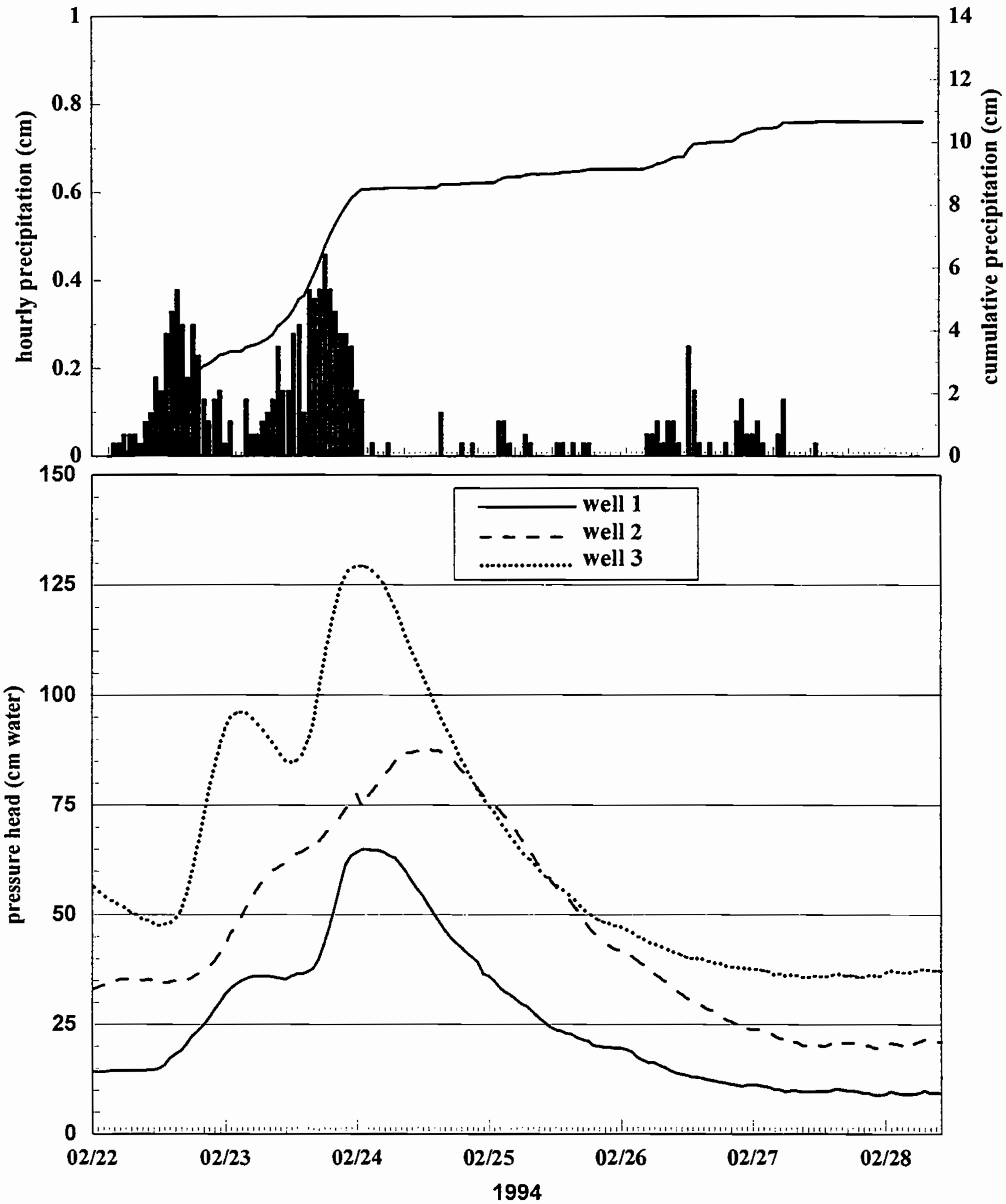

Figure 5.7 Observed pressure head at wells 1-3 during Storm 2.

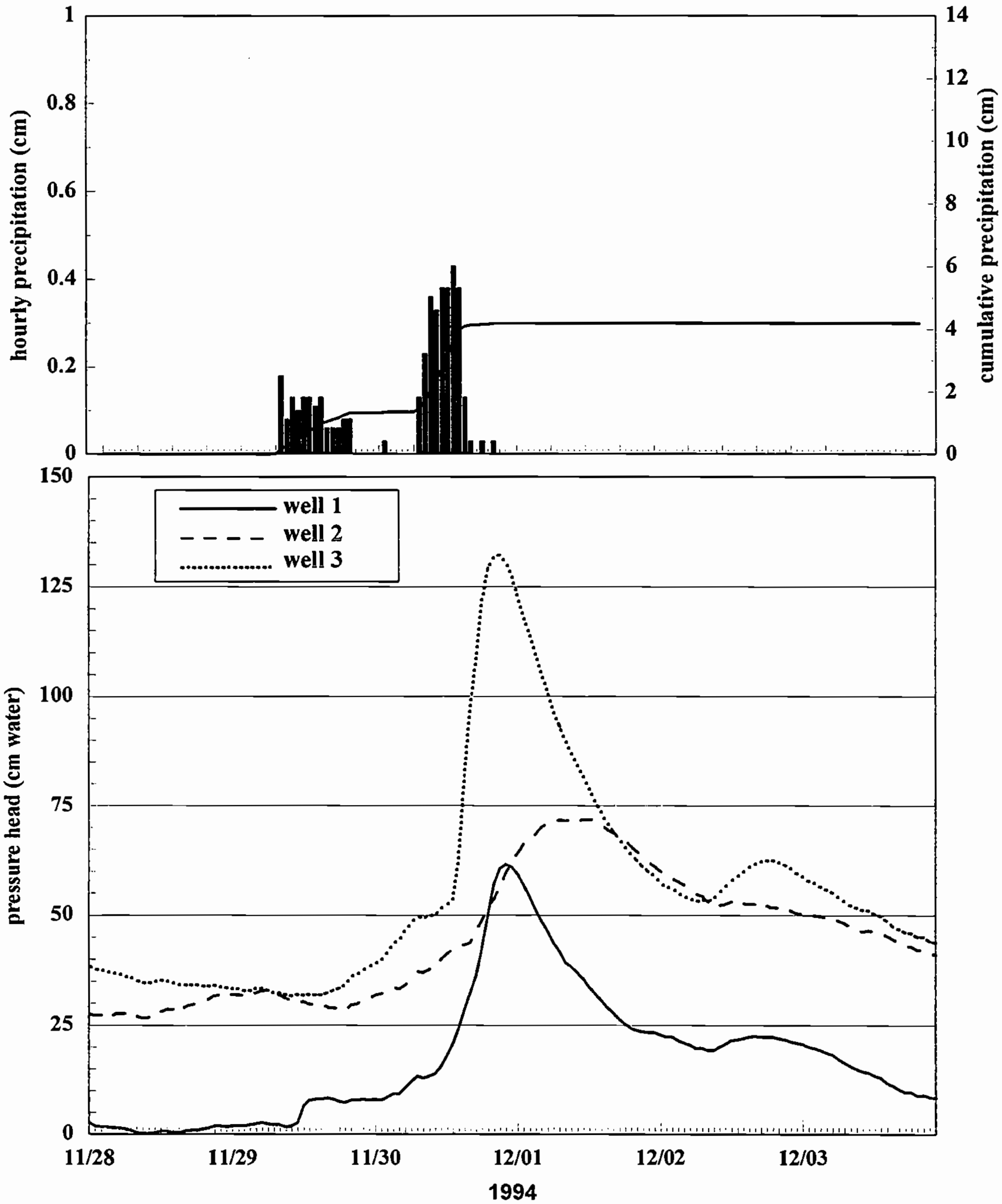

Figure 5.8 Observed pressure head at wells 1-3 during Storm 3.

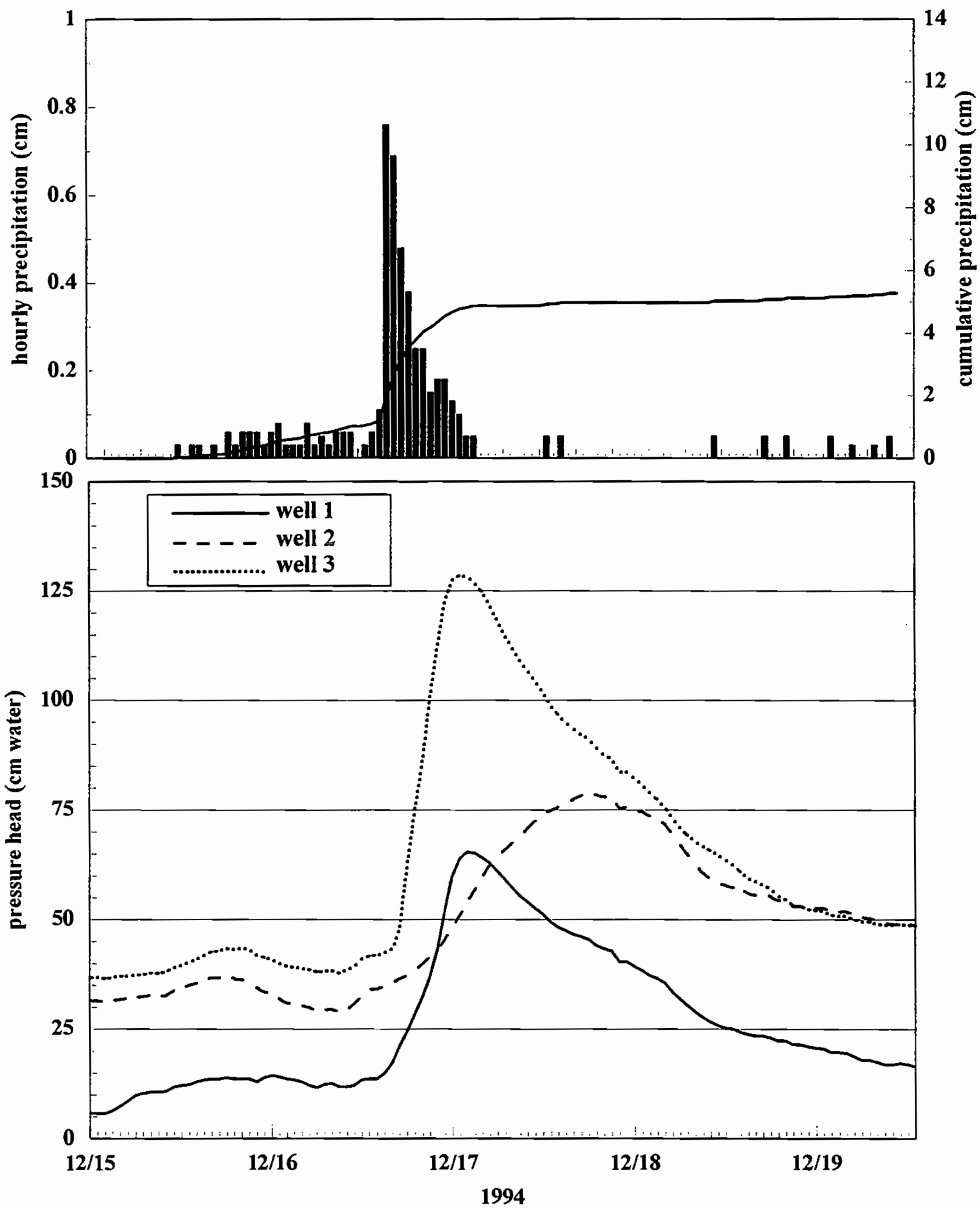

Figure 5.9 Observed pressure head at wells 1-3 during Storm 4.

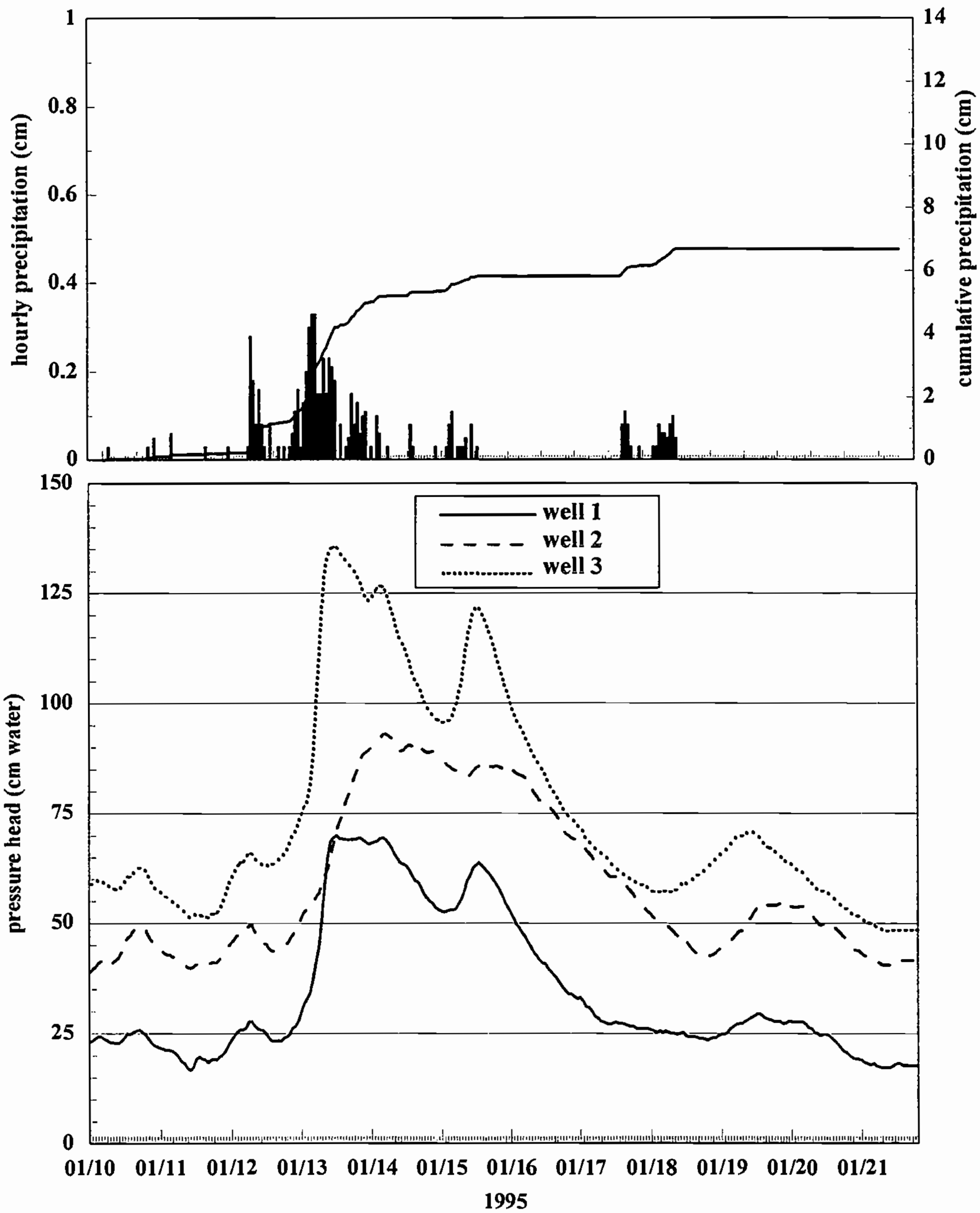

Figure 5.10 Observed pressure head at wells 1-3 during Storm 5.

The relationship between API and pressure head is both non-linear and hysteretic. Fedora (1987) found that API based models of streamflow typically over-predicted discharge on the rising limb of the hydrograph, and under-predicted peak and recession limb discharge due to hysteresis in the API - discharge relationship. It was determined that the degree of hysteresis in the pressure head - API relationship could be reduced by lagging the API variable relative to pressure head. However, the optimum time lag was not the same for all the storms. On average, the best time lag for the calibration storms was six hours. Therefore, API was delayed by six hours relative to pressure head for the regression analysis. Figure 5.11 shows a plot of pressure head at a well versus API_t and API_{t-6} for one storm event, showing the reduction in the hysteresis resulting from the time lag.

5.4.1.1 Single Storm Analysis

After determination of the optimal hydrograph recession coefficient, and calculation of API, regression analysis was carried out for the individual storms to develop a set of equations relating API to pressure head in the wells. Based on the non-linearity of the API - pressure head relationship, a second order term was added to the regression models. Following initial model development it was determined that improvements could be made by delaying the API values by six hours to reduce the degree of hysteresis in the relationship. While the magnitude of the regression

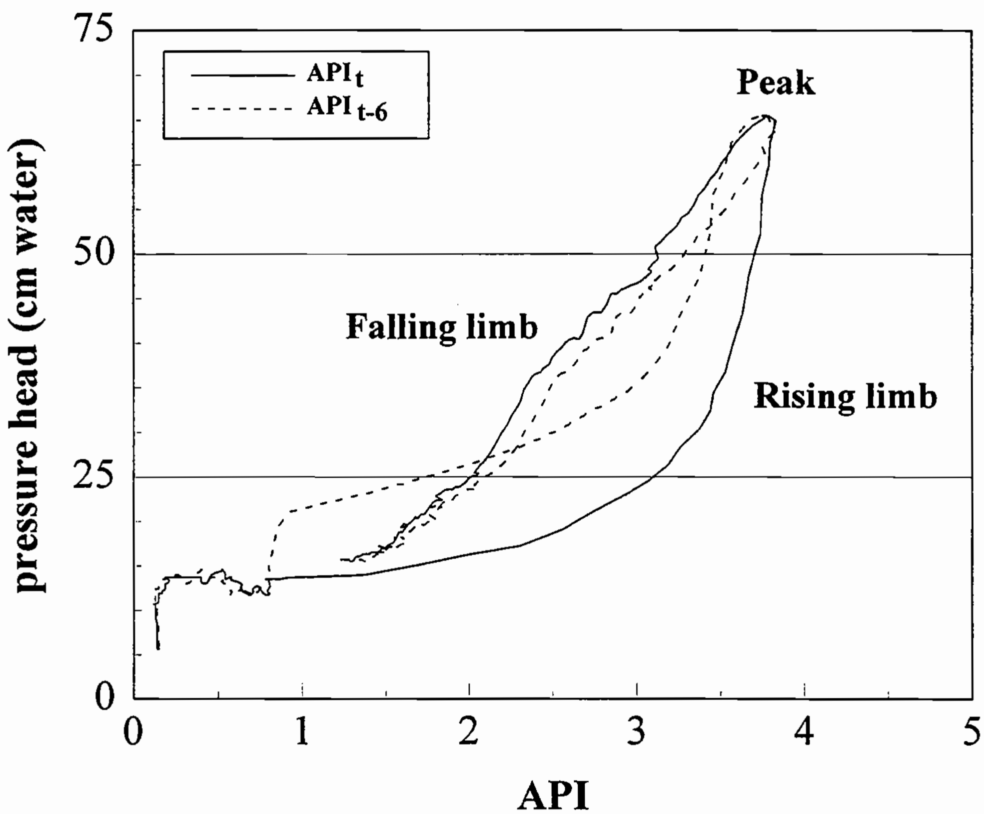

Figure 5.11 Plot of pressure head versus API for a storm event showing hysteretic relationship.

coefficients of the two models do not differ greatly, the resulting hydrograph is shifted in time for the majority of the storms. Resulting equations have the form

$$\hat{h}_t = \beta_0 + \beta_1 x API_i + \beta_2 x API_i^2 \tag{5.1}$$

where $\hat{h}_t$ is predicted pressure head at time t, β_0, β_1, β_2 are regression coefficients, *API* is the antecedent precipitation index and the subscript *i* denotes either API at time t or API at time t-6 hours. Table 5.5 shows the coefficients of the regression model with the independent variable API_{t-6}, for well 1 for the five largest storm events. Table 5.6 reports the coefficients of determination, r^2, of the regression models for wells 1-3 for the five storms for the same model. Figures 5.12-5.16 show observed and calculated pressure head values for the five storm events for well 1for both the API_t and API_{t-6} models.

Table 5.5 Coefficients of the API_{t-6} regression models for pressure head at well 1.

Storm	β_0	β_1	β_2
1	53	0.63	0.25
2	8.3	-3.3	1.4
3	0.50	9.6	2.0
4	12	2.6	4.3
5	18	5.2	2.9

Table 5.6 Adjusted coefficient of determination, r^2, of the API_{t-6} regression model for well 1-3 for the five largest storms.

Storm	Well	Adjusted r^2
1	1	0.57
	2	0.84
	3	0.81
2	1	0.84
	2	0.82
	3	0.67
3	1	0.91
	2	0.81
	3	0.87
4	1	0.98
	2	0.85
	3	0.76
5	1	0.78
	2	0.61
	3	0.75

5.4.1.2 Multiple Storm Analysis

The coefficients of the regression models for well 1 (Table 5.5) can be seen to differ significantly among storms. This is due to the variability in magnitude of API values and initial pressure head at inception of a storm. These factors would obviously make a particular model a poor predictive tool for a storm with dis-similar characteristics. To develop a more robust model, multiple consecutive storm events

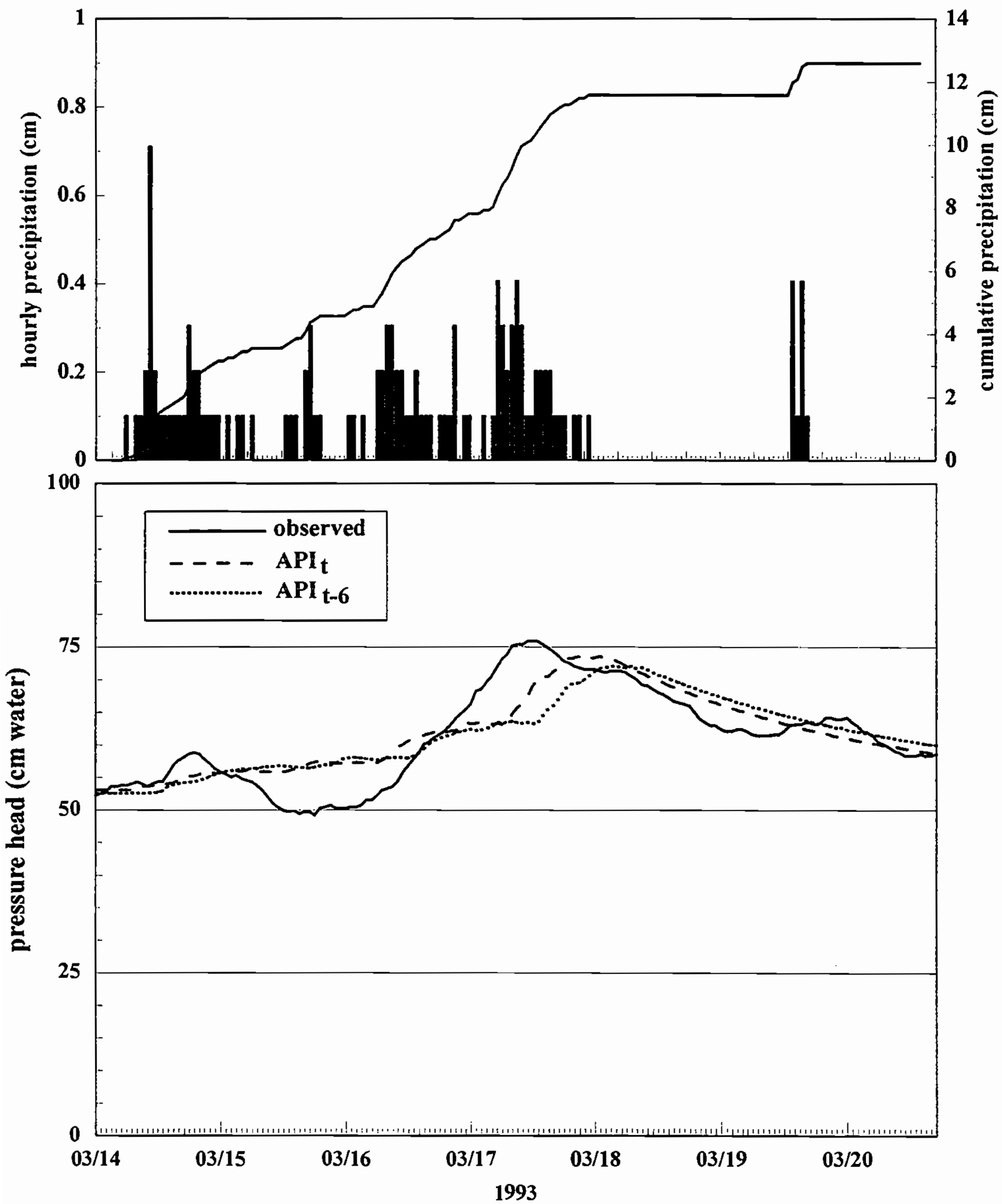

Figure 5.12 Observed and API calculated pressure head at well 1 for Storm 1.

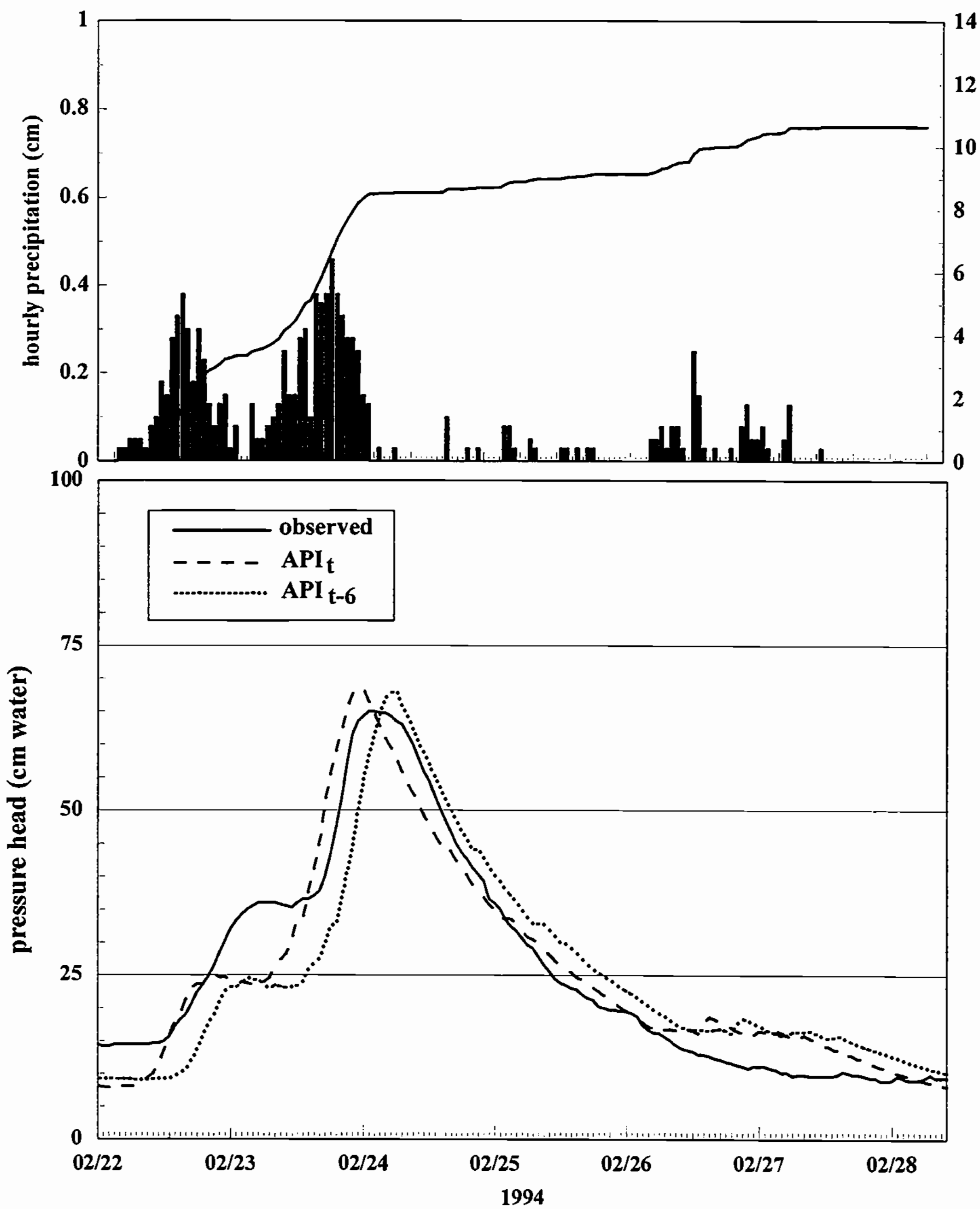

Figure 5.13 Observed and API calculated pressure head at well 1 for Storm 2.

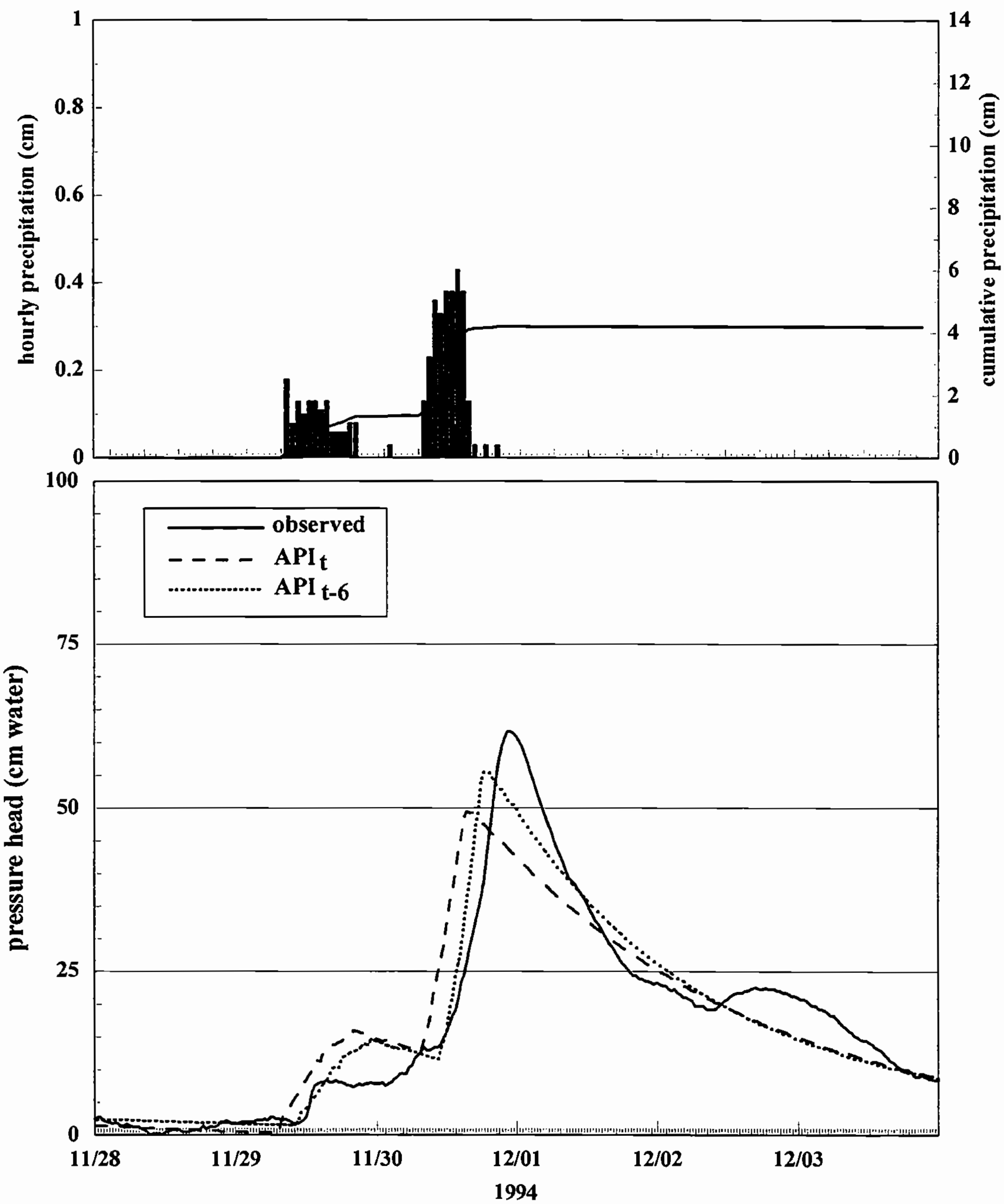

Figure 5.14 Observed and API calculated pressure head at well 1 for Storm 3.

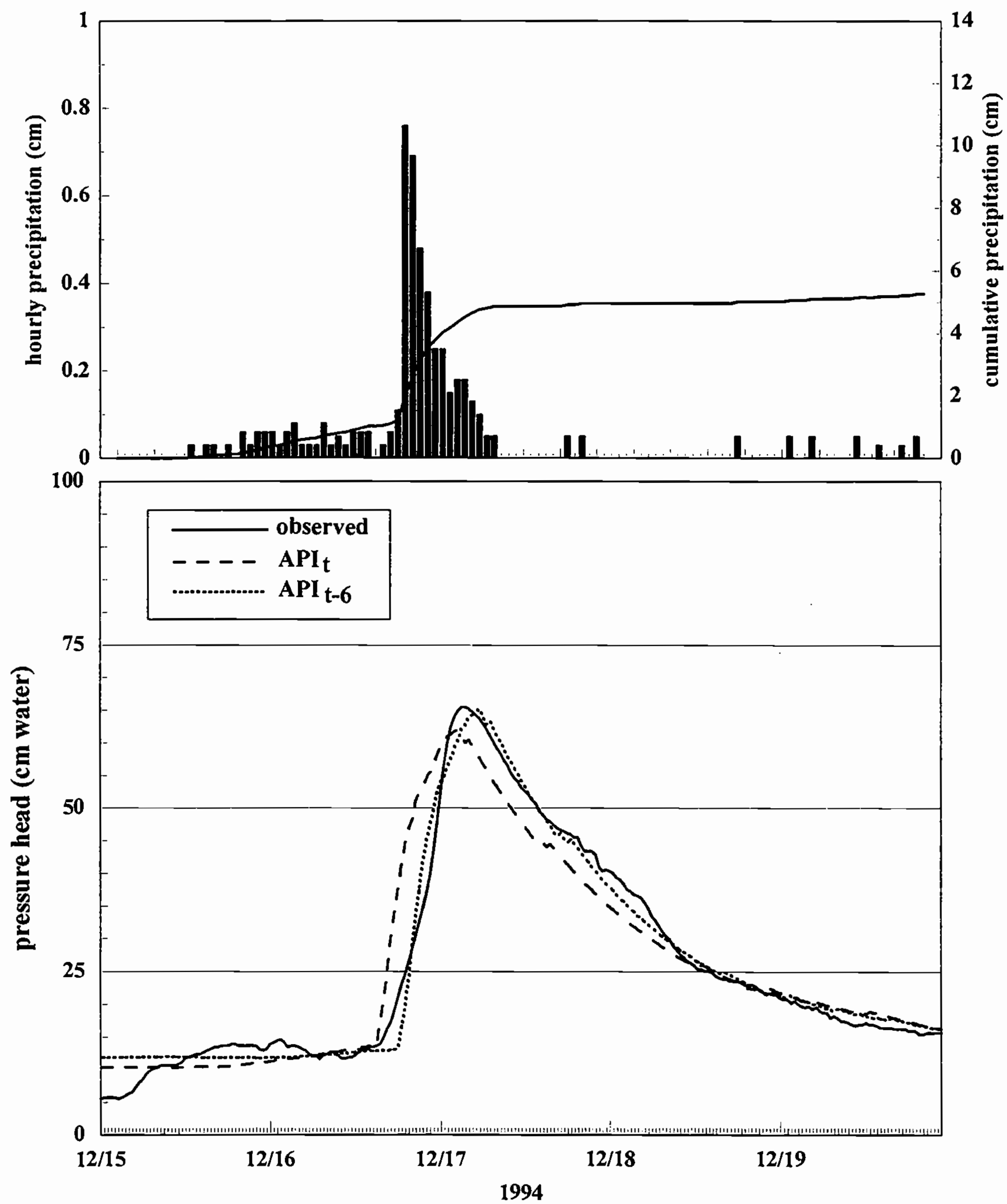

Figure 5.15 Observed and API calculated pressure head at well 1 for Storm 4.

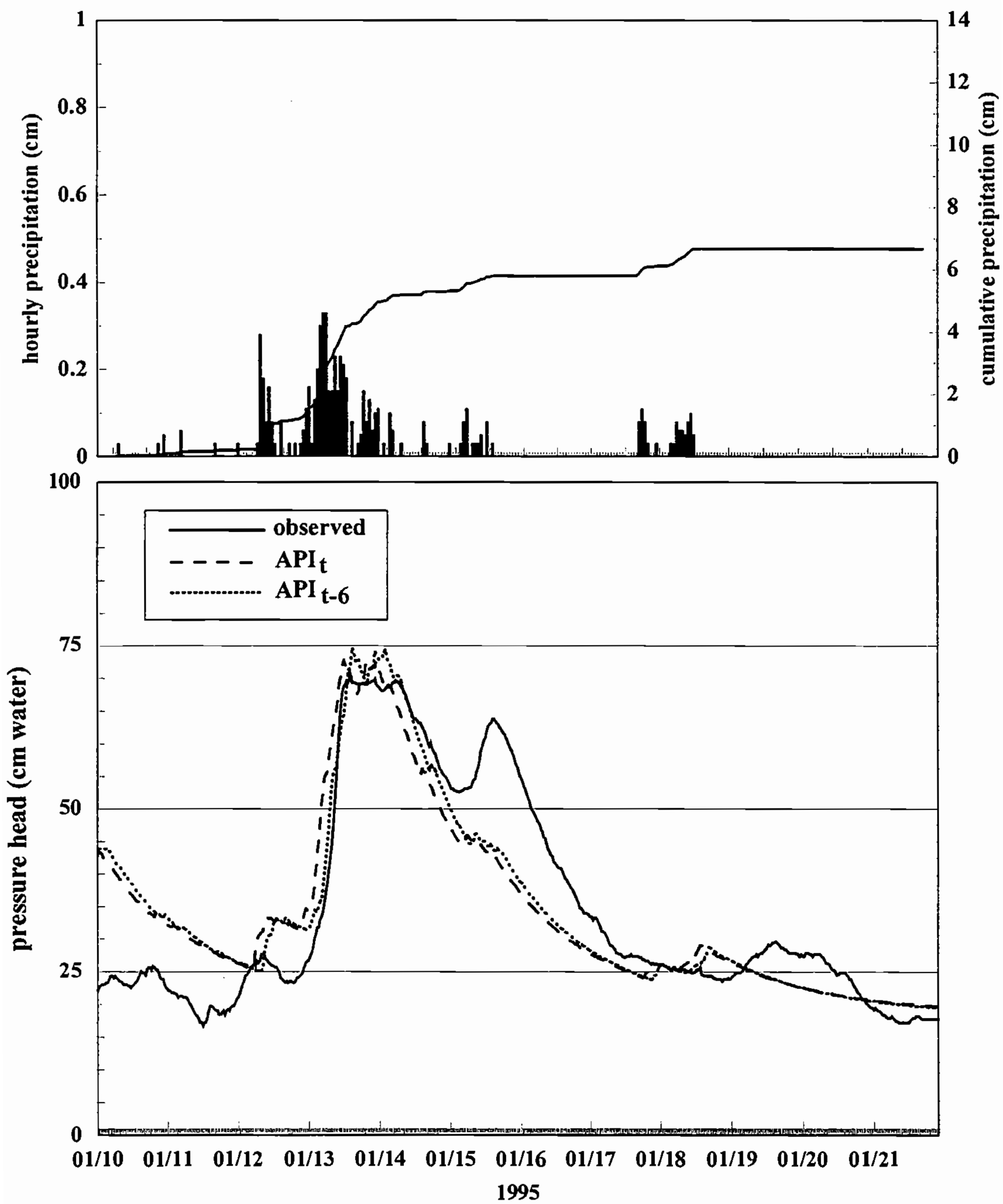

Figure 5.16 Observed and API calculated pressure head at well 1 for Storm 5.

were combined for analysis. Data for Storms 3 and 4 were combined and a single equation using API as the independent variable was developed. This equation was then used to predict the pressure head response in well 1 for Storm 5. Results of this analysis are shown in Figure 5.17 and Figure 5.18.

5.4.1.3 Two Sample Testing of Observed and Predicted Pressure Head

In order to determine whether the predicted pressure head values could be described as having similar measures of central tendency as the observed values, two sample testing of observed and predicted values of pressure head was done. One test paired the observed peak head value with the predicted peak head value for the five storms. A second test paired the difference between observed peak head and observed head at the beginning of the storm, with the difference between predicted peak head and predicted head at the beginning of the storm. The latter test was done to determine a measure of the quality of the predicted rising limb of the hydrograph. Tests of normality of the data suggested that the observed data were nearly normally distributed while the predicted values were less so. Peak values were more nearly normally distributed than were the differenced values. However, results of the Kolmogorov-Smirnoff two sample test suggested that the pairs of samples were not from different distributions.

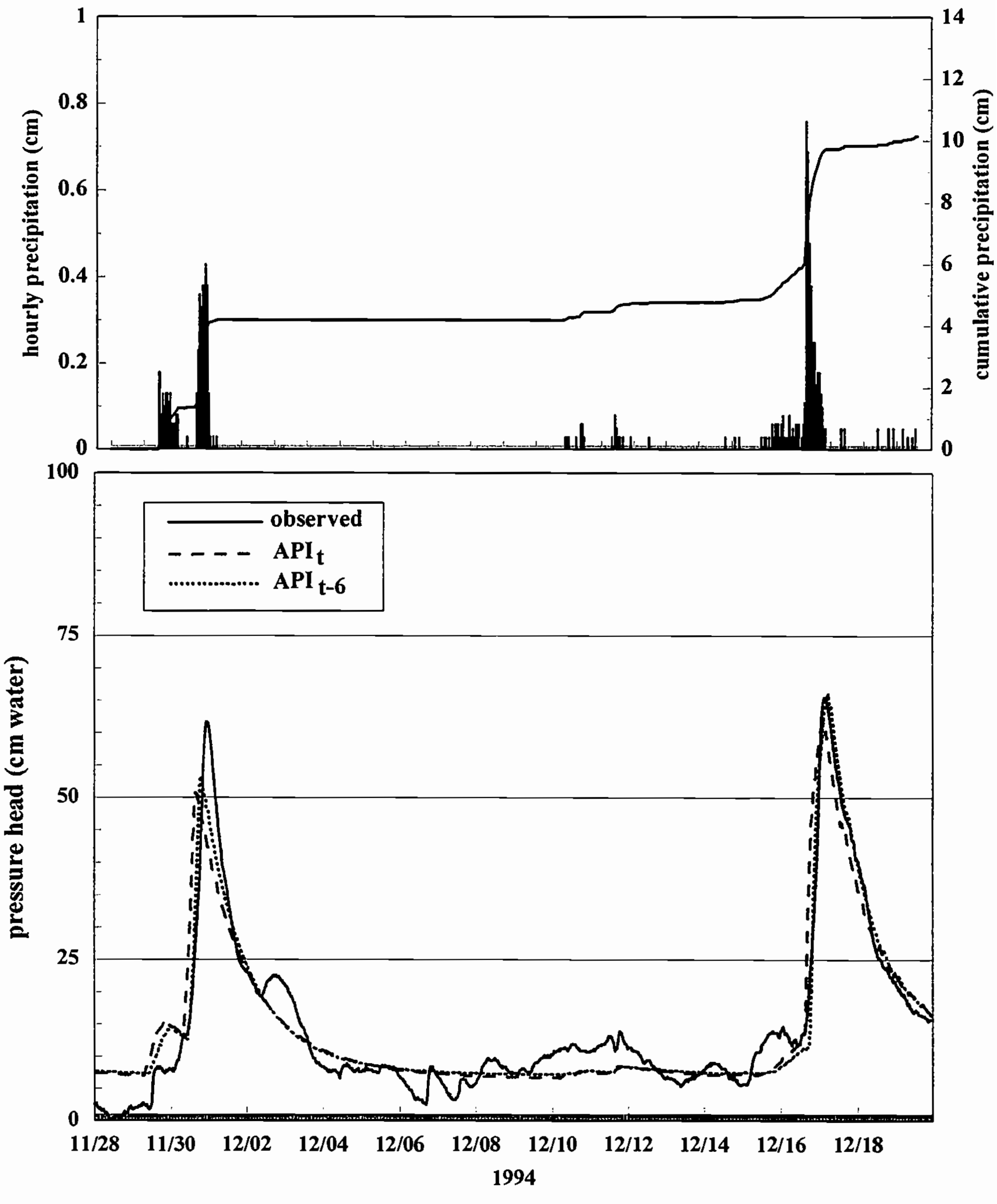

Figure 5.17 Observed and API calculated pressure head at well 1 for Storms 3 and 4 using multi-storm analysis.

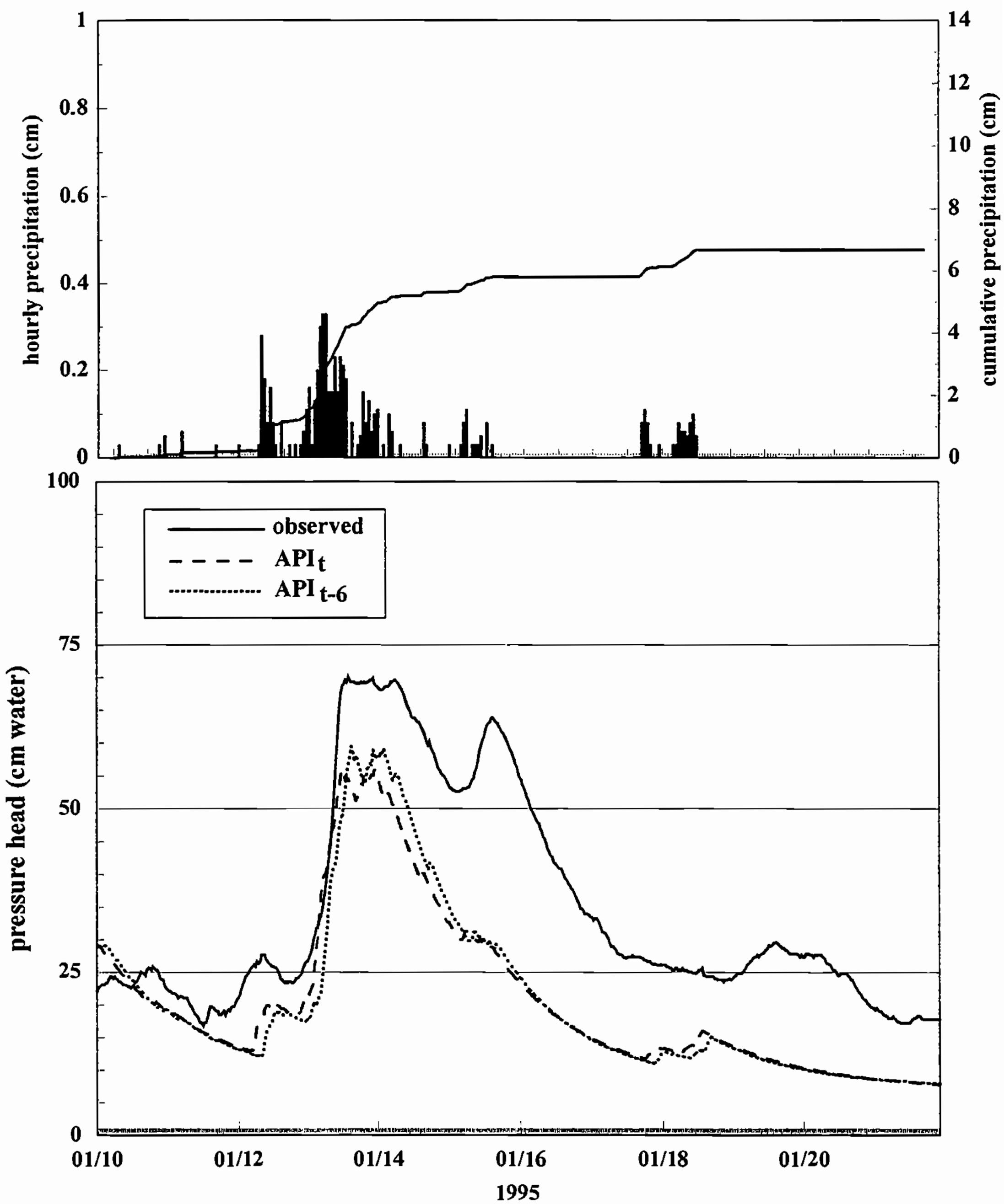

Figure 5.18 Verification of the multi-storm API model for pressure head at well 1 for Storm 5.

Based on these results, both a standard t-test and a non-parametric paired sample test was performed, with identical results. The Wilcoxon signed ranks nonparametric test results are presented in Table 5.7.

Table 5.7 Results of the Wilcoxon signed ranks tests for observed and calculated pressure heads.

	Test	
	Peaks	Differences
H_0 for means	$h_{obs}-h_{pred} = 0$	$(h_{peak}-h_0)_{obs}-(h_{peak}-h_0)_{pred} = 0$
H_A for means	$h_{obs}-h_{pred} \neq 0$	$(h_{peak}-h_0)_{obs}-(h_{peak}-h_0)_{pred} \neq 0$
α	0.05	0.05
$Z_{critical}$	1.96	1.96
Test Statistic	1.64	2.50
P value	0.10	0.012
Decision	**do not reject H_0**	**reject H_0**

5.4.2 Results of Kinematic Storage Modeling

Precipitation data and pressure head data from well 1 for Storms 2, 3, and 4 were used to calibrate the kinematic storage model described in Chapter 4. Storm 1 was not used in the calibration because of the uncharacteristic "flat" hydrograph observed for well 1. Table 5.8 shows the values of hillslope parameters used in the model runs.

Table 5.8 Hillslope parameter values used in calibration and verification of the kinematic storage model.

Parameter	Value
L	102 meters
D	1.4 meters
α	0.5411 rad
L_c / w	1.26

Three sets of model runs were performed using values of drainable porosity, θ_d, determined by the methods described in section 4.8.2.3. The value of saturated hydraulic conductivity, K_s, was adjusted to replicate the observed hydrograph of each of the three storms. Use of the drainable porosity determined by the method of Bear (1972) resulted in poor hydrograph fits. Results using the modified Bear and piezometric response methods were similar to each other, and much improved over the former results. The value of drainable porosity from the modified Bear method was almost identical to the average value from the piezometric response method for the three calibration storms. Simple arithmetic mean values of drainable porosity and saturated conductivity from the three calibration storms for the modified Bear method were then used in verification of the model using precipitation data from Storm 5. Results of the model calibration and verification are shown in Figure 5.19 - 5.22. Table 5.9 shows the values of drainable porosity and hydraulic conductivity used in the model runs.

Table 5.9 Drainable porosity determined by several methods, and corresponding saturated hydraulic conductivity, used in calibration and verification of the kinematic storage model.

	Bear (1972)	Modified Bear	Piezometric Response
Calibration			
Storm 2			
θ_d (cm^3/cm^3)	0.40	0.15	0.17
K_s (cm/s x 10^{-3})	13.9	16.7	16.0
Storm 3			
θ_d	0.40	0.15	0.10
K_s	5.6	8.6	8.6
Storm 4			
θ_d	0.40	0.15	0.12
K_s	5.6	7.6	9.2
Verification			
Storm 5			
θ_d	---	0.15	---
K_s	---	11.3	---

5.4.3 Comparison of Model Results

As a means of quantitatively measuring and comparing the results of the API and kinematic storage modeling, regression analysis was conducted. Predicted pressure head was regressed on observed head for the two API models (API_t and API_{t-6}), and the kinematic storage models for the three methods of estimating drainable porosity (Bear, modified Bear, and piezometric response). The results of the regression analysis are presented in Table 5.10 for the three calibration storms.

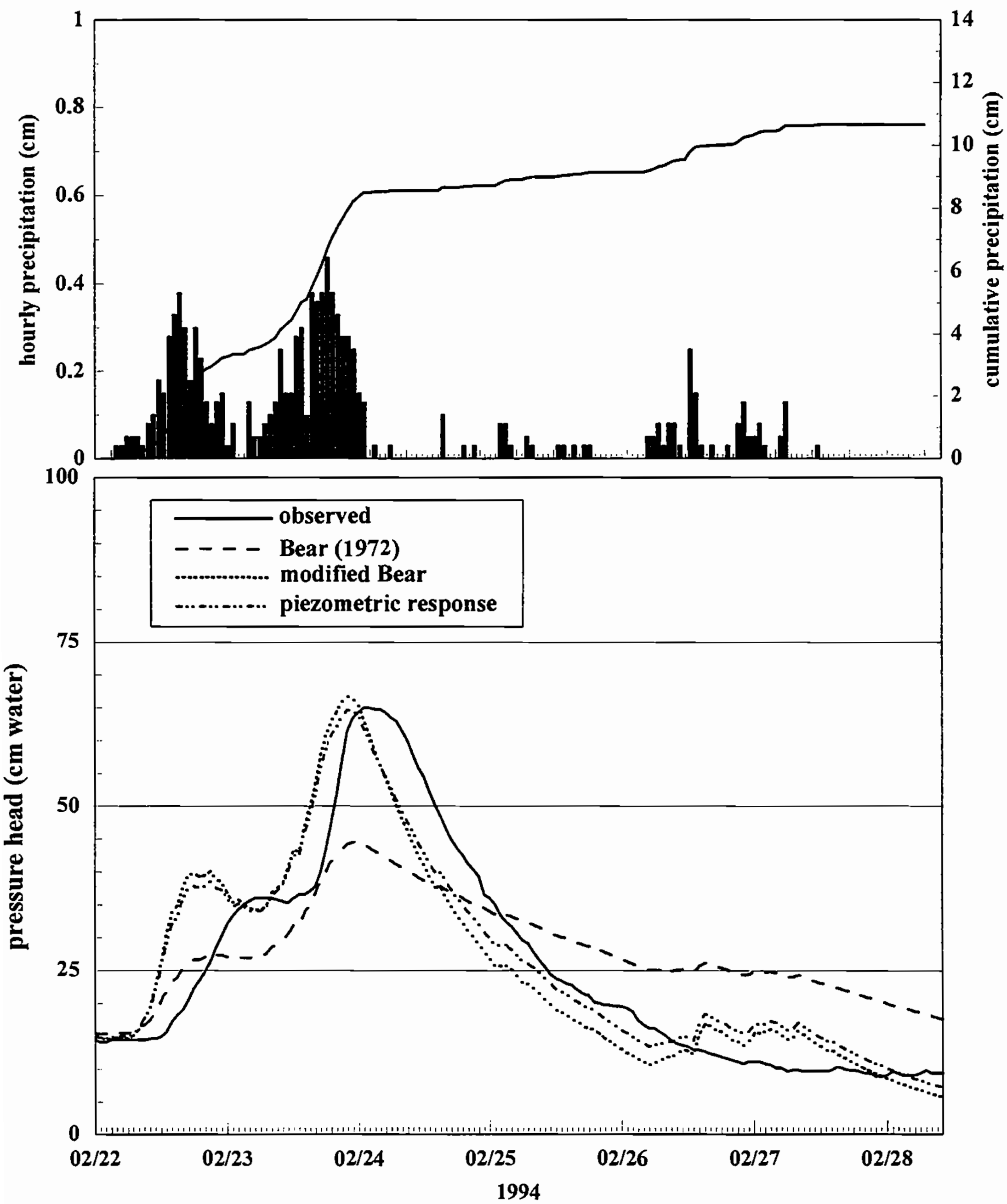

Figure 5.19 Observed and calculated pressure head using kinematic storage model at well 1 for Storm 2.

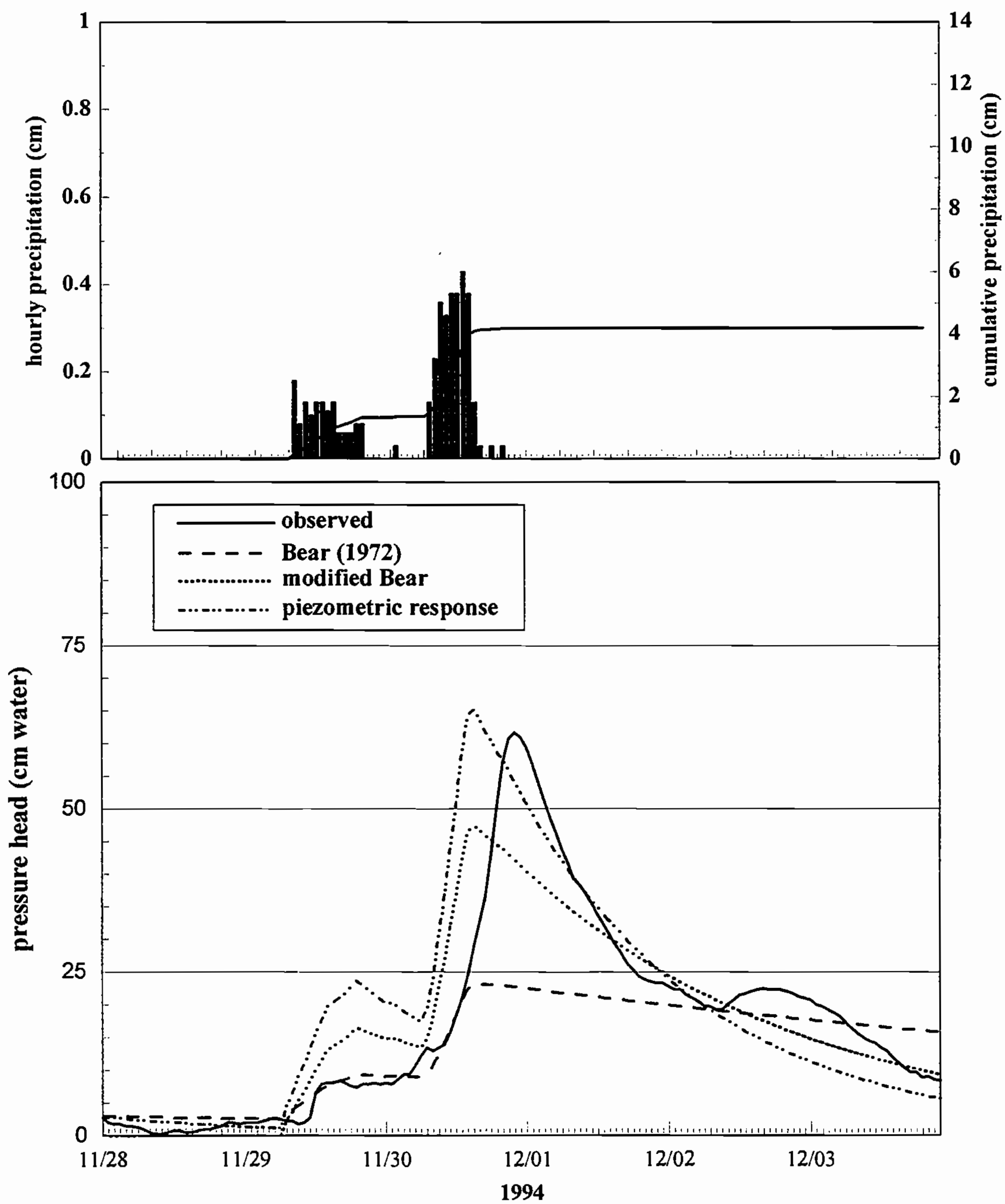

Figure 5.20 Observed and calculated pressure head using kinematic storage model at well 1 for Storm 3.

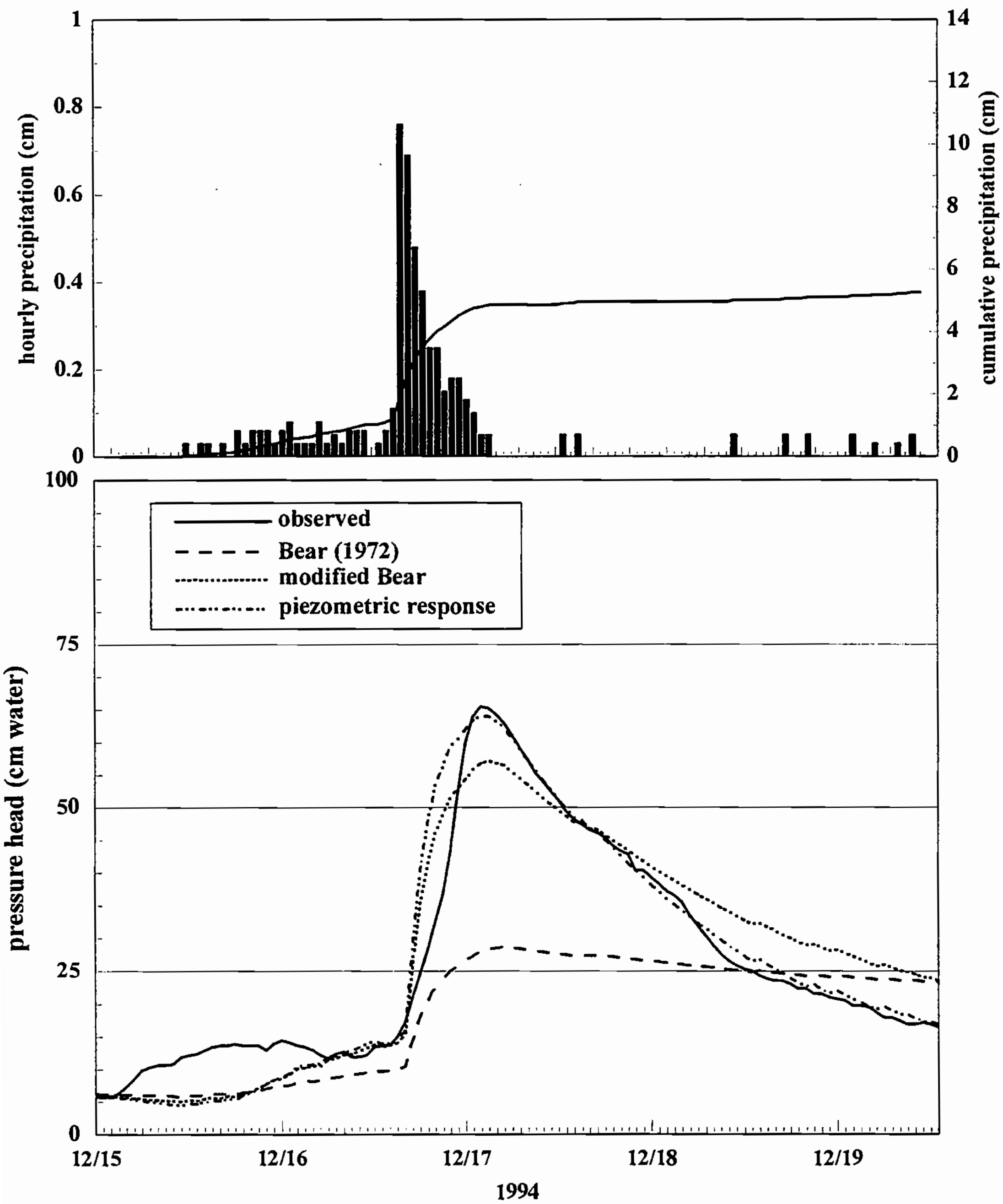

Figure 5.21 Observed and calculated pressure head using kinematic storage model at well 1 for Storm 4.

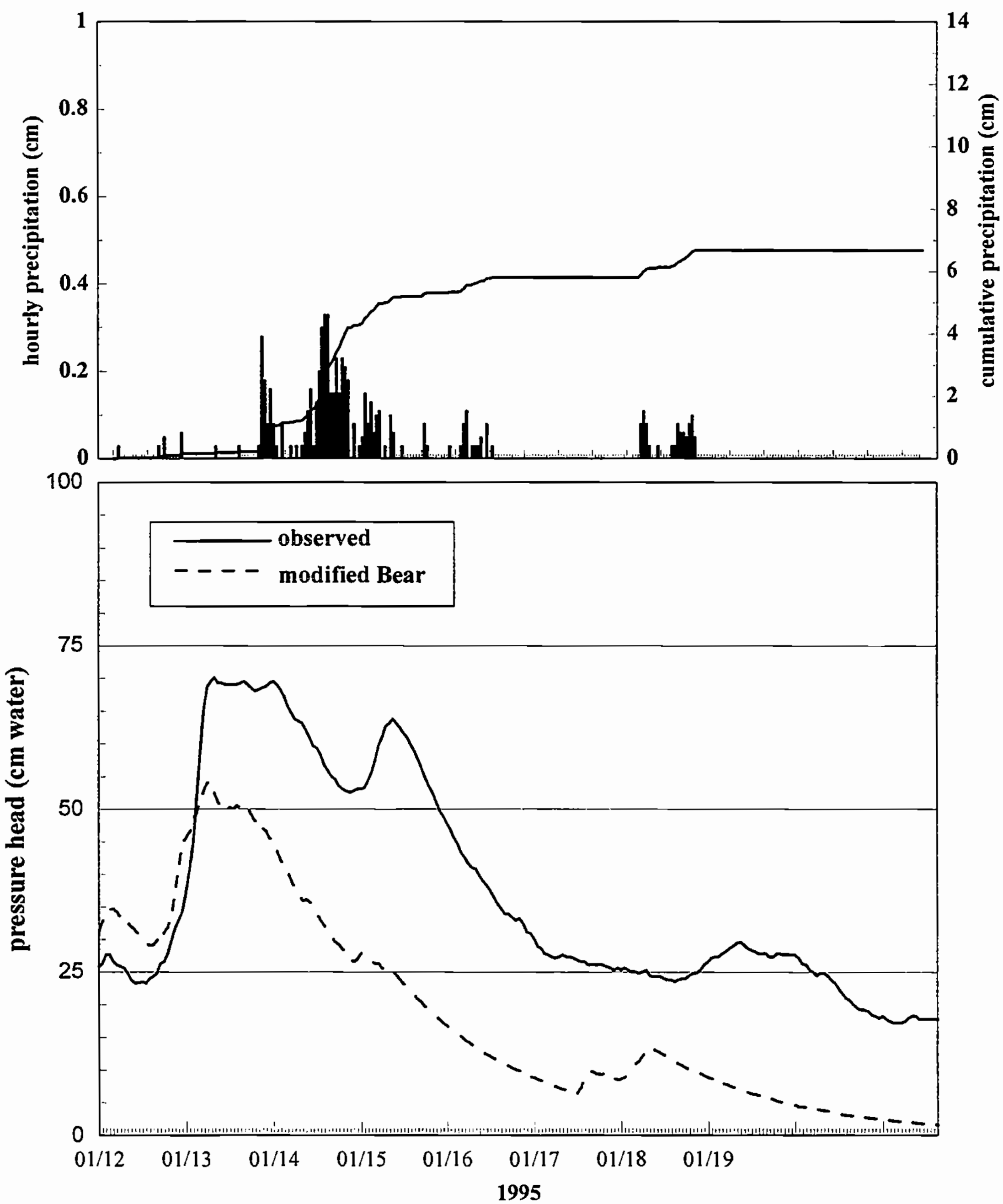

Figure 5.22 Verification of the kinematic storage model for pressure head at well 1 for Storm 5.

Table 5.10 Coefficient of determination, r^2, from regression of predicted head on observed head for the API and kinematic storage models.

	r^2 from regression of predicted head on observed head for the following models				
Storm	API		Kinematic Storage		
	API_t	API_{t-6}	Bear	modified Bear	piezometric response
2	0.91	0.84	0.83	0.79	0.84
3	0.80	0.91	0.71	0.80	0.67
4	0.90	0.98	0.61	0.89	0.93
mean r^2	0.87	0.91	0.72	0.83	0.81

5.5 Macropore Flow Measurements

Observations of macropores in the soil profile made during excavation suggested that macropore flow could be anticipated during wet antecedent conditions and high flow periods. A minimum of one event of macropore flow was considered necessary to allow testing of the macropore flow measurement scheme before data collection could begin. However, during three winters of monitoring, only three episodes of saturated flow above bedrock were observed at the trench face. None of the events allowed sufficient time to install and test the measurement equipment because of the highly transient nature of the saturated conditions. During Storm 1, some crude discharge measurements were made using a flask and stop watch, that allow some general comments to be made regarding macropore flow at the site.

On March 16, 1993 at 1400 hours, saturated flow at the trench face was observed at Site 2, including numerous active macropores. The largest macropores varied in size from approximately 2.5 centimeters to 7.5 centimeters in diameter. Pores of this size are among those thought to be involved in rapid movement of saturated flow through soils in the forest environment. All active macropores were located in the bottom 30 centimeters of the soil profile above bedrock. Figure 5.6 (Storm 1) shows the precipitation and pressure head hydrograph at well 1, just up-slope of the trench face, for the time period of the macropore flow observations. Three of the active macropores were discharging water in sufficient quantity to make crude measurements. One pore had a flow rate of approximately 8 liters/minute (133 cm^3/s); a second pore was discharging water at approximately 6 liters/minute (100 cm^3/s); a third pore, flowing less than full, was discharging at approximately 1 liter/minute (17 cm^3/s). At the remaining pores, it was not possible to make discharge measurements because water was exiting the pore and running down the face of the profile. The estimated discharge from the remaining active large (> 2.5 cm) macropores was 3 liters/min (50 cm^3/s). An estimate of total discharge at the face, including seepage flow from the soil matrix, was approximately 25 liters/minute (416 cm^3/s). From these measurements, the macropores were discharg-ing approximately 70% of the total flow at the face during this event. During two other events, saturated flow was observed exiting the profile above bedrock. In this instance, however, no active macropores were observed. Seepage flow was occur-ring in the lower 25 centimeters of the profile, and significant flow was occurring along bedrock at the base of the profile, as had been observed during and after numerous other storm events.

5.6 Pore-pressure Ratio Analysis

Slope stability models typically include a parameter describing the relationship between pore-pressure at a point and soil depth at that point. The dimensionless pore-pressure ratio, r_u, was described in section 4.9. Figure 5.23 shows a plot of r_u for wells 1-3 for Storm 2. Plots for the other storm events were similar in character. Results of this analysis will be discussed in the context of slope stability modeling.

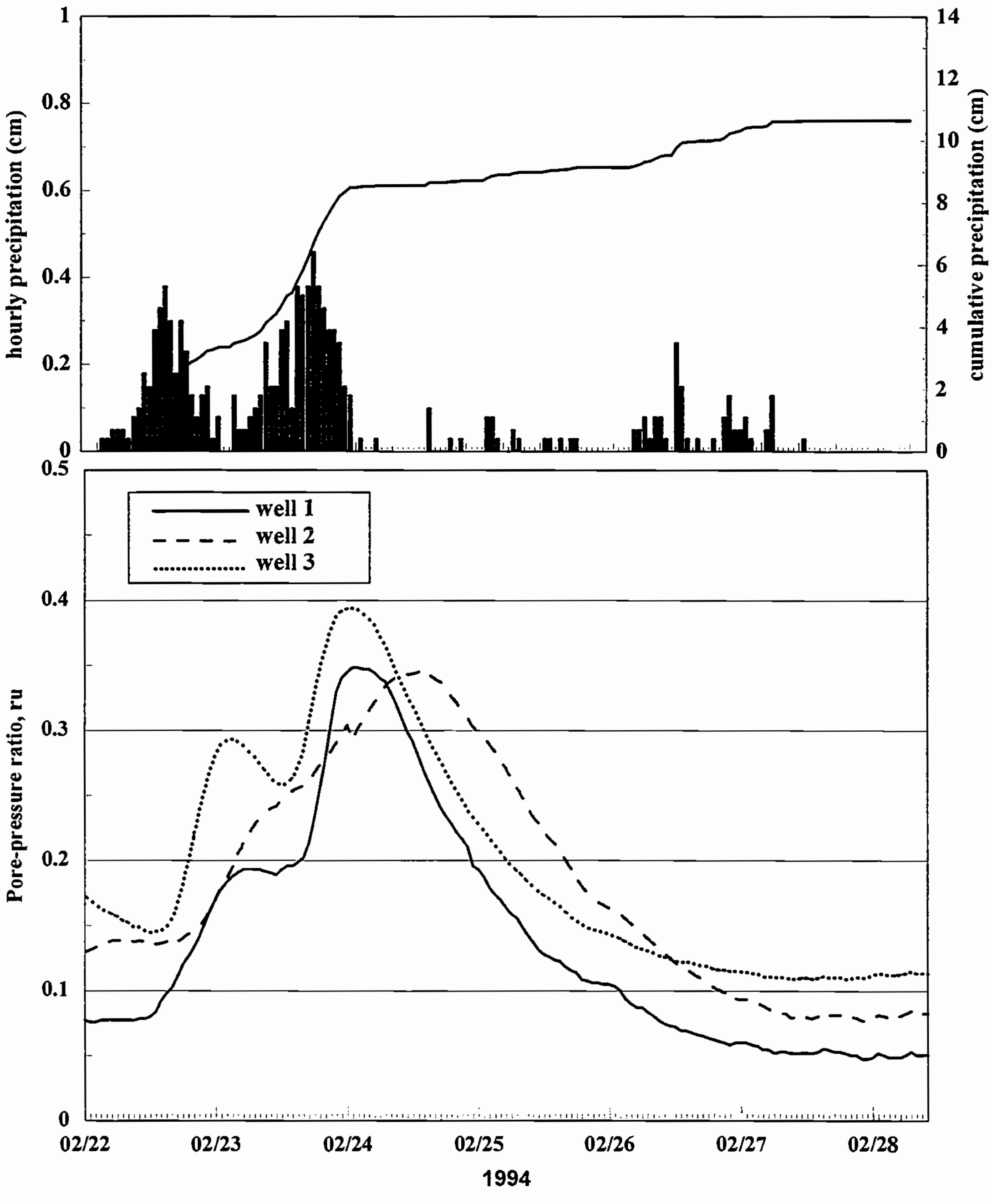

Figure 5.23 Pore pressure ratio, r_u, at wells 1-3 during Storm 2.

6. DISCUSSION

This section will begin with a discussion of the characteristics of the sites, the properties of the soil, and comparisons with published results. Secondly, components of the monitoring effort will be discussed. Lastly, results of the Antecedent Precipitation Index modeling and the kinematic storage modeling efforts will be evaluated. Data collection on the McDonald Research Forest (Site 1) was extremely limited due to site conditions and equipment malfunction. Consequently, discussion of results will focus on the Honey Grove Creek monitoring site (Site 2).

The two instrumented sites have properties that are common to headwalls in the Oregon coast range where landslide potential is considered to be of moderate to high risk. Both sites are steep, near-ridge depressions, with evidence of colluvial activity. Surface topography suggests converging groundwater flow would be expected, particularly on Site 2. At Site 2, surface water channelization occurs just downhill of a constricting topographic point. Large overstory vegetation is scarce on the depression, but is found primarily around the margins of the headwall. These features are common on unstable headwalls throughout the coast range.

Results of the soil testing suggest that the soils of Site 2 are quite similar to those found throughout forested slopes of the coast range. Testing of soil hydraulic properties also suggests similarities with other soils in the vicinity.

6.1 Soil Testing

Results of soil testing by this and a related investigation will be discussed. Soil index properties were determined by this study, and that of Morgan (1995) for different soil samples from Site 2. Soil strength parameters were determined by Morgan (1995) in an analysis of methodology for determination of strength properties of marginally stable forest soils.

6.1.1 Soil Index Properties

Forest soils of the Douglas-fir region are typically highly porous, and have low bulk density. As a result of these characteristics, the soils tend to have high infiltration rates and hydraulic conductivity (Heilman, et al. 1979). Precipitation rates rarely exceed infiltration rates, and overland flow is uncommon. The index properties of the soil on Site 2 are generally consistent with reported data for similar soils. The unit weight of the soil reported by Morgan (1995) ranged from 13.1 kN/m^3 to 13.4 kN/m^3. These values are considered to be at the upper end of the range of unit weights for forest soils of the region. At the lower end of the range, Bransom (1991) found an average unit weight of 9.75 kN/m^3 using a nuclear density gauge in forested headwall soils in the central Oregon coast range. During additional soil sampling for hydraulic property tests for the current investigation, calculation of unit weight from soil cores for the soil on Site 2 produced values averaging approximately 12.5 kN/m^3. The average soil unit weight determined by Yee (1975) for similar soils was 11.7 kN/m^3. Different testing methods may account for the slight differences in values reported.

The Unified Soil Classification System group SM is common for colluvial soils of the region. These soils are silty-sands with little or no fines. Of twelve soils tested by Bransom (1991) from similar geomorphic and topographic settings, eleven soils were classified as SM, or had a dual SP-SM classification designating slightly higher plasticity of the fines. Yee (1975) classified the soils from his nearby study site as SM as well. Atterberg Limits of the soil compare closely with those reported by Bransom (1991) and Yee (1975) as well. Total porosity of the soil for Site 2 is approximately 0.53, and is within the range of values determined for similar soils (Bransom, 1991).

6.1.2 Soil Effective Strength Parameters

Morgan (1995) found the average ϕ' to be 29.7° for all soil samples tested at low confining pressures, and a ϕ' of 32.5° for the single undisturbed sample tested at low confining pressures. Bransom (1991) found an average ϕ' value of 31.1° and an average c' value of 0.67 kPa for coast range headwall soils tested using similar procedures. Higher values have been reported by other workers for similar soils. Schroeder and Alto (1983) conducted CU tests of forest soils from the Oregon and Washington coast range and reported average values of ϕ' on the order of 37.8°. Schoenemann and Pyles (1990) using a statistical procedure for describing shear strength test results, reported a ϕ' of 39.9° for the Schroeder and Alto test data. Yee (1975) reported an average value of 40° for the forest soils he tested. He considered the high value to result from highly stable soil aggregates in his samples. Differences in sample collection and handling, and differences in test procedures likely account for much of the variability in test results. In general, the soils described by the current study bear a high degree of similarity to those of the other studies, suggesting similar engineering behavior for many of the soils in the central coast range.

Standard geotechnical testing procedure has employed high confining pressures during triaxial testing of soil materials. However, shallow soils on steep slopes in the forest environment typically experience low in situ vertical confining stresses. In a study of strength parameters from 12 headwall soils in forest environments, Bransom (1991) determined the average overburden stress at bedrock was 12.8 kPa at field moisture levels, excluding the weight of vegetation. This value increased to 15.5 kPa assuming fully saturated conditions. Low confining pressure tests would seem to be more appropriate for use in stability modeling of shallow forest soils (Morgan, 1995).

6.1.3 Soil Hydraulic Properties

Experimentally determined values of the hydraulic conductivity function parameters, λ and η, were found to be 0.34 and 3 respectively for the sub-soil at Site

2. These values do not agree well with average values given by Brooks and Corey (1966) and Corey (1969), who suggest values of 2 and 8 for λ and η respectively for a typical sand. However, Corey (1969) suggests that highly structured soils will have lower values of λ and η. Yee (1975), working with soils similar to that of this investigation, found that the soils exhibited an exceptionally high degree of aggregation and aggregate stability. Yee found values of η to be approximately 2 for that soil, generally in good agreement with the findings of this study. Values of the air-entry pressure, ψ_a, determined in this study, also agree closely with the values determined by Yee. The value of saturated hydraulic conductivity that was obtained from calibration of the kinematic storage model suggests that the soil is near the middle of the range of typical conductivities for coarse clean sands or sands and gravels (Bear 1972, Domenico and Schwartz 1990). However, the role of macropore flow was determined to be important under certain precipitation and antecedent soil moisture conditions. Thus, the saturated conductivity may not be simply a matrix flow conductivity value, rather, it likely represents an "effective" hillslope conductivity value that includes matrix flow and macropore flow.

6.2 Precipitation Measurements

During the winter of 1992-1993, the DP101 data logger on Site 1 failed, apparently due to moisture condensation on the inside of the data logger. During the early winter months the tipping bucket mechanism failed at Site 2 failed, causing the bucket to stick in one position. By the end of that winter, it was clear that Site 1 was not going to be a productive site in terms of measurable subsurface flow. When repairs were made to the defective equipment, two gages were placed at Site 2 to provide redundancy. One gage was placed on the instrumented portion of the site, while the second gage was placed in a nearby clearcut at the same elevation and aspect. No significant difference in precipitation measurements between the two gages was observed at any future time, and the redundant gage was eventually removed for use on another research project.

The greatest difficulty in precipitation data handling stemmed from incompatibility of time-of-event recording mode used in precipitation measurements, and user-defined time interval used in well and tensiometer data collection. This incompatibility resulted in need for special pre-processing to put the precipitation data in the same time format as the well and tensiometer data. As a result, not all storm events were processed in the manner described. Typical winter storms of moderate duration and low intensity, that occurred between the extreme events reported, were not pre-processed. As a result, these data were not available for use in some of the modeling work.

6.3 Tensiometry

Selection of the particular type of instrument used in this study was perhaps inappropriate for the soil conditions on these sites. Instruments were commercially produced ceramic tip tensiometers with water reservoir refill caps. It appears that the instruments were damaged during installation, resulting in micro-cracks in the ceramic tips, or small leaks elsewhere in the tensiometer. A commercial insertion tool designed to cut a slightly undersized hole was used for installation.

During each site visit, the tensiometers would be filled, then allowed to equilibrate with the soil, then refilled as necessary to bring the water column to the required position in the tensiometer. During subsequent site visits, it was observed that the tensiometers were often drained below ground level. This variable head of water, therefore, makes it impossible to determine the soil capillary pressure from the transducer voltage reading. While the transducer readings consistently indicated sub-atmospheric conditions within the tensiometer, the uncertainty of the magnitude of the capillary pressure values in the soil renders the data quantitatively void of meaning.

Secondly, large diurnal fluctuations in voltage reading were observed in the transducers used with the tensiometers. Although temperature compensated, exposure on the south facing slope apparently had a large effect on pressure measurements, particularly during spring and early fall. Fluctuations in readings on a diurnal scale were nearly identical to the manufacturers specifications for temperature coefficient of the span of the instrument. The combination of these two operational difficulties make quantitative analysis of unsaturated conditions impossible.

Qualitative observations can be made for a period when certainty of proper instrument function is high. The relative tensiometer response to precipitation shown in Figures 5.4 and 5.5 does suggest some consistency with expected conditions. Figure 5.4 shows the relative response at three depths on contour. The capillary pressure is shown to decrease with depth. The 46 cm depth instrument is on the centerline of the headwall, while the 30 cm and 61 cm instruments are on the margins. This placement explains why the 46 cm and 61 cm depths are at closer capillary pressure than are the 30 cm and 46 cm depths; soil at the center of the depression is consistently at higher moisture content at all depths than is the soil at the margins.

Soon after the onset of precipitation, the capillary pressure begins to drop at all three depths, at nearly the same time. It appears that a slight increase in water content produces a signinficant increase in conductivity and that the increased connectivity of the pore structure results in almost simultaneous response to precipitation throughout the soil profile. As precipitation continues, capillary pressure reaches a minimum and remains nearly constant. Once precipitation ceases, capillary pressures increase to approximately pre-storm values. This process is repeated during the second cell of precipitation. The third precipitous drop in capillary pressure that occurs late on December 1, well after the cessation of precipitation, is thought to result from snowmelt. The snowmelt was likely recorded during the second storm cell by the tipping bucket rain gage, which was elevated above the forest floor approximately 2 m. Residual snow on the forest floor may then have melted when air temperatures rose. Wells also show a slight increase in pressure head shortly after the capillary pressure drop occurs (Figure 5.8).

The relative capillary pressure for a constant depth at different slope positions is shown in Figure 5.5. Again the relative position of the plots is consistent with expectations. The lower slope position, just above the topographic constriction, is at a higher moisture content than the mid-slope and upper slope positions, supporting the idea that converging flow is occurring. As with the tensiometric response along contour, there is not a significant temporal delay in response of the three zones to precipitation. As precipitation begins to fall, both the upslope and low slope positions show a rapid drop in capillary pressure, while the mid-slope position shows a much more gradual pressure drop. As the second, larger event begins, all three zones experience rapid pressure drop. However, as capillary pressure in the low slope position begins to level out, as occurred during the previous event, it again experiences a large pressure drop. Converging flux from upslope is likely responsible for this drop. As precipitation stops, capillary pressures continue to drop, but begin to return to pre-storm values relatively quickly for all three zones. The low slope position shows the most rapid increase in capillary pressure at the end of the storm. The recession of the hydrograph for the well in this zone (well 1) is not as rapid as that of well 3 in the upslope position. One explanation for this would be that the hydraulic gradient becomes more vertical downward at the low slope position, causing a more rapid increase in capillary pressure at this depth, than occurs upslope. The presence of the free face just below well 1 and the low slope tensiometer is the likely cause of this. The natural condition at the site was a free face that was less steep than that created to monitor saturated throughflow. The degree to which the altered free face has influenced the subsurface condition is unknown. However, it would seem likely that the influence was significant.

Lack of sound quantitative data about the conditions in the unsaturated zone can frustrate attempts to develop good deterministic models of subsurface flow. The kinematic storage modeling work suggests that the model is extremely sensitive to changes in the initial volumetric water content of the unsaturated zone. As a result of the lack of good information, the unsaturated flow model is subject to a high degree of uncertainty. Further, the significance of unsaturated subsurface flow in routing significant quantities of water down slope has been reported by Yee (1975) and others; the implications of this for slope stability analyses need to be considered when estimating positive pore-water pressures based on precipitation input, such as might be done with the API method. A more thorough knowledge of unsaturated conditions in the headwall would have made results of modeling efforts more certain.

6.4 Piezometric Response to Precipitation

The well point used in this study was designed to overcome some of the limitations of conventional piezometers when used in highly transient subsurface flow conditions. Namely, the piezometer was designed to avoid the significant time delay that can occur when a change in pressure head in the formation must be translated into a fluid volume change inside the piezometer in order to be measured (Hvorslev 1949, 1951). With the exception of a transducer failure due to leakage of a seal, a problem that was corrected in all but one of the well points, the piezometers appear to have functioned properly. Without a conventional piezometer in the immediate vicinity of those used, there is no way to be certain that the design was a success in meeting the stated objective. However, it does not appear from looking at the piezometer data that any excessive time lag, relative to timing of precipitation input, resulted from use of the well point. Therefore, it appears that the design functioned at least as well as conventional piezometers, if not better.

On steep slopes such as the sites monitored in this study, the subsurface flow regime, specifically the hydraulic head distribution, is dominated by gravity. The values of pressure head observed in the wells are overshadowed by the elevation head changes along the centerline of the headwall. It should be noted that regardless of the characteristics of the storm event, eg. total precipitation, maximum intensity, average intensity, etc., the peak pressure head at any particular well varies over a narrow range for all the storms. As discussed previously, the presence of the free face at the downslope end of the headwall has the effect of distorting the flow field upslope of the face. The degree to which this controls the narrow range of peak pressure head is uncertain. It is conceivable that there is another geohydrologic control, but the presence of the free face seems the most obvious. Also, Figures 5.6 - 5.10 show that peak pressure head increases going upslope along the centerline of the headwall from well 1 to well 3, for four of the five extreme storm events. This observation may also result from the presence of the free face. Further implications of this will be discussed in the context of slope stability.

6.4.1 Antecedent Precipitation Index Modeling

It was recognized that there exists a correlation between precipitation, antecedent precipitation and pressure head at the wells. An Antecedent Precipitation Index (API) was developed to systematically reduce the effect of a unit of precipitation on pressure head as time passed. Regression equations were developed for prediction of pressure head using API as the independent variable. As shown by Figure 5.11, the relationship between API and pressure head is non-linear and hysteretic. The hysteresis seen in the API vs. pressure head relationship should theoretically result in over-prediction of pressure head on the rising limb of the hydrograph and under-prediction on the falling limb when fit with a single equation. However, it was determined that the degree of hysteresis could be reduced by introducing a time lag. That is, the value of pressure head at time t was better correlated with API from some previous time, than API for the same time t. The optimum value of the time lag was different for different storms, but on average, six hours represented the best value. A polynomial equation containing API_{t-6} and the square of API_{t-6} was determined to best fit the observed data. Figures 5.12-5.16 show the effect on predicted head of the time lag. For the majority of storms the predicted head was closer to both the magnitude and timing of the observed head than the model with no lag.

The value of the predictive model is maximized by conducting multiple event analysis. Ideally, one could start calculating API from the first winter storms and update the model as the number of events increased. The shortfall of single event analysis is that variability in magnitude of pressure head at the start of a storm, and magnitude of API, result in equations for two storm events that can have very different coefficients, as can be seen in Table 5.5.

The models appear to generally function well for the purpose of predicting magnitude and timing of hillslope discharge. Considering both the calibration and verification runs of API for the multi-event case (Figures 5.17, 5.18) the average percent difference between the predicted and observed peak pressure head (as a percent of observed peak head) is -9%. The percent difference for the verification run alone is -15%. This value would seem to be large, given the relatively small pressure head values involved. For the purposes of estimating peak pressure head in the soil for slope stability analyses, this non-conservative behavior is undesirable.

The simplicity of the API method has both advantages and disadvantages. As there are no soil or hillslope parameters directly in the API model, the technique is not capable of handling small scale heterogeneities such as a layered soil profile having different hydraulic conductivities. However, Table 5.6 shows that the API method is repeatable for different wells on the site, as suggested by the consistently high coefficients of determination (r^2) of the regression models. In reality, the recession coefficient, C, is the single parameter that describes all the soil and hillslope parameters. During analysis of the data, it was observed that C was not a constant for all wells. This is not particularly surprising, as small scale heterogeneities are likely to be present. In addition, it was determined that a single value of C did not provide the best correlation between API and pressure head for a particular well, from storm to storm. This is likely due to antecedent moisture conditions in the hillslope. However, the range of C values that resulted in the best correlation was narrow both between storms, and between wells on the site, suggesting that use of an average value would result in an acceptable model.

The uses of the API method are several. The basic requirement, however, is both hydraulic head and precipitation data for a site of interest in order to calibrate the model. After calibration, the model can be coupled with a slope stability model to develop a design storm that would bring the site to limit equilibrium and produce failure of some portion of the site. This storm could be compared to frequency data for observed storms to aid in design of roads, road drainage structures, or other engineered structures where subsurface flow and runoff are of concern. If a model was available for a small watershed, the conditions during failure of a site could be recreated to make estimates of strength parameters or other variables. This technique could also be used to monitor and predict movement of large, slow moving soil slips.

Collection of groundwater and precipitation data is costly and time consuming. The amount of data can be large, and analysis laborious. The API method provides a means of acquiring subsurface information while monitoring only atmospheric conditions, namely precipitation. Following a period of calibration, monitoring of groundwater could be discontinued and the API relationship used to provide an estimate of hydraulic head conditions based on ongoing precipitation data collection.

6.4.2 Kinematic Storage Modeling

In order to have a basis with which to compare and contrast the API model results, a kinematic storage model was used to predict hydraulic head in well 1 for several of the extreme storms. The kinematic storage model was chosen because it is capable of matching the performance of more complex mathematical models having greater data requirements (Sloan and Moore, 1984). The data requirements for the coupled unsaturated-saturated flow storage model include knowledge of the hydraulic conductivity function, including saturated conductivity, drainable porosity of the media, and average initial water content at the beginning of a storm. A number of other, more easily determined, hillslope parameters are also required. The model is easily coded for computer solution, and storage requirements and runtime are minimal.

Typical application of the kinematic storage model is for planar-hillslope subsurface flow. Because the objective of this modeling effort was to use a common, simple groundwater model, the more complex storage model for converging flow was not developed. However, hydraulic head from the planar hillslope model was scaled to account for converging flow consistent with physical features of the site. A necessary condition for the scaling is that the magnitude of input to the saturated zone from the unsaturated zone be small relative to the velocity of flow through the saturated zone. This saturated flow velocity is a constant, for a constant saturated conductivity, by the kinematic assumption that the hydraulic gradient equals the slope of the impermeable bed of the flow region. For the site and storm conditions of this study, it was the case that saturated flow velocity dominated. As a result, the unsaturated flow component of the model was uncoupled from the saturated flow component, and head was scaled to account for downslope convergence of the control volume.

The two soil hydraulic parameters that can be adjusted in the model are the saturated conductivity and drainable porosity. From early model runs it was apparent that values of drainable porosity determined by the method of Bear (1972) overestimated the parameter. This technique considers the drainable porosity to be the difference between the volumetric water content at saturation and the water content at field capacity (see Figure 4.4), where field capacity is defined as the value of water content remaining in a unit volume of soil after downward gravity drainage has ceased. The value of water content at field capacity was estimated from the near vertical portion of the main draining soil moisture characteristic curve at higher capillary pressures. When using the value of drainable porosity determined this way, calculated head values would rise to a relatively low peak, and then fall much more slowly than observed values (Figures 5.19-5.22). Adjusting saturated conductivity to reproduce the observed peak head did not result in good replication of the recession limb.

The modified Bear method of estimating drainable porosity (see Figure 4.4(b)), from desaturation as a function of soil depth, produced much better model results. Peak pressure head values were more consistent with observed values, and recession limbs of the hydrographs were similar in shape and magnitude to those observed. The final method of estimating drainable porosity, called the piezometric response method, compared the depth of precipitation input to the change in piezometric level at a well. The ratio of these two quantities was used as an estimate of the drainable porosity. Data from wells on the perimeter of the study site were used, to minimize the effects of converging flow. The modified Bear and piezometric response methods produced similar results. In fact, the average value of drainable porosity determined by the piezometric response method for the three calibration storms (0.13) was nearly identical to the value determined by the modified Bear method (0.15). The modified Bear method is, perhaps, the most appropriate method to use, given that piezometric response is what is being modeled and that soil hydraulic property data would typically be available. Therefore, the value of drainable porosity determined by the modified Bear method was used in the verification run of the kinematic storage model for Storm 5. The model did not perform as well for this storm. The percent difference in observed and calculated peak head was -23%. However, this value is not significantly larger than that for the API verification result for the same storm. In general, the kinematic storage model performed well for these storm events.

Producing satisfactory model results using the full coupled unsaturated-saturated flow model requires relatively good knowledge of parameter values. It was determined that the saturated flow model is not sensitive to changes in initial saturated thickness at the outlet, H_0, is slightly sensitive to changes in saturated conductivity, K_s, and is highly sensitive to changes in drainable porosity, θ_d. The coupled unsaturated-saturated flow model is slightly sensitive to changes in drainable porosity, moderately sensitive to changes in saturated conductivity and air-entry pressure, ψ_a, and extremely sensitive to changes in θ_{u0}. The precise value of θ_{u0} is not known without some form of continuous monitoring on-site, although a reasonable estimate of the value could be made from the soil moisture characteristic curve. Therefore, model results may be dependent, to some degree, on a priori knowledge of the site conditions. In addition, the model data requirements may be difficult to obtain with a great degree of certainty for sites with significant heterogeneity. Steps can be taken to eliminate uncertainty in site conditions and soil hydraulic parameters as was done by Reddi and Wu (1991), using the kinematic storage model with Bayesian updating of parameter values. However, the need for initial conditions remains. In cases where the unsaturated model can be disregarded, as in the case of this study, several of the difficulties just described are eliminated. There is no need for knowledge of a hydraulic conductivity function, or for other unsaturated zone conditions.

6.4.3 Comparison of Model Results

For the calibration storms (Storms 2,3, and 4) the best results for the two classes of models were produced using API_{t-6}, as the independent variable in the antecedent precipitation index model, and the modified Bear method of estimating drainable porosity in the kinematic storage model. Table 5.10 shows the coefficient of determination, r^2, from regression of predicted head on observed head from all the models. The best model results, using r^2 as a comparison criteria, are the two API models. However, API_t, and modified Bear and piezometric response methods in the kinematic storage model are very similar.

Both API_{t-6} and kinematic storage model using modified Bear underestimate the observed peak head for the one verification storm. The percent difference is -15% for the API model, and -23% for the kinematic storage model. The effect of this difference when calculating the factor of safety for the slope is much less however. Using the one-dimensional infinite slope model with parameter values determined for the study site, the result of the factor of safety calculations was a 7.5% difference when using the observed and the API predicted head, and 9% for the kinematic storage predicted head. This suggests that for the magnitude of pressure head values observed, the two models can be used to predict head for the purpose of calculating factor of safety with satisfactory results. However, as values of head increase, the percent difference in factor of safety increases geometrically. For example, using a value of head that would result in a factor of safety of 1.0, and a head -20% different, the percent difference in factor of safety is approximately 17%.

While the two models perform similarly, the kinematic storage model potentially requires more site information than API. As mentioned previously, it may not be reasonable to expect to ever know the average initial water content of the entire unsaturated zone. However, if the unsaturated model can be uncoupled, the data requirements drop significantly, and the saturated flow model alone has been shown to perform reasonably well.

The API model also performs reasonably well, without requiring a great deal of knowledge about site parameters. There is, of course, the requirement for both head and precipitation data for a calibration period in order to develop the model. The recommendation at this time would be to conduct multi-storm analysis from the beginning of winter storms. The work involved could be significantly reduced by tailoring the data acquisition system to generate similar time history for both well and precipitation data.

There appears to be one or more storm characteristics that affect the ability of the models to accurately predict head. The pattern of rainfall seems to have a strong influence on the model results. It seems from comparisons of the observed and predicted hydrographs (Figure 5.12 - 5.22) that the ability to predict the timing and magnitude of head is, to some degree, influenced by the shape of the hyetograph (the precipitation depth vs. time plot). The API model, in particular, seems to perform better for a "bell shaped" storm, where precipitation intensity starts low, increases, then tapers off, e.g. Storm 4, than for a "rectangular" storm, where intensity is relatively constant, e.g. Storm 3. The verification run of the models may have performed poorly as a result of the broken pattern of precipitation observed in Storm 5. However, there may be additional storm characteristics that are responsible for the observed results.

Finally, additional extreme storm events could be used to develop better calibrations for both the kinematic storage model and the API model. The lack of quantitative data about the unsaturated zone limited the ability to calibrate the full kinematic storage model as effectively as one would like, but storm and site conditions allowed use of just the saturated flow component of the model. Either model would seem to hold promise for purposes of classifying headwalls on the basis of landslide risk.

6.5 Macroporosity and Rapid Subsurface Flow

A primary objective of the study was to further the fundamental understanding of the role of macroporosity in the rapid routing of subsurface flow on steep slopes. As indicated in Chapter 5 only one event of sustained macropore flow was measured, and that by hand, rather than with the intended measurement system. The presence of the free face at the outlet of the headwall has been implicated in an alteration of the moisture and energy conditions in the headwall. Therefore, the fact that macropores were active during a storm may have resulted from the altered conditions. However, measurement of macropore flow at this location does allow for some speculation about the role of this drainage component in an undisturbed zone.

The macropores that were active during the reported event were routing the majority of throughflow at the free face. Measurements indicate that approximately 70% of flow discharging at the face was flowing in macropores greater than 2.5 cm in diameter. If the macropores are linked to form an extensive network in the hillslope, they are clearly capable of delivering the bulk of subsurface flow down slope, under certain conditions of subsurface moisture. We can not definitively say what those conditions are based on our observations. However, the storm that generated the macropore flow was that having the longest duration of the extreme events monitored. The storm also had the second highest one-hour intensity of all the storms monitored. These storm characteristics appear to have led to the wettest soil conditions in the vicinity of the free face, as evidenced by the fact that pressure head at well 1 was highest for this storm. It seems, then, that storms of long duration and moderate to high intensity, coupled with wet antecedent conditions, are most likely to result in macropore flow. The exact hydraulic mechanisms involved in this drainage remain unclear. It can only be concluded from this work that macropores appear to play a significant role in subsurface flow under certain soil hydrologic and atmospheric conditions in the forest environment. The extent to which this component of hillslope drainage either increases or reduces the stability of the slope is not known.

6.6 Pore-pressure Ratios and Slope Stability

The results of the piezometric data analysis showed that the pressure head in the hillslope increased in the upslope direction for the majority of the extreme storm events. This is counter to the common assumption in slope stability analyses that the maximum pressure head occurs at the toe of the slope. However, as discussed previously, comparisons of the effect of pressure head on stability from point to point in a slope must consider not just the magnitude of pressure head, but some form of a ratio of pressure head to soil depth.

A comparison of Figure 5.7 and Figure 5.23 shows that for this particular site, under the conditions observed, that while the magnitude of pressure head does increase in the upslope direction, the value of the peak pore-pressure ratio, r_u, is relatively constant along the slope. Comparisons of plots of pressure head and r_u for the other storms analyzed showed similar results. Values ranged from approximately 0.30 to 0.40 for wells 1-3 for the five storms. This observation does not seem to have a physical basis, and for this reason it is not suggested that this is the general case for hillslopes. It does, however, suggest that care should be exercised in making assumptions about how the peak pore-pressure ratio may vary in the slope being modeled for stability. Finally, many slope stability models assume saturated conditions to the soil surface as a matter of course; for worst case analyses this is reasonable. However, from observations on the study site, and the results of the pore-pressure ratio analysis, this may be a rare condition.

7. CONCLUSIONS

Subsurface flow conditions are an important component of the stability dynamics of steep slopes. On steep forested slopes in the Oregon coast range, subsurface flow is highly transient and may be dominated by macropore flow under certain precipitation and antecedent soil moisture conditions. One tool needed by land managers for classification of landslide risk is a simple groundwater model. Commonly used groundwater models have significant data requirements that are often difficult to obtain. Characterizing variability in soil and hydraulic properties is complicated by the heterogeneous nature of many forest soils. Finally, extensive testing and monitoring is often required in order to obtain sufficient information to calibrate a groundwater model. For purposes of classifying sites on the basis of failure potential, such testing and monitoring may not be justifiable.

Two simple models for prediction of groundwater levels on a steep forested slope were developed and tested. The first model is based on an Antecedent Precipitation Index (API). The API model requires only precipitation time history, following development of a regression equation for pressure head or hydraulic head, using API as the independent variable. A second model was used to compare and contrast the ability of the API model to predict groundwater response to precipitation. This model, the kinematic storage model, is a mass balance model that treats the entire hillslope as the control volume and predicts hydraulic head at a downslope outlet. An infiltration model is typically coupled to the saturated flow model. For the coupled model, data requirements are not trivial, and include extensive knowledge of conditions in the unsaturated zone.

7.1 Summary of Principle Findings

A summary of key findings of the soil testing, subsurface monitoring and piezometric response modeling follows:

- Soil index properties, strength parameters, and hydraulic properties determined for the Oregon coast range headwall are consistent with properties of soils in similar topographic and geographic locations reported in the literature.

- The ability of both the API model and the kinematic storage model to accurately predict head seems to be influenced by storm pattern. The models appear to perform better for a "bell-shaped" storm with varying precipitation intensities than for a "rectangular" storm of uniform precipitation intensity.

- The API model typically over-predicts pressure head on the rising limb of the hydrograph, and under-predicts on the falling limb. This results from hysteresis in the API - pressure head relationship. It was determined that the degree of hysteresis could be reduced by shifting the API variable forward in time, correlating it with pressure head from a later time. A six-hour time lag produced the best overall results for the extreme storms.

- Pressure head values generally increased in the upslope direction. However, pore-pressure ratios varied over a narrow range at the wells for all storms. Peak pressure head at the individual wells tended to vary over a narrow range for all storms. These observations may result from the free face at the toe of the slope, and its potential effect on moisture and energy conditions upslope.

- Macropore flow was determined to be a significant component of subsurface flow under certain precipitation and antecedent soil moisture conditions. While the hydraulic mechanisms involved in macropore flow are not well understood, it is clear that this component plays an important role in hillslope drainage. Flow measurements during one storm event suggest that macropore flow accounted for approximately 70% of the discharge from the hillslope.

7.2 Conclusions

Overall, both the API model and the kinematic storage model performed reasonably well in prediction of the timing and magnitude of peak pressure head for the extreme storms. The planar hillslope kinematic storage model performed well, even though site conditions indicate strong converging flow. Neither model is capable of handling small scale heterogeneities in soil hydraulic properties. Rather, "effective" hillslope properties are used, either directly, as with saturated hydraulic conductivity in the kinematic storage model, or indirectly, as with the recession coefficient, C, in the API model. This may be the best method, however, for handling the combined matrix flow-macropore flow thought to be common in forest soils under certain storm and antecedent conditions.

In order to expand the usefulness of the API model, a statistically sound sample of headwall sites should be instrumented and monitored. Variability in the magnitude of the recession coefficient, C, could be characterized. This would allow determination of whether site specific, watershed scale, or a regional predictive equation, or set of equations, would be necessary.

The well point used in this study was designed to eliminate or reduce time-lag between changes in hydraulic head in the formation, and measurement of that change by the instrument. This design was appropriate for the highly transient conditions observed on the hillslope. Manufacturing cost was high, relative to standard piezometers. A low-cost alternative that incorporated the same features as the instrument used would allow for multiple installations on an increased number of sites at reasonable cost.

Hydraulic conditions on the hillslope are thought to have been affected by the presence of the free face created to monitor saturated throughflow. As no measure of this influence can be made, observations cannot be corrected for any affect the free face may have had. In order to analyze the role of macropores and macropore flow, a less direct, less visual approach may be desirable and necessary. The use of tracers may allow estimates of effective hydraulic conductivity to be made. Piezometers can be used as injection points, but recovery in downslope piezometers could be difficult under the shallow, highly transient flow conditions observed. However, piezometer injection or surface application, followed by excavation could serve the purpose. Destructive sampling, of course, must be carried out at the end of the monitoring period.

Slope stability concerns in forested regions of the Pacific Northwest will continue to be raised as rare, extreme storm events produce landslides on managed and unmanaged lands. Engineers and others with need for simple tools to predict groundwater response to such storms face a number of obstacles. The work reported herein is considered to be a first step along a course of action that may lead to the development of a widely useful predictive model for groundwater levels on steep slopes. There remains much about the methodology that may benefit from refinements. However, the techniques appear to be fundamentally sound. It has been shown that a simple model can be as good as a more complex model in predicting hillslope piezometric levels during storms. This can hopefully serve as the basis for further work to improve the state of knowledge, and the ability to carry out necessary engineering analyses.

LITERATURE CITED

Andersson, J. and A.M. Shapiro. 1983. Stochastic Analysis of One-Dimensional Steady State Unsaturated Flow: A Comparison of Monte Carlo and Perturbation Methods. Water Resources Research 19 (1): 121-133.

Atkinson, T.C. 1978. Techniques for measuring subsurface flow on hillslopes. IN M. J. Kirkby (Ed.) Hillslope Hydrology. Wiley and Sons, Publishers, New York. pp 73-120.

Aubertin, G.M. 1971. Nature and extent of macropores in forest soils and their influence on subsurface water movement. Upper Darby Pennsylvania. U.S. Forest Service. Northeast Forest Experiment Station. Research Paper NE-192 33 pp.

Bakr, A.A., LW. Gelhar, A.L. Gutjahr, and J.R. MacMillan. 1978. Stochastic Analysis of Spatial Variability in Subsurface Flows 1. Comparison of One- and Three-Dimensional Flows. Water Resources Research 14 (2):262-271.

Baldwin, E.M. 1981. Geology of Oregon. 3rd ed. Kendall/Hunt Publishing Co., Dubuque, IA. 170 pp.

Barcelo, M.D. and J.L. Nieber. 1982. Influence of a soil pipe network on catchment hydrology. Am. Soc. Ag. Eng. 82-2027:1-27.

Bear, J. 1972. Dynamic of Fluids in Porous Media. Dover Publications, Inc. New York.764 pp.

Beasley, R.S. 1976. Contribution of Subsurface Flow from the Upper Slopes of Forested Watersheds to Channel Flow. Soil Sci. Soc. Am. J. 40:955-957.

Beven, K.J. 1977. Hillslope Hydrographs By The Finite Element Method. Earth Surface Processes. 2:13-28.

Beven, K. 1981. Kinematic subsurface stormflow. Water Resources Research 17(5):1419-1424.

Beven, K. 1982. On Subsurface Stormflow: Predictions With Simple Kinematic Theory for Saturated and Unsaturated Flows. Water Resources Research 18(6):1627-1633.

Beven, K. and P. Germann. 1982. Macropores and water flow in soils. Water Resour. Res. 18(5):1311-1325.

Bishop, A.W. and N.R. Morgenstern. 1960. Stability Coefficients for Earth Slopes. Geotechnique, 10(4): 129-150.

Bouwer, H. 1978. Groundwater Hydrology. McGraw Hill, New York. 480 pp.

Bransom, M. 1991. Soil Engineering Properties and Vegetative Characteristics for Headwall Slope Stability Analysis in the Oregon Coast Range. MS Thesis, Oregon State Univ., Corvallis. 82 pp.

Bren, L.J., P.W. Farrell, and C.J. Leitch. 1987. Use of Weighted Integral Variables to Determine the Relation Between Rainfall Intensity and Storm Flow and Peak Flow Generation. Water Resources Research 23(7):1320-1326.

Brooks, R.H. and A.T. Corey. 1966. Properites of porous media affecting fluid flow. Proc. Am. Soc. Civil. Eng. J. Irrig. and Drainage. 92(IR 2): 61-88.

Burroughs, E.R. 1984. Landslide hazard rating for portions of the Oregon coast range. IN Symposium on the effects of forest land use on erosion and slope stability. Environment and Policy Institute, East-West Center, Univ. Hawaii, Honolulu. pp 265-274.

Childs, E.C. 1969. An Introduction to the Physical Basis of Soil Water Phenomena. Wiley and Sons, New York.

Chow, V.T. 1964. Runoff. In V.T. Chow (ed.) Handbook of applied hydrology. McGraw-Hill, New York. pp 1-56.

Corey, A.T. 1969. Flow in Porous Media. Colorado State University, Agricultural Engineering Department. Fort Collins, CO.259 pp.

Crozier, M.J. and R.J. Eyles. 1980. Assessing the Probability of Rapid Mass Movement. New Zealand Institute of Engineers, Proceedings of Technical Groups 6, 1 (G), Part 2. p 2.47-2.51.

Darcy, H. 1856. Les fontaines publiques de la ville de Dijon. Victor Dalmont, Paris.

Domenico, P.A. and F.W. Schwartz. 1990. Physical and Chemical Hydrogeology. John Wiley & Sons. 824 pp.

Fedora, M. 1987. Simulation of Storm Runoff in the Oregon Coast Range. MS Thesis. Oregon State University. 142 pp.

Freeze, R.A. and P.A. Witherspoon. 1966. Theoretical analysis of regional groundwater flow: 1. Analytical and numerical solutions to the mathematical model. Water Resour. Res. 2:641-656.

Freeze, R.A. 1978. Mathematical models of hillslope hydrology. IN M.J.Kirkby (ed) Hillslope Hydrology. Wiley and Sons, New York. pp 177-225.

Freeze, R.A. and J.A. Cherry. Groundwater. 1979. Prentice-Hall, Inc., 604 pp.

Gardner, W.R. 1958. Some Steady State Solutions of the Unsaturated Moisture Flow Equation with Application to Evaporation from a Water Table. Soil Sci. 85(4): 228-232.

Germann, P. and K. Beven. 1981. Water Flow in Soil Macropores III. A Statistical Approach. J. Soil Sci. 32: 31-39.

Gomez-Hernandez, J.J. and J. Carrera. 1994. Using linear approximations to rank realizations in groundwater modeling: Application to worst case scenario. Water Resources Research 30 (7): 2065-2072.

Haines, W.B. 1930. Studies in the physical properties of soils. V. The hysteresis effect in capillary properties and the modes of moisture distribution associated therewith.. J. Agr. Sci. 20: 97-116.

Harr, R.D. 1977. Water Flux in Soil and Subsoil on a Steep Forested Slope. J. Hydrol. 33:37-58.

Heilman, P.E., H.W. Anderson, and D.M. Baumgartner, Eds. 1979. Forest Soils of the Douglas-fir Region. Washington State Univ. Coop. Ext. Serv.298 pp.

Hewlett, J.D. and A.R. Hibbert. 1963. Moisture and energy conditions within a sloping soil mass during drainage. J. Geophys. Res. 68(4):1081-1087.

Hewlett, J.D. and A.R. Hibbert. 1965. Factors affecting the response of small watersheds to precipitation in humid areas. In W.E.Sopper and H.W.Lull (eds.) Forest hydrology: Proc.Nat. Sci. Foundation Sem. Pergamon Press, New York. pp. 275-290.

Hewlett, J.D., J.C. Forston, and G.B. Cunningham. 1977. The Effect of Rainfall Intensity on Storm Flow and Peak Discharge from Forest Land. Water Resources Research 13 (2): 259-266.

Hewlett, J.D. 1984. Additional Tests on the Effect of Rainfall Intensity on Storm Flow and Peak Flow from Wild Land Basins. Water Resources Research 20(7):985-989.

Hillel, D. 1982. Introduction to Soil Physics. Academic Press, Inc. 364 pp.

Holbo, H.R., E.L. Miller,and R.C. Sidle. 1985. Scanning recording system for multiple capacitive water-depth transducers. J. Hydrol. 79:311-318.

Holtz, R.D. and W.D. Kovacs. 1981. An Introduction to Geotechnical Engineering. Prentice-Hall, Inc. 733 pp.

Hubbert, M.K. 1940. The theory of groundwater motion. J. Geol. 48:785-944.

Hvorslev, M.J. 1949. Subsurface Exploration and Sampling of Soils For Civil Engineering Purposes. Soil Mechanics and Foundations Division, ASCE. 521 pp.

Hvorslev, M.J. 1951. Time lag and soil permeability in groundwater obsevations. Corp of Engineers, U.S. Army Waterways Exp. Sta. Bull. No. 36. Vicksburg, MI.

Istok, J.D. and L. Boersma. 1986. Effect of Antecedent Rainfall on Runoff During Low-Intensity Rainfall. J. Hydrol. 88: 329-342.

Jury, W.A., W.R. Gardner, and W.H. Gardner. 1991. Soil Physics. John Wiley & Sons, Inc. 328 pp.

Knapp, B.J. 1973. A system for the field measurement of soil water movement. Tech. Bull. Brit. Geomorph. Res. Grp. 9:26 pp.

Lambe, T.W. 1951. Soil Testing for Engineers. John Wiley & Sons, Inc. 165 pp.

MacDonald, L.H. 1987. Forest harvest, snowmelt and streamflow in the central Sierra Nevada. Forest Hydrology and Watershed Management. Proc. Vancouver Sym. pp. 273-283.

Megahan, W.F.and J.L. Clayton. 1983. Tracing Subsurface Flow on Roadcuts on Steep, Forested Slopes. Soil Sci. Soc. Am. J. 47(6):1063-1067.

Morgan, D. 1995. Strength Parameters and Triaxial Strength Testing of Soils of the Oregon Coast Range. Master of Science Engineering Report, Department of Civil Engineering, Oregon State Univ., Corvallis. 94 pp.

Morgenstern, N.R. and D.A. Sangrey. 1978. Methods of Stability Analysis. In Schuster, R.L. and R.J. Krizek (eds.) Landslides: Anlaysis and Control. Special Report 176 Transportation Research Board. National Academy of Sciences, Washington D.C.
pp 155-171.

Mosely, M.P. 1982. Subsurface Flow Velocities Through Selected Forest Soils, South Island, New Zealand. J. Hydrol. 55:65-92.

Mualem, Y. 1976. A New Model for Predicting the Hydraulic Conductivity of Unsaturated Porous Media. Water Resources Research 12(3): 513-522.

NOAA Climatological Data - Oregon. Monthly and Annual Precipitation Records. U.S. Dept. of Commerce.

O'Rourke, J.E.,J.R. Essex and B.K. Ranson. 1977. Field permeability test methods with applications to solution mining. U.S. Dept. Commerce Nat.Tech.Info.Serv.PB-272452.

Philip, J.R. 1964. Similarity hypothesis for capillary hysteresis in porous materials. J. Geophys. Res. 69: 1553-1562.

Pierson, T.C. 1977. Factors Controlling Debris-Flow Initiation On Forested Hillslopes in the Oregon Coast Range. Ph.D. Thesis, Univ. of Washington, Seattle. 166 pp.

Reddi, L.N. and T.H. Wu. 1991. Probabilistic Analysis of Ground-Water Levels in Hillside Slopes. J. Geotech. Eng., ASCE, 117 (6):872-890.

Reid, M.E., H.P. Nielsen, and S.J. Dreiss. 1988. Hydrologic Factors Triggering a Shallow Hillslope Failure. Bull. Assoc. Eng. Geol. 25(3):349-361.

Reiter M. 1991. Subsurface Flow of a Forested Riparian Area in the Oregon Coast Range. MS Thesis, Oregon State Univ., Corvallis. 108 pp.

Richards, L.A. 1931. Capillary conduction of liquids in porous mediums. Physics 1:318-333.

Rijtema, P.E. 1965. An analysis of actual evapotranspiration. Report 659, Center for Agri. Publ. And Docs. Wageningen, Netherlands. 107 pp.

Schoenemann, M.R. and M.R. Pyles. 1990. Statistical Description of Triaxial Shear Test Results. Geotech. Testing, J. Am. Soc. Testing and Materials. p 58-62.

Schroeder, W.L. and J.V. Alto. 1983. Soil Properties for Slope Stability Analysis; Oregon and Washington Coastal Mountains. For. Sci. 29(4):823-833.

Sidle, R.C. 1985. Shallow groundwater fluctuations in unstable hillslopes of coastal Alaska. Z. Gletscherkunde und Glazialgeol. 20(2):79-95.

Sidle, R.C. 1986. Groundwater Accretion in Unstable Hillslopes of Coastal Alaska. IN Conjunctive Water Use. IAHS Publication 156. p 335-343.

Sloan, P.G. and I.D. Moore. 1984. Modeling Subsurface Stormflow on Steeply Sloping Forested Watersheds. Water Resour. Res. 20(12):1815-1822.

Swanston, D.N.,G.W. Lienkaemper, R.C. Mersereau, and A.B. Levno. 1988. Timber Harvest and Progressive Deformation of Slopes in South-western Oregon. Bull. Assoc. Eng. Geol. 25(3):371-381.

Troendle, C.A. 1985. Streamflow Generation from Subalpine Forests. In E.B.Jones and T.J.Ward (eds) Watershed Management in the Eighties. Proc. Sym. Watershed Management. pp 240-247.

Tsukamoto, Y. and T. Ohta. 1988. Runoff Process on a Steep Forested Slope. J. Hydrol. 102:165-178.

van Genuchten, M.Th. and D.R. Nielson. 1985. On describing and predicting the hydraulic properties of unsaturated soils. Ann. Geophy. 3: 615-628.

Verma, R.D. and W. Brutsaert. 1971. Similitude criteria for flow from unconfined aquifers. Am. Soc. Civil Eng., J. Hydraul. Div. 97(HY9)):1493-1509.

Wang, H.F. and M.P. Anderson. 1982. Introduction to Groundwater Modeling - Finite Difference and Finite Element Methods. San Francisco: W.H. Freeman. 237 pp.

Whipkey, R.Z. 1965. Subsurface stormflow from forested slopes. Bull. Int. Assoc. Sci. Hydrol. 10(3):74-85.

Whipkey, R.Z. 1967. Theory and Mechanics of Subsurface Stormflow. In W.E.Sopper and H.W.Lull (eds.) Forest hydrology: Proc.Nat. Sci. Foundation Sem. Pergamon Press, New York. pp 255-260.

Wilson, C.J. and W.E. Dietrich. 1987. The contribution of bedrock groundwater flow to storm runoff and high pore pressure development in hollows. IN R.L.Beschta et. al. (eds) Erosion and Sedimentation in the Pacific Rim. Proc. Sym. pp 49-59.

Yee, C.S. 1975 Soil and Hydrologic Factors Affecting the Stability of Natural Slopes in the Oregon Coast Range. Ph.D. Dissertation, Oregon State University, Corvallis 204 pp.

Zeimer, R.R. 1984. Response of progressive hillslope deformation to precipitation. IN Symposium on Effect of Forest Land Use on Erosion and Slope Stability. East-West Center, Honolulu. pp 91-98.

Zeimer, R.R. and J.S. Albright. 1987. Subsurface pipeflow dynamics of north-coastal California swale systems. IN Erosion and Sedimentation in the Pacific Rim. IAHS Publication 165. pp 71-80.